



Cite this: *Chem. Soc. Rev.*, 2023, 52, 3035

# Photocontrolled RAFT polymerization: past, present, and future

Yungyeong Lee,<sup>a</sup> Cyrille Boyer<sup>id</sup>\*<sup>c</sup> and Min Sang Kwon<sup>id</sup>\*<sup>ab</sup>

In this review, we provide a brief history, progress, and applications, and discuss the remaining challenges of photocontrolled reversible addition–fragmentation chain transfer (RAFT) polymerization (i.e., photoinduced electron/energy transfer-RAFT (PET-RAFT), photoiniferter, and photomediated cationic RAFT polymerization). Among these, visible-light-driven RAFT polymerization has attracted particular attention in recent years due to its benefits, including low energy consumption and the safe reaction procedure. Moreover, the incorporation of visible-light photocatalysis in the polymerization has conferred attractive features, such as spatiotemporal control and oxygen tolerance; however, a clear understanding of the reaction mechanism has not been completely provided. We also present recent research efforts to elucidate the polymerization mechanisms with the aid of quantum chemical calculations combined with experimental evidence. This review offers an insight into the better design of polymerization systems for desired applications and helps realize the full potential of photocontrolled RAFT polymerization in both academic- and industrial-scale applications.

Received 7th December 2022

DOI: 10.1039/d1cs00069a

rsc.li/chem-soc-rev

<sup>a</sup> Department of Materials Science and Engineering, Seoul National University, Seoul 08826, Republic of Korea. E-mail: minsang@snu.ac.kr

<sup>b</sup> Research Institute of Advanced Materials, Seoul National University, Seoul 08826, Republic of Korea

<sup>c</sup> Cluster for Advanced Macromolecular Design (CAMD), School of Chemical Engineering, and Australian Centre for NanoMedicine, UNSW Sydney, Kensington, NSW 2052, Australia. E-mail: cboyer@unsw.edu.au

## 1. Introduction

### 1.1. Visible light as an energy source for photomediated reactions

Visible light refers to electromagnetic waves with wavelengths in the range of approximately 400–750 nm that are detectable by the human eye.<sup>1</sup> As visible light constitutes approximately half of the solar energy reaching the surface of earth, tremendous efforts have been devoted to utilize visible light as an energy source in the field of solar energy utilization including photovoltaics and solar



Yungyeong Lee

*Yungyeong Lee received her B.S. and M.S. degrees in Chemistry from Ulsan National Institute of Science and Technology (UNIST) in 2017 and 2019, respectively. Since 2021, she has been pursuing a PhD in Materials Science and Engineering (MSE) at Seoul National University (SNU) under the supervision of Prof. Min Sang Kwon. Her research interest focuses on the development of organic photocatalysts, investigation of their photophysical and electrochemical properties, and application to visible-light-mediated polymerization reactions particularly in aqueous systems.*



Cyrille Boyer

*Prof Cyrille Boyer is a Full Professor in the School of Chemical Engineering, Deputy Head of School, and Co-Director of Australian Centre for Nanomedicine. In 2022, he was awarded an Australian Laureate Fellowship. Cyrille's research interests mainly cover the preparation of functional macromolecules using photocatalysts, which find applications in various areas, including in nanomedicine and in energy storage. The research of his group has been recognized by several research awards, including 2018 IUPAC-Polymer International Young Researcher award, 2016 ACS Biomacromolecules/Macromolecules Young Researcher Award, Le Fevre Memorial Prize for Chemistry; and 2015 Malcolm McIntosh Prize for Physical Science.*



fuels. Owing to Ciamician's pioneering insight, influenced by photosynthesis in nature,<sup>2</sup> light has been consistently used as an energy source for organic reactions.<sup>3</sup> Because most organic molecules do not absorb light in the visible range, ultraviolet (UV) light has long been employed as the primary energy source for photochemical reactions. However, due to its high energy, UV light often causes substantial side reactions and thereby reduces the reaction efficiency, which consequently limits the scope of photochemical reactions. Therefore, compared to conventional thermal reactions, photochemical reactions have been considerably underexplored.

In 2008, MacMillan,<sup>4</sup> Yoon,<sup>5</sup> and Stephenson<sup>6</sup> and coworkers reported that complex organic reactions proceed very efficiently in the presence of photoredox catalysts (PCs) under visible light irradiation. From these pioneering studies, organic chemists recognized that low-energy visible light could be a suitable energy source for various organic reactions, which led to the origin of a new field called "visible-light photocatalysis".<sup>7–9</sup> Thereafter, for more than a decade, visible-light photocatalysis has indeed been used as a mild and efficient method to activate molecules for a wide range of organic transformations that cannot be realized by other methodologies of chemical catalysis.<sup>10–13</sup> Under irradiation, excited-state PCs engage in electron or energy transfer and consequently generate highly reactive radical species from the corresponding stable substrates. These previously inaccessible reaction scaffolds have enabled significant development of radical chemistry in organic synthesis.

## 1.2. Visible-light-driven reversible deactivation radical polymerization

Reversible deactivation radical polymerization (RDRP) is a powerful technique to prepare polymers with controlled molecular weights, narrow molecular weight distributions (MWDs), compositions, functionalities, and architectures that impact the properties of polymers.<sup>14,15</sup> As this method provides appropriate controllability and compatibility with various monomers under mild conditions, it has been employed in numerous applications such as coatings, adhesives, cosmetics, ink materials for printing, detergents, paints,

and surfactants.<sup>16</sup> In RDRP, heat is typically utilized as an energy source for polymerization in the presence of an initiator or a catalyst.<sup>17,18</sup>

Consistent efforts have been made to utilize light as an energy source for RDRP because of the potential benefits, including spatiotemporal control over polymerization and fast kinetics at ambient temperature as compared to conventional thermal processes.<sup>19–21</sup> Early systems for photomediated RDRP, which utilized high-energy UV light, had mostly relied on (i) a traditional photoinitiating system based on Norrish type I/II reactions,<sup>22</sup> (ii) a catalytic species with absorption only in the UV range,<sup>23,24</sup> or (iii) a chain transfer agent (CTA) (*i.e.*, RAFT agent) that undergoes photolysis under UV light irradiation.<sup>25–27</sup> However, these processes typically exhibited insufficient controllability of polymerization, side reactions and/or too fast kinetics due to the high energy of UV light. Nevertheless, it should be noted that in the field of polymer chemistry, a variety of UV-light-induced photoinitiating systems had been actively investigated before the emergence of visible-light photocatalysis owing to their utility in industrial applications such as photoresists and/or photocuring systems.

With regard to the milder reaction conditions of polymerization, visible light has been introduced as an energy source for RDRP since the early 2010. Inspired by visible-light photocatalysis, in 2012 Hawker and Fors demonstrated atom transfer radical polymerization (ATRP) of methacrylates using tris(2-phenylpyridine)iridium ( $\text{Ir}(\text{ppy})_3$ ) as a PC and a 50 W fluorescent lamp.<sup>28</sup> Matyjaszewski and coworkers reported another photomediated ATRP using a copper (Cu) complex under violet and blue light irradiation (392 and 450 nm, respectively),<sup>29</sup> where photoinduced reduction of the  $\text{Cu}^{2+}$  complex and subsequent activation of the alkyl halide initiator were achieved by irradiation rather than heating. By the addition of visible-light-absorbing dyes to indirectly reduce the  $\text{Cu}^{2+}$  complex and generate initiating radicals, Yagci and coworkers further expanded the polymerization wavelength to 400–500 nm.<sup>30</sup> In the case of RAFT polymerization, in 2014, Boyer and coworkers employed  $\text{Ir}(\text{ppy})_3$  to activate the reversible addition–fragmentation chain transfer (RAFT) polymerization of various vinylic monomers (including (meth)acrylamides, (meth)acrylates, styrene, and vinyl esters) under blue light irradiation (435 nm).<sup>31</sup> In 2015, Boyer,<sup>32</sup> Qiao,<sup>33</sup> and coworkers separately reported the successful RAFT polymerization of (meth)acrylates under blue or green light irradiation (435 and 530 nm, respectively) in the absence of PCs. These visible-light-driven RDRPs retained excellent controllability of polymerization similar to conventional thermal RDRPs. Since these initial studies, various types of visible-light-driven RDRPs have been extensively studied from different perspectives such as (i) reaction optimization, (ii) mechanistic studies, (iii) understanding the unique features of each polymerization, (iv) catalyst/reagent developments, (v) syntheses of polymers with a novel structure, and (vi) new applications.<sup>19,20,34–36</sup>

## 1.3. Visible-light-driven RAFT polymerization

In conventional RAFT polymerization, an initiator generates radicals typically by thermal decomposition and a CTA ensures



**Min Sang Kwon**

currently an Associate Professor of MSE. He has a broad interest in organic chemistry, photochemistry, and polymer chemistry.

*Min Sang Kwon received his B.S. degrees in Chemistry and MSE from SNU. Then, he did his PhD in Chemistry at SNU under the guidance of Prof. Eun Lee. After finishing his postdoctoral studies at SNU with Prof. Soo Young Park, he moved to University of Michigan to work with Prof. Jinsang Kim. In 2016, he began his independent career at UNIST as an Assistant Professor. In 2020, he moved back to his alma mater, SNU, where he is*



the controllability of polymerization *via* RAFT equilibrium.<sup>37</sup> In contrast, in photomediated RAFT polymerization, a photo-initiating system mostly driven by UV light has replaced the conventional thermal initiator. Despite the simplicity and convenience of photomediated polymerization, which proceeds by irradiation rather than heating, the high energy of UV light caused undesired side reactions and lowered the controllability of polymerization.<sup>38</sup> Boyer and coworkers pioneered the use of low-energy visible light for photomediated RAFT polymerization in 2014 by the incorporation of PCs, named photoinduced electron/energy transfer-RAFT (PET-RAFT) polymerization.<sup>31</sup> In 2015, Boyer,<sup>32</sup> Qiao,<sup>33</sup> and coworkers separately reported visible-light-driven photoiniferter polymerization of specific (meth)acrylates. The proposed PET-RAFT polymerization was based on electron/energy transfer between a visible-light-absorbing PC and a CTA,<sup>31</sup> whereas photoiniferter polymerization was based on visible-light-driven photolysis of a CTA in the absence of PCs and had been previously demonstrated only under UV light.<sup>39,40</sup> More recently, cationic RAFT polymerization, which involves the formation of carbocations as propagating species,<sup>41,42</sup> was realized under visible light in the presence of a PC, as reported by Fors and coworkers.<sup>43</sup> Since then, numerous studies have improved the utility of reaction systems, for example, by investigating PCs and/or CTAs to enhance the rate of polymerization under a broad range of irradiation wavelengths. It has also been revealed that these visible-light-driven RAFT polymerizations exhibit decent controllability of polymerization as well as attractive features including spatiotemporal control, oxygen tolerance, and unique selectivity of polymerization, which are dependent on reaction conditions (*i.e.*, irradiation wavelengths and the combination of a CTA, monomer, and PC if employed), and high compatibility with other polymerization

methods, which was not observed in conventional RDRP.<sup>44</sup> Therefore, visible-light-driven RAFT polymerization has enabled the preparation of polymers with high levels of structural complexities and functionalities and reached a wide range of advanced applications, such as advanced manufacturing, nanomedicine, and energy. Fig. 1 depicts the timeline of milestones toward the development of visible-light-driven RAFT polymerization.

#### 1.4. Scope of this review

Given these attractive and unique features, several highly cited review articles have already discussed photocontrolled RAFT polymerization either as a part of photomediated RDRP or photoredox catalysis,<sup>19,20,45–47</sup> or as an independent topic with a particular emphasis on mechanistic studies,<sup>48</sup> oxygen tolerance,<sup>49</sup> spatio-temporal regulation of the reaction system by light,<sup>50,51</sup> fabrication of advanced materials,<sup>52</sup> and environmental compatibility of polymerization.<sup>44</sup> The recent review articles have provided an insight into the remaining challenges and underscored the promising future of photomediated RAFT polymerization for its wide applicability in the industry.<sup>34,53</sup> However, as compared to PET-RAFT polymerization, only a few articles<sup>54,55</sup> have paid considerable attention to photoiniferter polymerization until Hartlieb in 2022 outlined the progress of photoiniferter polymerization from early systems to the current state.<sup>56</sup> It was because photoiniferter polymerization has mostly utilized UV light thus far, in contrast to PET-RAFT polymerization which utilized the milder visible light.

Visible light is more than an energetically mild and environmentally benign energy source. Convergence of visible-light photocatalysis and photomediated RDRP has also brought decent controllability of polymerization and distinct features such as oxygen tolerance. Furthermore, visible and near-infrared (NIR) light allows utilizing wavelength-orthogonal chemistry for activating wavelength-selective photoinduced reactions in an orthogonal manner. In this regard, it is timely to provide a detailed review on photocontrolled RAFT polymerization reactions (*i.e.*, PET-RAFT, photoiniferter, and photomediated cationic RAFT polymerization) with a particular emphasis on visible-light-driven systems, and summarize their concept, method, mechanism, and applications. In addition to the unprecedentedly wide versatility of the polymerization ranging from precision polymer synthesis in academic fields to 3D/4D printing technologies in industrial fields, we describe the recent increasing efforts to uncover and elucidate the underlying mechanistic backgrounds from a photophysical point of view with the help of computational studies. As the broad applicability of the polymerization originates from the mechanism, this review provides an overview of the current status and the remaining challenges in photocontrolled RAFT polymerization.

## 2. Mechanism

In this section, the basic mechanisms and current studies related to the mechanistic understanding of various visible-light-driven RAFT polymerizations are described. The methods mostly do not require exogenous initiators and share a RAFT process, which underpins the controllability similar to that in conventional

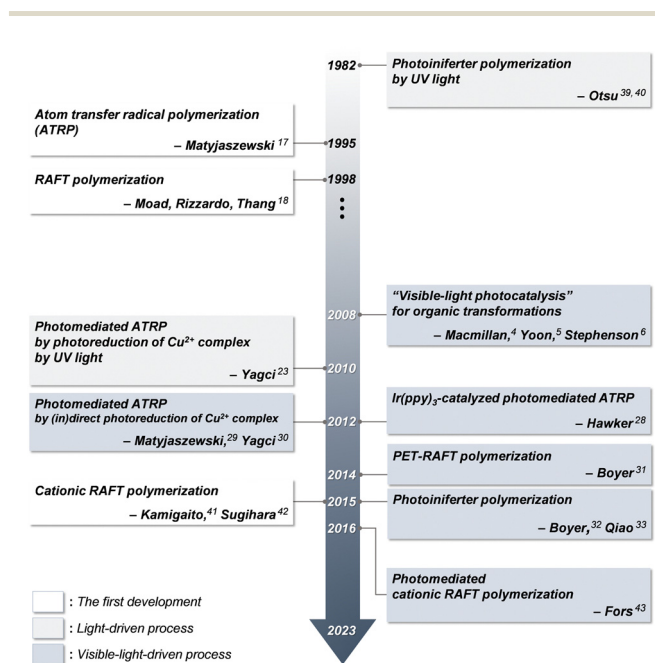


Fig. 1 Timeline of milestones toward the development of photocontrolled RAFT polymerization.





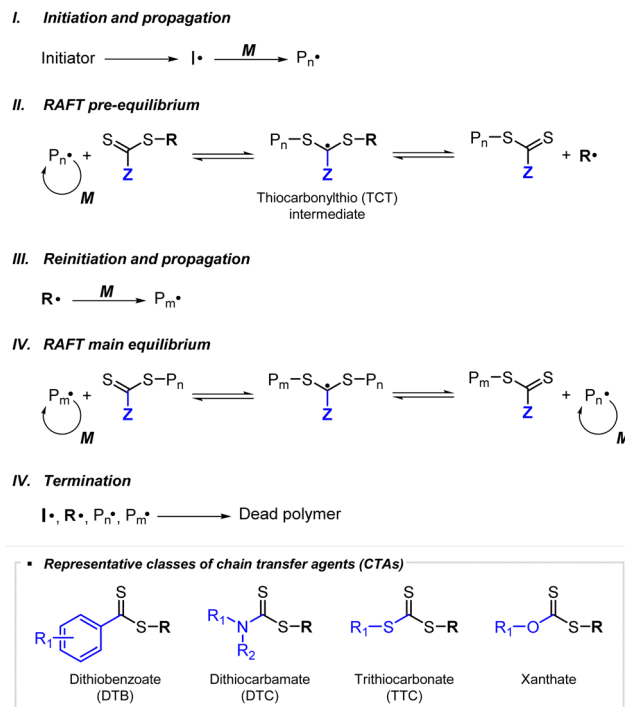
thermal RAFT polymerization. Based on the initiation mechanism, the methods can be categorized as follows.

In PET-RAFT polymerization, an initiating radical is generated by the interaction between an excited-state PC and a CTA followed by (i) fragmentation of the reduced CTA *via* either an oxidative<sup>31</sup> or a reductive quenching cycle,<sup>57</sup> and/or (ii) homolysis of the CTA *via* energy transfer.<sup>46</sup> The CTA can be oxidized as in the case of photomediated cationic RAFT polymerization.<sup>43</sup> Photoiniferter polymerization includes direct homolysis of the CTA under irradiation in the absence of a PC.<sup>40,58</sup> Very recently, the RAFT process has been combined with inner-sphere electron transfer (ISET)<sup>59</sup> and hydrogen atom transfer (HAT).<sup>60</sup>

Despite the burgeoning applications of visible-light-driven RAFT polymerization in numerous fields, several questions, such as whether it is electron or energy transferred from the excited-state PC to the CTA, still remain unsolved. It is also noteworthy that the electron/energy transfer processes may also depend on the type of PC and CTA. Herein, the importance of enhancing fundamental understanding of the mechanism and thereby the recent efforts utilizing quantum chemical (QC) calculations, kinetic modeling, laser flash photolysis, or transient absorption spectroscopy to answer these unsolved questions are summarized.

## 2.1. Conventional RAFT polymerization (RAFT process)

RAFT polymerization, which was firstly developed by Rizzardo, Moad, Thang, and coworkers in 1998,<sup>18</sup> relies on degenerative chain transfer to reversibly deactivate active propagating radicals. By the addition of a CTA possessing a thiocarbonylthio (TCT) group to conventional radical polymerization, the RAFT process successfully realized RAFT polymerization with controlled and living behavior (Scheme 1). Firstly, an external initiator is fragmented, typically by heat or light, to generate initiating radicals. After several additions of monomers, the propagating radical is added to the CTA. The resulting TCT intermediate radical undergoes fragmentation to liberate the R group as another propagating radical. These two propagating radicals are reversibly added and fragmented to become dormant and active species for polymerization, respectively, which is called RAFT main equilibrium. *Via* this RAFT main equilibrium, the propagating radicals share equal probabilities for chain growth. It is noted that addition and fragmentation occur faster than propagation, which prevents bimolecular termination between two radical species. Therefore, polymers possessing TCT groups exhibit low dispersity and can be reactivated by adding new monomers. As controlled and living radical polymerization is realized through an efficient RAFT process, for each monomer family, a CTA with appropriate R and Z groups must be chosen to ensure energetically favorable addition, fragmentation, and propagation. Dithiobenzoates (DTBs), dithiocarbamates (DTCs), trithiocarbonates (TTCs), and xanthates are representative classes of CTAs categorized based on the Z groups. Since the development of RAFT polymerization, the influence of R and Z groups on polymerization control has been thoroughly studied. The well-established general guidelines for the selection of CTAs for a certain monomer are well described



Scheme 1 Mechanism of conventional RAFT polymerization.

in the review articles by the inventors of RAFT polymerization in the Commonwealth Scientific and Industrial Research Organization (CSIRO)<sup>61</sup> and Perrier.<sup>37</sup>

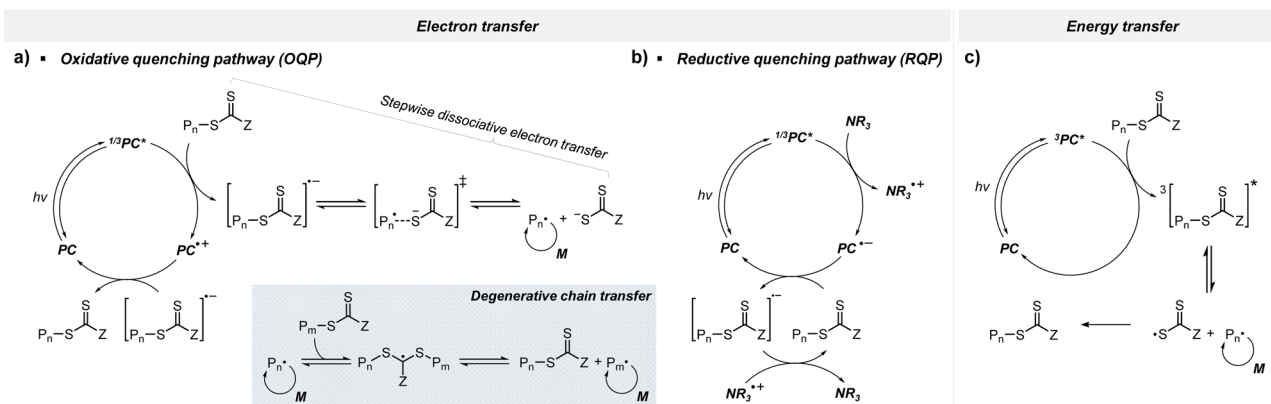
## 2.2. Visible-light-driven RAFT polymerization

**2.2.1. PET-RAFT polymerization.** Despite the recent remarkable advancements of PET-RAFT polymerization, its mechanism remains elusive as it involves multiple competing pathways (*i.e.*, electron and/or energy transfer; see below). The complexity of the PET-RAFT polymerization mechanism primarily arises from the fact that CTAs have relatively high oxidizing powers and hence high ground-state reduction potentials ( $-1.0 \text{ V} < E_{\text{red}}^0 < -0.4 \text{ V}$ ; *vs.* saturated calomel electrode (SCE)), low energies at the lowest triplet excited state ( $T_1$ ) ( $1.5 \text{ eV} < E_{00}(T_1) < 1.8 \text{ eV}$ ), and moderate visible-light absorption abilities. The high  $E_{\text{red}}^0$ s allow the reduction of the CTA by PC intermediates *via* electron transfer, whereas the low  $T_1$  energies allow energy transfer from an excited-state PC to the CTA. Finally, several visible-light-absorbing CTAs can be directly excited by absorbing visible light ( $< 530 \text{ nm}$ ) by themselves in the absence of a PC (please see Section 2.2.2). Among the different pathways, three pathways involving PCs are depicted in Scheme 2: one energy transfer pathway and two electron transfer pathways which are divided into the oxidative quenching pathway (OQP) and the reductive quenching pathway (RQP) depending on the fate of excited-state PCs during the photocatalytic cycle. Most PCs can, in principle, induce polymerization *via* all the pathways, which greatly limits the complete understanding of the precise mechanism. Propagating radical species are generated regardless of the pathways, but their reaction intermediates (*i.e.*, TCT anion and TCT radical) are different.





## PET-RAFT polymerization



**Scheme 2** Mechanism of PET-RAFT polymerization. Electron transfer via (a) oxidative quenching pathway (OQP) and (b) reductive quenching pathway (RQP) in the presence of a reducing agent (e.g., tertiary amine). (c) Energy transfer.

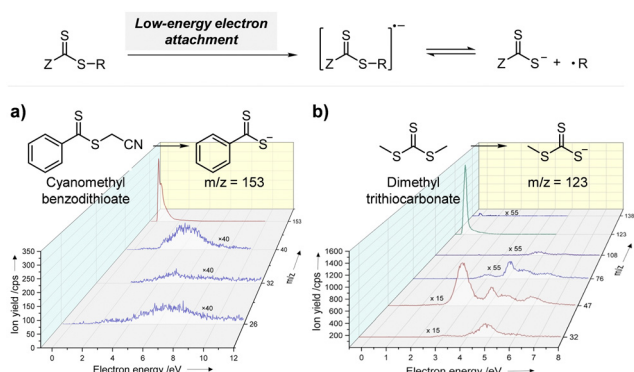
### 2.2.1.1. Electron transfer: oxidative quenching pathway (OQP).

The OQP involves oxidation of an excited-state PC. Electron transfer from an excited-state PC to a ground-state CTA leads to the formation of a one-electron-oxidized PC ( $PC^{\bullet+}$ ) and an anionic intermediate of the CTA, which then undergoes fragmentation to afford a propagating radical and a TCT anion. Stepwise dissociative electron transfer (DET) is considered to occur during the activation step (Scheme 2a). Based on the transfer coefficient ( $\alpha$ ) measured by cyclic voltammetry (CV), Moad, Strover, and coworkers claimed that electron transfer from the excited-state PC to the CTA and dissociation of the C–S bond occur in a stepwise manner.<sup>62</sup> More recently, Denifl, Moad, Coote, and coworkers thoroughly investigated the reduction of the selected CTAs (cyanomethyl benzodithioate and dimethyl trithiocarbonate) and their subsequent chemical reactions by performing low-energy electron attachment experiments in the gas phase (Fig. 2).<sup>63</sup> Interestingly, in these experiments, the authors observed that anion intermediates were (i) generated and (ii) selectively dissociated into TCT anions and carbon radicals through C–S bond cleavage. These observations strongly supported

the involvement of stepwise DET in the electron-transfer-driven RAFT process.

Recently, the research groups of Boyer and Liu,<sup>64</sup> and Kwon<sup>65</sup> separately reported that the selectivity for the CTA in PET-RAFT polymerization is closely related to the stepwise DET mechanism. Boyer and coworkers observed that metal naphthalocyanine (MNC)-catalyzed PET-RAFT polymerization of methyl acrylate (MA) under NIR light irradiation (780 nm) showed substantial monomer conversion and decent control for TTCs with a tertiary R group, whereas no polymerization occurred for TTCs with a secondary R group.<sup>64</sup> QC calculations combined with experiments revealed that an activation barrier exists for the dissociation of the C–S bond of a CTA anion intermediate, depending on the R group. Similar results were also reported by Kwon and coworkers.<sup>65</sup> Using  $Ag_2S$  nanocrystals (NCs) as a PC under red light irradiation (635 nm), PET-RAFT polymerization of methacrylates was achieved for TTCs (CDTPA), whereas no polymers were obtained for DTBs (CPADB). According to QC calculations, a significantly higher activation energy was obtained for the stepwise dissociation of the anion intermediate of CPADB compared to that of CDTPA (45.47 vs. 21.86 kJ mol<sup>−1</sup>), implying that anion intermediates generated by photoinduced electron transfer play an essential role in the observed Z-group selectivity (Fig. 3).

Although OQPs mostly rely on photoinduced outer-sphere electron transfer (OSET) between the PC and CTA, Pan and coworkers recently reported PET-RAFT polymerization based on photoinduced ion-pair ISET (IP-ISET) (Scheme 3).<sup>59</sup> The authors demonstrated successful PET-RAFT polymerization of various vinylic monomers under visible-light irradiation in the presence of a zwitterionic borane catalyst ( $[L_2B]^+X^-$ ) and CTA. Based on QC calculations combined with experiments,  $[L_2B]^+[ZCS_2]^-$  generated *in situ* from  $[L_2B]^+X^-$  and CTA was considered to be an active catalytic species. The stability of  $[L_2B]^+$  formed by ion-pair electron transfer and the very long excited-state lifetime of  $[L_2B]^+*$  allowed the reaction to proceed well even at extremely low catalyst concentrations as low as 1 ppb, which is approximately three orders of magnitude lower than those of OSET-based systems. Unlike the



**Fig. 2** Electrochemical activation of the CTA by low-energy electron attachment and intensity map of TCT anions generated from subsequent dissociation of (a) cyanomethyl benzodithioate and (b) dimethyl trithiocarbonate. Adapted with permission from ref. 63 (Copyright 2021 John Wiley & Sons, Inc.).

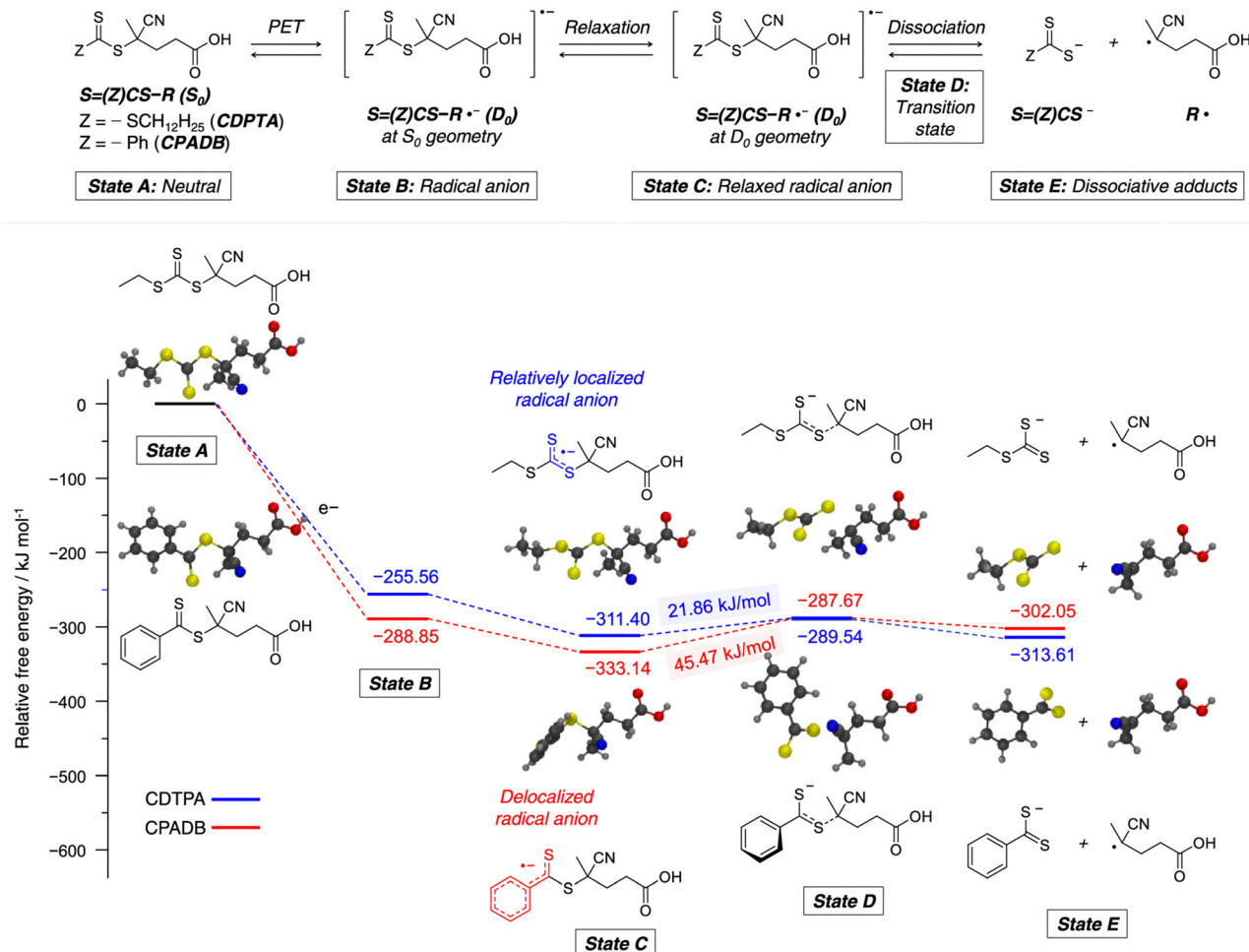


Fig. 3 Calculated energy profiles for stepwise dissociation of anion intermediates of CDTPA (blue) and CPADB (red). Adapted with permission from ref. 65 (Copyright 2023 American Chemical Society).

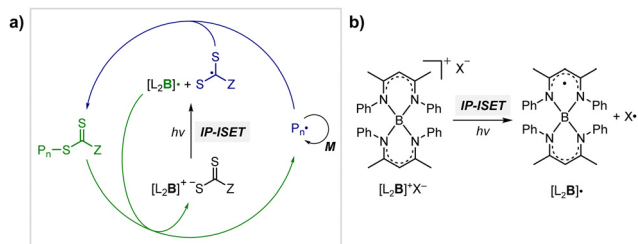
reported PET-RAFT polymerization, this method showed excellent tolerance to phenolic radical inhibitors, owing to the strong hydrogen bond between the phenolic group of the inhibitor and  $X^-$  of  $[L_2B]^+X^-$ .

#### 2.2.1.2. Electron transfer: reductive quenching pathway (RQP).

The RQP involves reduction of an excited-state PC by adding a sacrificial reducing agent (Scheme 2b). A one-electron-reduced PC ( $PC^{\bullet-}$ ) is initially formed through electron transfer from a sacrificial reducing agent to an excited-state PC. Subsequently,

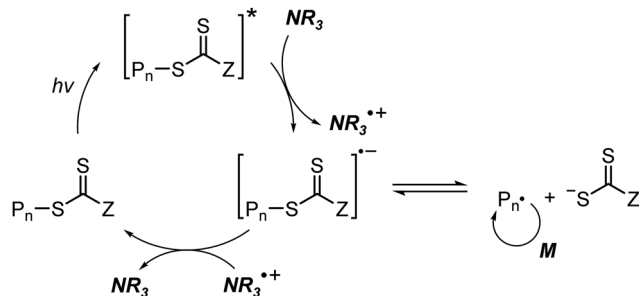
one electron was transmitted from  $PC^{\bullet-}$  to the CTA, generating propagating radical species and a TCT anion through a TCT anionic intermediate. In 2015, Boyer and coworkers proposed PET-RAFT polymerization *via* RQP using a tertiary amine as a sacrificial reducing agent.<sup>66</sup> This protocol provided faster kinetics and enhanced oxygen tolerance without severely sacrificing controllability compared to PET-RAFT polymerization *via* OQP (*i.e.*, in the absence of tertiary amines). Since this report, PET-RAFT polymerization *via* RQP has been widely used when fast polymerization kinetics under ambient conditions, such as polymerization under biorelevant conditions, are required.<sup>67–70</sup>

At approximately the same time in 2015, the use of tertiary amines in photocontrolled RAFT polymerization in the absence of PCs was proposed by Qiao and coworkers (Scheme 4).<sup>71</sup> Herein, the CTA directly absorbed light and tertiary amines, as a catalyst, reduced the excited-state CTA. This electron transfer from the tertiary amine to the excited-state CTA generated the anionic intermediate of the CTA, which then underwent fragmentation to provide a propagating radical and a TCT anion. Qiao and coworkers used 365 nm UV LEDs as the light source, and Konkolewicz and coworkers later demonstrated that the polymerization could proceed properly under visible light



Scheme 3 (a) Mechanism of PET-RAFT polymerization based on photo-induced inner-sphere electron transfer (ISET). (b) Chemical structures of  $[L_2B]^+$  and  $[L_2B]^{\bullet-}$ .<sup>59</sup>





**Scheme 4** Mechanism of tertiary amine-catalyzed generation of the TCT anion in the absence of a PC.

(< 530 nm).<sup>72</sup> It is noted that this mechanism of tertiary amine-catalyzed generation of the TCT anion in the absence of a PC cannot be excluded in PET-RAFT polymerization *via* RQP, which complicates a complete understanding of the polymerization results.

In PET-RAFT polymerization *via* RQP, the polymerization features, such as the rate of polymerization, oxygen tolerance, and controllability, were found to be sensitive to the type<sup>73</sup> and amount of tertiary amines,<sup>71,72</sup> as well as the irradiation wavelength.<sup>57</sup> This sensitivity likely arises because the rate of electron transfer from a tertiary amine to an excited-state PC (or an excited-state CTA) relies on the amount and redox potentials of the amine. Furthermore, one-electron-oxidized tertiary amines may cause various side reactions by providing hydrogen and/or generating reactive  $\alpha$ -amino radical species,<sup>74,75</sup> leading to poor controllability. However, the effects of tertiary amine intermediates on the polymerization have not been thoroughly analyzed and hence, combined efforts involving QC calculations, kinetics simulations, and chromatographic analyses are required.

**2.2.1.3. Energy transfer.** An alternative pathway involves photoinduced energy transfer, in which energy is transferred from an excited-state PC to a CTA, promoting the CTA to an electronically excited state. Then, active propagating radicals are generated *via* homolytic C–S bond cleavage of the excited-state CTA (Scheme 2c). Energy transfer is likely to occur from the  $T_1$  state of the PC to the triplet excited states of the CTA.

Energy transfer is a photophysical process by which energy is transferred from one molecular entity (donor, D) in an excited state to another molecular entity (acceptor, A) to be raised to a higher energy state. The process can be distinguished into three types:<sup>76,77</sup> primitive energy transfer by emission-reabsorption, Förster resonance energy transfer, and Dexter energy transfer. In photocatalysis of organic molecules, Dexter energy transfer is of predominant relevance.<sup>77</sup> As Dexter energy transfer is based on simultaneous electron exchange between D and A, which requires the overlap of the wavefunctions, the energy transfer occurs over very short distances within approximately 10 Å, which approaches the collisional diameter.<sup>78,79</sup> In addition, the electron exchange is governed by the Wigner spin conservation rule and hence, the spin-allowed processes are single-singlet and triplet-triplet energy transfer. Among these, triplet-triplet energy transfer is preferred owing to the typically longer lifetime

of triplet states compared to singlet states. The longer lifetime increases the probability of collisions. Because this is essentially an electron transfer process, the kinetics can be described using Marcus theory.<sup>80</sup> Therefore, the rate of Dexter energy transfer is strongly influenced by the thermodynamic driving force, reorganization energy, and electronic coupling between D and A; nevertheless, in the synthetic community, the thermodynamic driving force (*i.e.*, the energy gap between the lowest triplet state of D and A) is mostly utilized to estimate the energy transfer efficiency because the reorganization energy and electronic coupling are rather difficult to measure. When the thermodynamic driving force is large as in exergonic energy transfer, the energy transfer gets faster close to the diffusion limit. The studies on the energy transfer pathway in PET-RAFT polymerization are discussed in the next section.

#### 2.2.1.4. Mechanistic understanding of PET-RAFT polymerization.

The important debate with respect to the mechanism of PET-RAFT polymerization is how an excited-state PC interacts with a CTA: *via* either electron transfer or energy transfer. Substantial research efforts to answer this difficult question have been continuously made until recently, and these efforts are well summarized in a recent review article by Konkolowicz and coworkers.<sup>48</sup> Smith and coworkers supported an electron transfer mechanism based on calculations of the energetics of selected PCs (ZnTPP and pheophorbide A (PheoA)), various CTAs, and charge-transfer complexes that can be formed between them.<sup>81</sup> Falvey and coworkers also supported an electron transfer mechanism based on studies using laser flash photolysis for (i) triplet-triplet energy transfer between a triplet sensitizer (*e.g.*, anthraquinone, Rose Bengal, and benzophenone) and a CTA, and (ii) subsequent decomposition of an excited-state CTA.<sup>82</sup> Although energy transfer from the sensitizer to the CTA was efficient, decomposition of the CTA was rarely observed, suggesting that radical generation by energy transfer is rather limited compared to radical generation by electron transfer. Very recently, Kwon and coworkers successfully resolved the mechanistic complexity of PET-RAFT polymerization by using appropriately designed Ag<sub>2</sub>S NCs as a PC.<sup>65</sup> Owing to the small bandgap and moderate  $E_{ox}^*$  of the Ag<sub>2</sub>S NCs, PET-RAFT polymerization proceeded solely through electron transfer. Successful polymerization of methyl methacrylate (MMA) in the presence of Ag<sub>2</sub>S NCs confirmed that the electron transfer readily occurs in PET-RAFT polymerization. However, it is noteworthy that the mechanism depends on the type of PCs. In the case of [Ru(bpy)<sub>3</sub>]<sup>2+</sup> and Ir(ppy)<sub>3</sub>, the research groups of Allonas and Boyer<sup>83,84</sup> and Konkolewicz<sup>85</sup> provided evidence for an energy transfer process. Allonas, Boyer, and coworkers calculated the Gibbs free energy change during electron transfer ( $\Delta G_{ET}$ ) and triplet-triplet energy transfer ( $\Delta G_{ETT}$ ) based on the redox potentials and triplet energies of PCs and a series of CTAs obtained from QC calculations and CV measurements.<sup>83,84</sup>  $\Delta G_{ET}$  and  $\Delta G_{ETT}$  were then plotted against the rate constant for quenching ( $k_q$ ) of an excited-state PC obtained from laser flash photolysis experiments. A substantial correlation was observed between  $k_q$  and  $\Delta G_{ETT}$ , whereas no relationship was found between  $k_q$  and  $\Delta G_{ET}$ , suggesting that energy transfer likely





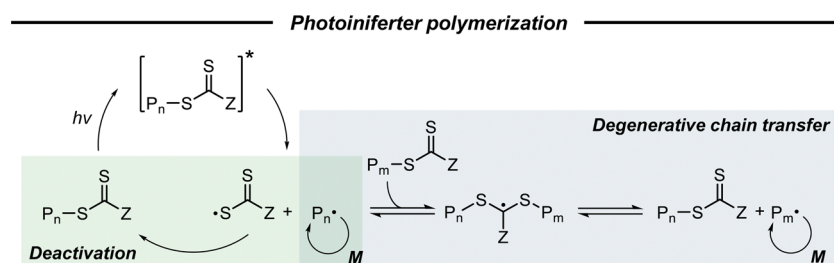
occurs between an excited-state PC and a CTA. Konkolewicz and coworkers also supported an energy transfer mechanism based on the simulation results of polymerization kinetics.<sup>85</sup> Using PET-RAFT polymerization of MA using Ir(ppy)<sub>3</sub> and TTC as a model system, the kinetics data obtained by experiment were compared with the data simulated using kinetic models of possible PET-RAFT mechanisms. Among them, the energy transfer mechanism was found to be the best fit.

In addition to the abovementioned issue, several issues remain unsolved, as introduced by Konkolewicz and coworkers.<sup>48</sup> First, the mechanism of electron transfer during OQP needs to be reconsidered. According to the current mechanism where the TCT anion is mainly involved in the regeneration of the ground-state PC, PET-RAFT polymerization could be significantly retarded or even stop at very low catalytic loading of the PC, as demonstrated by Konkolewicz and coworkers.<sup>85</sup> This finding is inconsistent with the previously reported experimental results. As such, in-depth studies are required to determine which pathways are involved in the reduction of oxidized cationic PC intermediates. Second, more in-depth understanding of the overall picture of what drives electron or energy transfer is required. The experimental results thus far suggest that the mechanism is dependent on the reaction system composition (*i.e.*, combination of PC, CTA, and monomer), whereas the exact mechanistic background remains unknown. Third, the fate of TCT radicals, which can be generated in PET-RAFT polymerization *via* energy transfer or photoiniferter polymerization, needs to be understood better. Herein, excessive TCT radicals could be accumulated by the termination of propagating radical species, as observed for TCT radicals generated by electron transfer, consequently leading to significant rate retardation. However, this retardation was not observed in the experimental studies and could be related to the formation of disulfide compounds that have not been much investigated. Fourth, the process of C–S bond dissociation in the energy transfer process remains unclear. As studied by Falvey and coworkers, C–S bond dissociation of the CTA in the triplet excited state was not sufficiently efficient to drive polymerization.<sup>82</sup> However, the study was performed in the absence of a monomer and thus, additional experiments in the presence of a monomer are necessary to draw a clear conclusion. Last, the direct spectroscopic observation of essential intermediates such as one-electron-oxidized/reduced PC, TCT anions, and TCT radicals would help to unambiguously identify the underlying mechanisms.

## 2.2.2. Photoiniferter polymerization

**2.2.2.1. Basic mechanism.** Photoiniferter polymerization under UV light irradiation, firstly proposed by Otsu and coworkers in 1982 as a type of RDRP,<sup>39,86</sup> has garnered renewed interest since Boyer,<sup>32</sup> Qiao,<sup>33</sup> and coworkers separately expanded the energy source of polymerization to visible light. Herein, a TCT-based CTA is a key agent that simultaneously acts as an initiator, a transfer agent, and a reversible terminator (*ini-fer-ter*), thereby eliminating the need for a PC or an exogenous initiator. As depicted in Scheme 5, the CTA directly absorbs light to become an excited state, which is followed by the homolysis of the C–S bond to produce an active initiating/propagating radical and a persistent TCT radical.<sup>56</sup> The propagating radicals can participate in degenerative chain transfer, a key mechanistic aspect of RAFT polymerization, and the TCT radical can deactivate active radical species in a reversible fashion as seen in ATRP. As this process requires the absorption of light by the CTA, the irradiation wavelength for photoiniferter polymerization is quite limited in contrast to PET-RAFT polymerization.

**2.2.2.2. Mechanistic understanding of photoiniferter polymerization.** The most essential issue in photoiniferter polymerization is to clearly understand the mechanism of photolysis of the C–S bond, an important process that determines the concentrations of radicals and CTAs during polymerization. Recently, Konkolewicz and coworkers reported that the rate of photoiniferter polymerization of MMA was significantly affected by the Z group of DTBs.<sup>87</sup> The rate of polymerization was nicely correlated with the redox potentials of CTAs, implying that the homolysis of the C–S bond is closely related to the electronic properties of CTAs. Falvey and coworkers suggested that higher singlet excited states such as S<sub>2</sub> states are involved more in the photolysis than S<sub>1</sub> or T<sub>1</sub> states based on energetics considerations.<sup>82</sup> Although these studies provided useful mechanistic insights into photolysis of the C–S bond, a precise understanding of the entire process of photoiniferter polymerization is still lacking and is expected to be provided through advanced QC calculations combined with well-designed experiments. For example, Kwon, Min, and coworkers very recently proposed that S<sub>1</sub>/S<sub>0</sub> conical intersection (CI) acted as an activation barrier for photolysis of the C–S bond.<sup>88</sup> CDTPA under 515 nm irradiation (10 mW cm<sup>−2</sup>) led to controlled and quantitative polymerization of MMA, whereas polymerization of MA provided adducts of (MA)<sub>n</sub>–CDTPA rather than polymers. QC calculations of reaction intermediates proposed that relative



Scheme 5 Mechanism of photoiniferter polymerization.



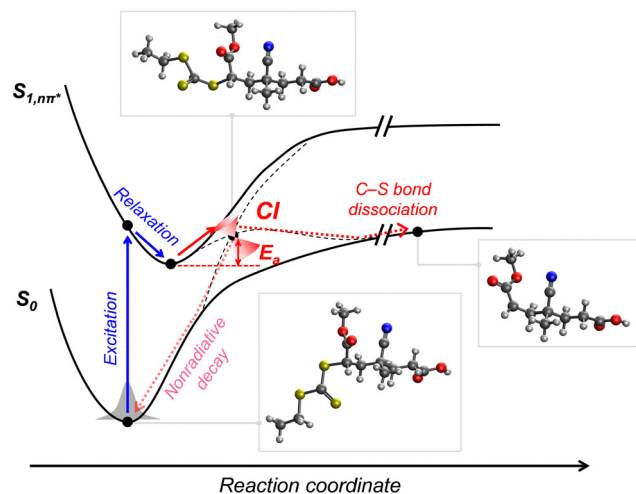


Fig. 4 Pathway for photolysis of the C-S bond in MA-CDTPA proposed by QC calculations.<sup>88</sup>

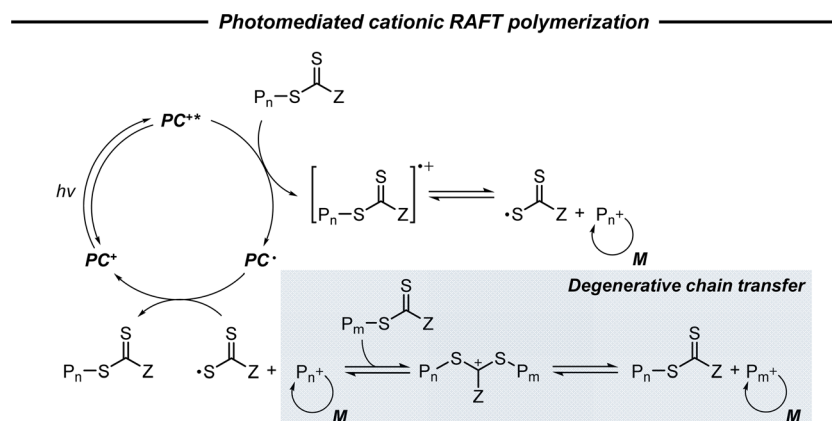
energies at the adiabatic  $S_1$  state, CI, and after dissociation were critical for the observed monomer-CTA selectivity (Fig. 4). Energy profiles for the process from Frank-Condon excitation, structural relaxation, and CI were similar for adducts of both monomers, whereas energy profiles for the process from CI to bond dissociation were more favorable in MMA-CDTPA due to the large stabilization energy of generated radicals. Other possible processes from CI include nonradiative decay channels, hindering the C-S bond photolysis and subsequent polymerization.

Next, two different mechanisms (*i.e.*, degenerative chain transfer and reversible deactivation) can affect the control of RAFT polymerization, depending on the type of CTA employed in the reaction. These two mechanisms could jointly operate in the case of xanthate (with a low transfer constant).<sup>56</sup> In contrast, in the other study using TTC (with a higher transfer constant), preliminary calculations suggested that the reversible deactivation did not contribute primarily to the control over polymerization.<sup>89</sup> Quantitative analysis of the contribution of two mechanisms needs to be provided by further investigation using experimental and theoretical studies.

Lastly, as in PET-RAFT polymerization, the fates of the CTA and the corresponding TCT radical need to be clarified. Although the photodegradation of TCT groups under UV light irradiation with high energy has been reported,<sup>19,26</sup> the case under visible-light irradiation with low energy has not been observed.

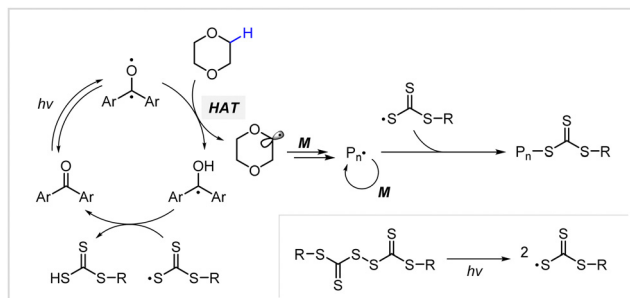
### 2.2.3. Photomediated cationic RAFT polymerization and others

**2.2.3.1. Photomediated cationic RAFT polymerization.** Cationic RAFT polymerization was firstly reported by the research group of Kamigato<sup>41</sup> and Sugihara.<sup>42</sup> Herein, in the presence of protonic acid initiators to protonate a CTA, the fragmentation of the CTA cation generated carbocations as propagating species, which were polymerized in a controlled fashion *via* degenerative chain transfer. Fors and coworkers then developed a photomediated version of cationic RAFT polymerization by introducing highly oxidizing 2,4,6-tris(*p*-methoxyphenyl)pyrylium tetrafluoroborate as a PC to oxidize a CTA and generate a carbocation (Scheme 6).<sup>43</sup> One-electron oxidation of the CTA by the excited-state PC upon irradiation was followed by mesolytic cleavage of the resulting CTA radical cation to yield the CTA radical and carbocation as propagating intermediates. Similar to conventional cationic RAFT polymerization, the polymerization was controlled *via* degenerative chain transfer. The use of a PC provided additional regulation over the propagation step by photo-reversible generation of the carbocation. Reduction of the CTA radical by the one-electron-reduced PC generated the CTA anion and PC, which capped the carbocation chain-end and closed the catalytic cycle. Therefore, the photocontrolled behavior of polymerization (*i.e.*, the generation of the propagating carbocation and thus polymerization only proceed under light irradiation) could only be provided by a PC that possessed proper  $E_{ox}^*$  and  $E_{red}^0$  for favored one-electron oxidation of the CTA and reduction of the CTA radical, respectively.<sup>90</sup> Based on the investigation of the detailed mechanism using selected PCs and CTAs, Fors and coworkers concluded that in the case of pyrylium derivatives, a singlet excited state might involve electron transfer as the low fluorescence quantum yield ( $\Phi_{FL}$ ) of the PC led to a lower polymerization rate. The concern over the direct oxidation of the monomer instead of the



Scheme 6 Mechanism of photomediated cationic RAFT polymerization.





Scheme 7 Mechanism of hydrogen atom transfer (HAT)-mediated photomediated cationic RAFT polymerization.<sup>60</sup>

CTA by the excited-state PC was also resolved by Stern–Volmer analysis and CV measurements. Both the CTA and isobutyl vinyl ether (IBVE) monomer could be oxidized, but it was revealed that the oxidation of the CTA was favored by lower  $E_{\text{ox}}^0$ . The bimolecular quenching constant between the excited-state PC and CTA determined by Stern–Volmer analysis was two orders of magnitude higher than that between the PC and IBVE. Lastly,  $E_{\text{red}}^0$  of the PC was important for efficient capping of the propagating chain-end and deactivation of polymerization, providing perfect temporal control.

**2.2.3.2. Hydrogen atom transfer (HAT)-mediated photomediated RAFT polymerization.** Fors and coworkers introduced a HAT manifold into photomediated RAFT polymerization.<sup>60</sup> Herein, a benzophenone analogue capable of Norrish type II reaction was used as a PC and TTC-derived disulfide was used as a CTA precursor, unlike in conventional PET-RAFT polymerization. Under irradiation using a compact fluorescent lamp (CFL), the PC absorbed light to generate a PC intermediate with diradical character (Scheme 7). This PC intermediate abstracted the C–H bond of the substrate through hydrogen abstraction, and the resulting radical intermediates of the substrate initiated the polymerization. On the other hand, the disulfide generated two TCT radicals through S–S bond homolysis. One TCT radical was combined with the propagating radical to generate a macro-CTA, whereas the other TCT radical reacted with the PC intermediate, ketyl radical derived from benzophenone, to generate trithiocarbonic acid and regenerate the PC. As stated by the authors, this method will be useful to graft CTA moieties into hydric C–H bonds of substrates (e.g., biomolecules and backbone of commodity polymers) for subsequent polymerization.

### 3. Distinct features

In addition to the use of green and abundant visible light as an energy source, the distinct features of visible-light-driven RAFT polymerization endow the reaction system with controllability and the synthesized polymers with structural diversity, functionality, and excellent livingness, which otherwise are not realizable *via* conventional thermally initiated reactions. These features are attributed to the abovementioned mechanisms and can be primarily categorized into (i) spatiotemporal control,

(ii) selectivity, (iii) orthogonality, and (iv) oxygen tolerance. It is noted that PET-RAFT polymerization distinctly demonstrates all four features. As active species are generated by light irradiation, spatiotemporal control is commonly achieved regardless of the polymerization mechanism (Section 3.1). Except for photomediated cationic RAFT polymerization, in PET-RAFT and photoiniferter polymerizations, active species are radicals so that the reactions can simultaneously occur with other reactions possessing different (such as ionic) intermediates and can be orthogonally controlled by turning the light on/off (Section 3.3). Meanwhile, the other two features (*i.e.*, selectivity and oxygen tolerance) have mainly been examined for PET-RAFT polymerization and still remain elusive for other methods.

#### 3.1. Spatiotemporal control

Every photomediated RAFT polymerization operates by the absorption of light by either a PC or a CTA, and is therefore inherently a spatiotemporally controlled process that only occurs where and when the light is irradiated. Perfect temporal control directs the mechanism of the reaction toward a photo-controlled process necessitating the use of light and compounds that appropriately absorb light and play the role. For example, imperfect control or increase in monomer conversion even without light irradiation, which has been observed in some photomediated cationic RAFT polymerizations, has been ascribed to the decomposition of the PC or slow deactivation of the CTA owing to improper balance between ground- and excited-state redox potentials of the PC and CTA.<sup>43,90–92</sup> Slow deactivation of the CTA results in longer lifetime of active propagating species such that these species remain after the cessation of irradiation and consume monomers. This loss of control caused by the remaining radicals, however, can be utilized to induce latent RAFT polymerization in the dark using the energy stored during precedent irradiation.<sup>93</sup> Here, eosin Y (EY)-mediated photoinduced conversion of triplet oxygen into singlet oxygen which was then reduced by ascorbic acid in the dark generated the initiating hydroxyl radical.

On the other hand, PET-RAFT polymerization can be temporally switched by other stimuli (e.g., temperature, pH, atmosphere, external magnetic field, and chemical reagents) in combination with light under which the photocatalytic activity of the PC is reversibly controllable (Fig. 5). The listed examples of dual-gated polymerizations have significant prospects for industrial applications as they offer additional means of control other than light and/or easy separation of PCs from the polymerization mixture for reuse.

Johnson and coworkers embedded 10-phenylphenothiazine (PTH) in a poly(*N*-isopropylacrylamide (NIPAm))-based gel in which at temperatures above the lower critical solution temperature (LCST), the PC could not be accessed by light and other reagents, and consequently the polymerization could not proceed (Fig. 5a).<sup>94</sup> Polymerization only proceeded at temperatures below the LCST and under light irradiation. In contrast, in nanocomposites composed of cross-linked hyperbranched polyglycerol, polyfluorene backbones decorated with poly(NIPAm)





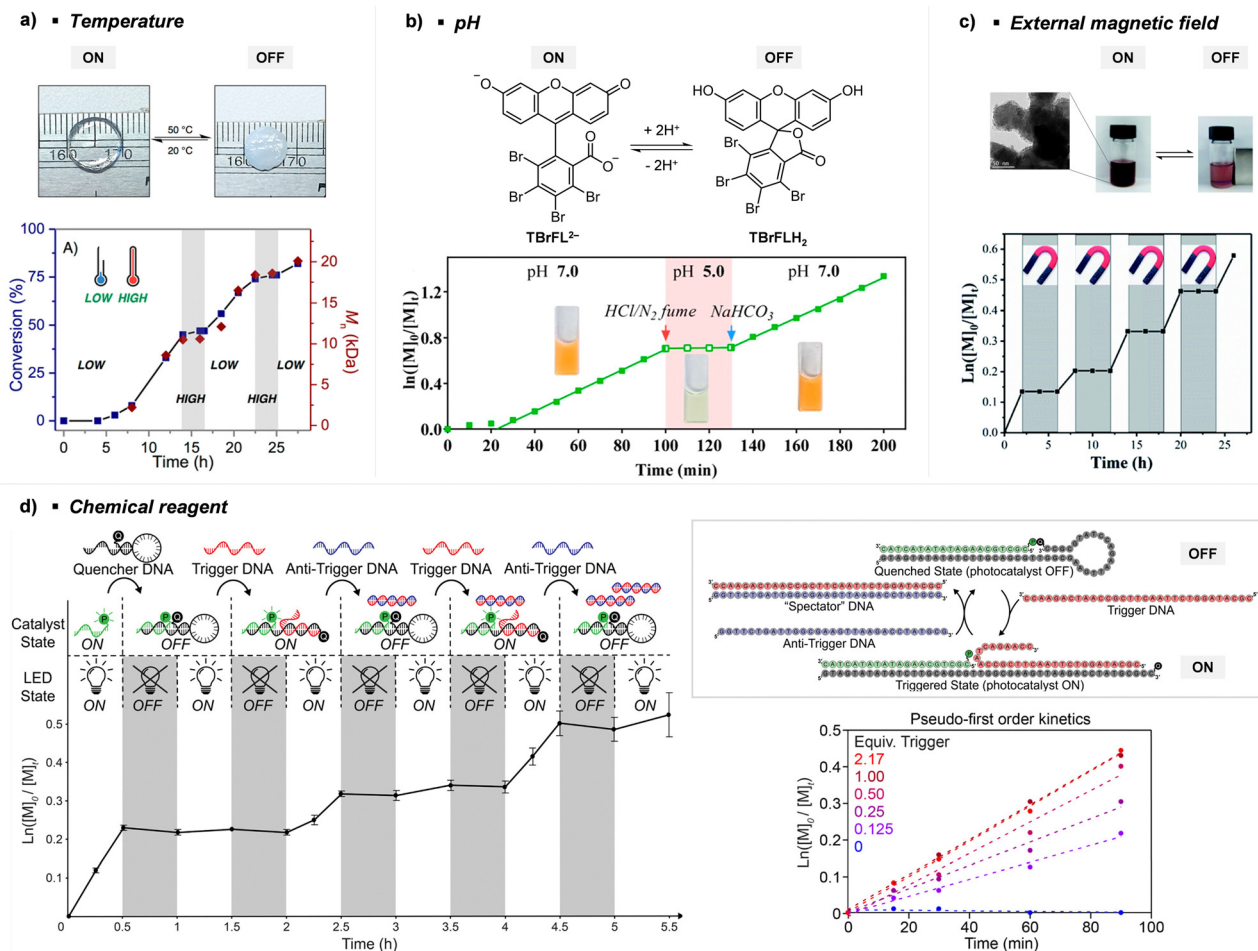


Fig. 5 Temporal control of PET-RAFT polymerization by various stimuli other than light: (a) heat, (b) pH, (c) external magnetic field, and (d) chemical reagents. Adapted with permission from (a) ref. 94 (Copyright 2017 American Chemical Society), (b) ref. 96 (Copyright 2019 American Chemical Society), (c) ref. 103 (Copyright 2020 The Royal Society of Chemistry), and (d) ref. 104 (Copyright 2023 American Chemical Society).

brushes, and  $\text{Ru}(\text{bpy})_3\text{Cl}_2$ , heat-driven shrinkage of poly(NIPAm) chains generated open pores for reagents to enter and polymerization proceeded.<sup>95</sup>

Boyer and coworkers discovered a pH-switchable xanthene-based PC TBrFL (Fig. 5b).<sup>96</sup> Because of the pH-responsiveness of xanthene dyes, at pH = 5, TBrFL became colorless and inactive to catalyze PET-RAFT polymerization, whereas at pH = 7, the original visible-light absorption property was restored to turn on the reaction. pH was lowered by adding gaseous  $\text{HCl/N}_2$  or  $\text{CO}_2$  and was recovered by  $\text{NaHCO}_3$  or  $\text{N}_2$ , respectively. This pH-responsive photocatalytic performance of xanthene dyes was retained in heterogeneous PCs where Erythrosin B (EB) and Rose Bengal were conjugated to porous polymers.<sup>97</sup>  $\text{ZnTPPS}_4^-$  demonstrated pH-dependent polymerization kinetics.<sup>98</sup> The polymerization kinetics were retarded by lowering the pH of the reaction mixture from 8.6 to 3.5. This was presumably because higher concentration of the hydroxide ion at higher pH weakened the coordination of the zinc core of  $\text{ZnTPPS}_4^-$  with the CTA or monomer and promoted the absorption of light by  $\text{ZnTPPS}_4^-$  and subsequent polymerization, as evidenced by the higher molar absorption coefficient of the reaction mixture at irradiation wavelength. In contrast,

$\text{ZnOETPP}$  exceptionally utilized oxygen for the polymerization process so that polymerization did not occur in the presence of  $\text{CO}_2$  or  $\text{N}_2$ .<sup>99</sup> This role of oxygen contradicted its conventionally recognized role of inhibiting polymerization by scavenging the propagating radicals (for a detailed explanation, please see Section 3.4). Copolymerization of macrocyclic allylic sulfones with acrylate and acrylamide monomers was reversibly switched by alternate introduction of Ar and  $\text{SO}_2$ .<sup>100</sup> During radical ring-opening cascade polymerization, macrocyclic allylic sulfones release  $\text{SO}_2$  and the resulting secondary alkyl radicals participate in propagation. However, the gradually accumulated  $\text{SO}_2$  in the reaction system recombined with the alkyl propagating radicals and inhibited polymerization in the late stages particularly at low reaction temperature. Density functional theory (DFT) calculations and electron paramagnetic resonance (EPR) spectroscopy evidenced that Gibbs free energy change upon extrusion and recombination of  $\text{SO}_2$  from the monomer was relatively small such that  $\text{SO}_2$  could negatively affect the polymerization behavior. Thus, the introduction of Ar re-initiated the  $\text{SO}_2$ -inhibited polymerization, whereas the introduction of exogenous  $\text{SO}_2$  switched off the polymerization.



The hybrid nanocomposites of magnetic  $\text{Fe}_3\text{O}_4$ , silica, and PCs ( $\text{Ir}(\text{ppy})_3$ <sup>101</sup> and  $\text{ZnTPP}$ <sup>102</sup>) reported by Cai, Zhang, and coworkers or  $\gamma\text{-Fe}_2\text{O}_3$  nanoparticles (NPs) doped with carbon dots reported by Qiao, Pang, and coworkers<sup>103</sup> were responsive to an external magnetic field. Upon applying a magnetic field, these nanohybrid PCs exhibited agglomeration and could not catalyze polymerization. This was attributed to the reduced visible-light absorption and limited access and electron transfer between PCs (bound to the surface of the nanocomposites) and CTA (Fig. 5c).

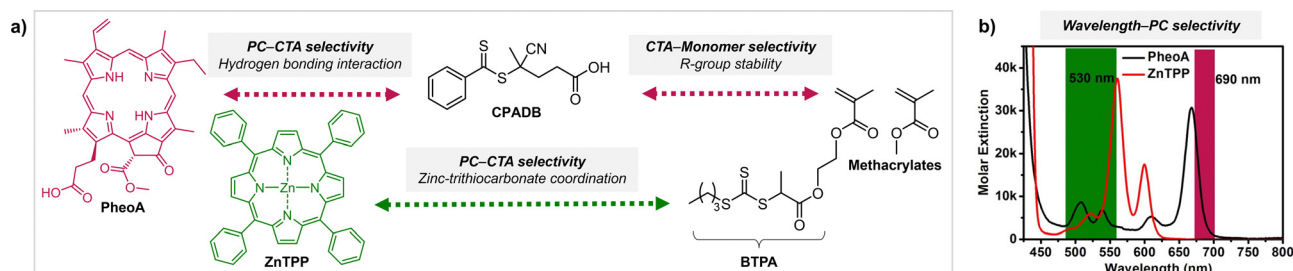
Lastly, Martell and coworkers conjugated DNA aptamers and a quencher dye with EY to switch on the photocatalytic activity of EY by adding chemical reagents that could be hybridized with the DNA (Fig. 5d).<sup>104</sup> As absorption of the quencher dye overlaps with emission of EY, fluorescence and photocatalytic activity of EY were switched off when the quencher dye and EY were in proximity through static quenching and Förster resonance energy transfer (FRET). The added chemical reagent non-covalently hybridized with the DNA to induce a conformational change, remove the proximity between the quencher dye and EY, and switch on the photocatalytic activity of EY. In particular, when trigger DNA was used as the chemical reagent, anti-trigger DNA with complementary sequences could inactivate the trigger DNA resulting in double-stranded spectator-DNA and a photocatalytically inactivate PC. Therefore, the activity of the PC could be reversibly switched, and the polymerization rate could be modulated by the amount of trigger-DNA relative to that of quencher-DNA. As sequences and secondary structures of DNA aptamers can be designed to specifically fit diverse trigger molecules such as glucose, hydrocortisone, and zinc ions, these switchable DNA-PC conjugates were expected to be expanded to various PCs and chemical reagents, only if appropriate pair of PC and quencher dye possessing overlapping emission and absorption spectra could be identified.

### 3.2. Selectivity

For successful photocontrolled RAFT polymerization, effective photolysis of the CTA (activation), insertion of the monomer, and deactivation of the CTA are required. It has been shown that each step is highly selective toward reagents and reaction conditions. First of all, the irradiation wavelength should match the absorption profile of either PC or CTA (depending on the type of polymerization) for their excitation. In PET-RAFT

polymerization the (de)activation of the CTA by the PC at the initiation stage and that of the CTA with monomers inserted at the propagation stage are mainly governed by thermodynamic constraints where the reactivity of the excited-state PC is determined by the energy absorbed at the irradiation wavelength. In addition to irradiation at the appropriate wavelength, selectivity of the PC toward the CTA and selective insertion of the monomer into the CTA have been observed. These selectivity issues can be leveraged to prepare polymers with desired sequences and complex architectures.

**3.2.1. Selectivity of the PC toward the CTA.** After successful excitation of the PC, selectivity in the transfer of electron or energy from the excited-state PC to the CTA arises from selective interaction between the PC and the CTA. Specific coordination of zinc of  $\text{ZnTPP}$  to a TTC resulted in photoinduced reduction of BTPA (a TTC) than CPADB (a DTB) despite the lower  $E_{\text{red}}^0$  of BTPA.<sup>105</sup> Upon changing the solvent from dimethyl sulfoxide (DMSO) to *N,N*-dimethylformamide (DMF) which competes with BTPA for the coordination, the coordination between  $\text{ZnTPP}$  and BTPA was reduced to retard the polymerization. On the other hand, interaction of CPADB with PheoA probably due to hydrogen bonding between its acid group and pyrrole of PheoA was evidenced by NMR and UV/Vis spectroscopy.<sup>106</sup> These selective interactions were considered to enhance electron transfer by the proximity effect. Later, Smith, Seal, and coworkers theoretically investigated these experimentally observed selectivity trends based on QC calculations using DMSO as a model solvent.<sup>81</sup> The authors ruled out the energy transfer pathway and considered that electron/charge transfer from the  $S_1$  state of the PC to CTA was the crucial step for CTA activation, which would be facilitated by the favored pre-complexation of the PC and CTA. From the analysis of the excited-state molecular orbitals of PC-CTA complexes, the selectivity of  $\text{ZnTPP}$  toward TTC and that of PheoA toward CPADB were indicated by the lowest energy gap between the initial optically excited state and the charge-transfer state along with the facilitated perturbative coupling between these two states, which enhanced electron transfer. Combined with the intrinsic monomer compatibility of the given CTA,<sup>37</sup> careful design of the reaction system using a mixture of multiple pairs of PC, CTA, and monomer that could be selectively activated at distinct irradiation wavelengths (Scheme 8) enabled the facile



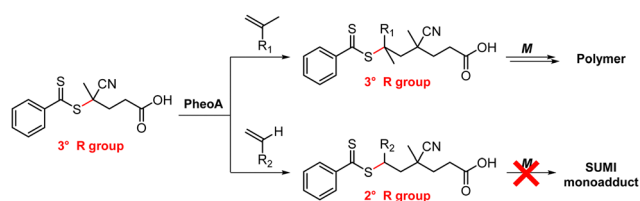
**Scheme 8** (a) Selectivity issues in PET-RAFT polymerization from a reaction mixture of two PCs (PheoA and  $\text{ZnTPP}$ ), two CTAs (CPADB and BTPA), and methacrylate monomers. The two PCs can be selectively activated at different wavelengths as per (b) UV-vis absorption profiles. Adapted with permission from (b) ref. 106 (Copyright 2016 American Chemical Society).



synthesis of well-defined graft copolymers,<sup>106</sup> as discussed in Section 4.3.2. For selective activation, irradiation wavelengths at which the absorption profiles of two PCs do not overlap are required. Selective activation of a certain PC and concomitant selective polymerization of the monomer that is compatible with a certain CTA can be achieved even in a mixture of all reagents. However, it is noted that the time of monomer addition should be carefully considered, as certain monomers, once reacted, block the successive insertion of the other type of monomers, leading to failed polymerization.

### 3.2.2. Selective insertion of the monomer into the CTA.

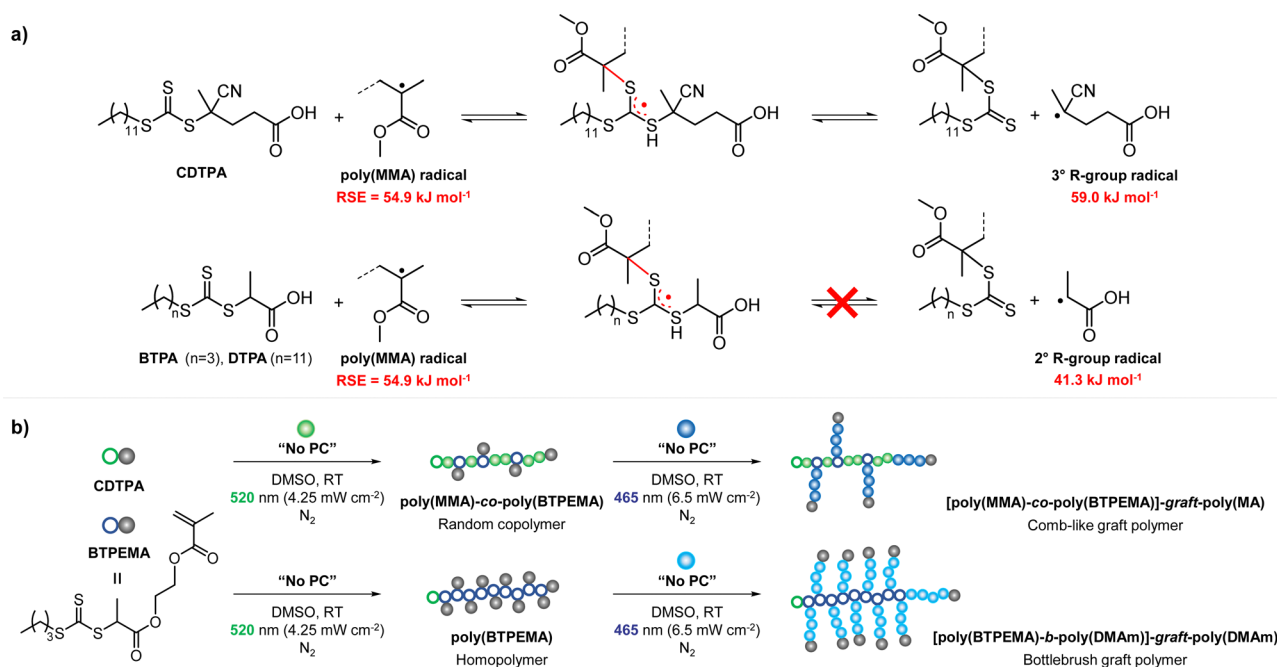
Such blocking of further propagation prevents the subsequent incorporation of upcoming monomers into the CTA, and thus is called single unit monomer insertion (SUMI). For successive polymerization, fragmentation of the propagating radical from the RAFT intermediate and additional insertion of the monomer are required. For example, after the insertion of MA into CPADB, the tertiary carbon radical of the R group of CPADB transformed into a less stable secondary radical that could no longer be activated by PheoA, whereas MMA with a tertiary carbon radical had no problem in polymerization.<sup>106</sup>



Scheme 9 Monomer-dependent selective photoactivation of CPADB.<sup>106</sup>

PheoA-catalyzed PET-RAFT polymerization for 20 hours of different monomers (typically 20 equivalents to CPADB) that yielded propagating radicals with secondary radicals, including styrene, acrylates, and acrylamides, other than methacrylates, all provided the same results (Scheme 9).<sup>106</sup> In contrast, AIBN-initiated RAFT polymerization afforded oligomeric products under otherwise identical reaction conditions, which was consistent with the previous studies which reported that AIBN was not a suitable initiator due to the possible formation of initiator-derived byproducts.<sup>107</sup> Furthermore, a very short reaction time was essential to prevent multiple insertions of monomers and to ensure high end-group fidelity if a certain number of SUMI reactions of different monomers had to be repeated.<sup>108</sup> Therefore, the unique selectivity of PET-RAFT and photoiniferter polymerizations even with mild reaction conditions and the absence of an exogenous initiator successfully afforded polymers with controlled monomer sequences of precisely positioned functionalities *via* SUMI.<sup>109</sup>

CTAs possessing the same Z group but different R groups can also be selectively fragmented. Matyjaszewski and coworkers in collaboration with Boyer reported that during photoiniferter polymerization of MMA in the presence of CDTPA and BTPA, only CDTPA was consumed for polymerization.<sup>110</sup> This was because the photolysis of CDTPA was favored owing to the higher stability and radical stabilization energy (RSE) of the tertiary R group, whereas BTPA with the secondary R group did not undergo fragmentation or participate in chain transfer with the poly(MMA) radical (Scheme 10a). The retarded polymerization rate upon the addition of an excess amount of BTPA or DTPA evidenced that both CTAs participated in the formation of the intermediate adduct radical, whereas only the adduct with CDTPA resulted in the fragmentation and release of the R group



Scheme 10 (a) Selective fragmentation of CTAs after the addition of the poly(MMA) radical. (b) Stepwise synthesis of comb-like and bottlebrush polymers *via* selective fragmentation of CTAs under irradiation at different wavelengths.<sup>110</sup>



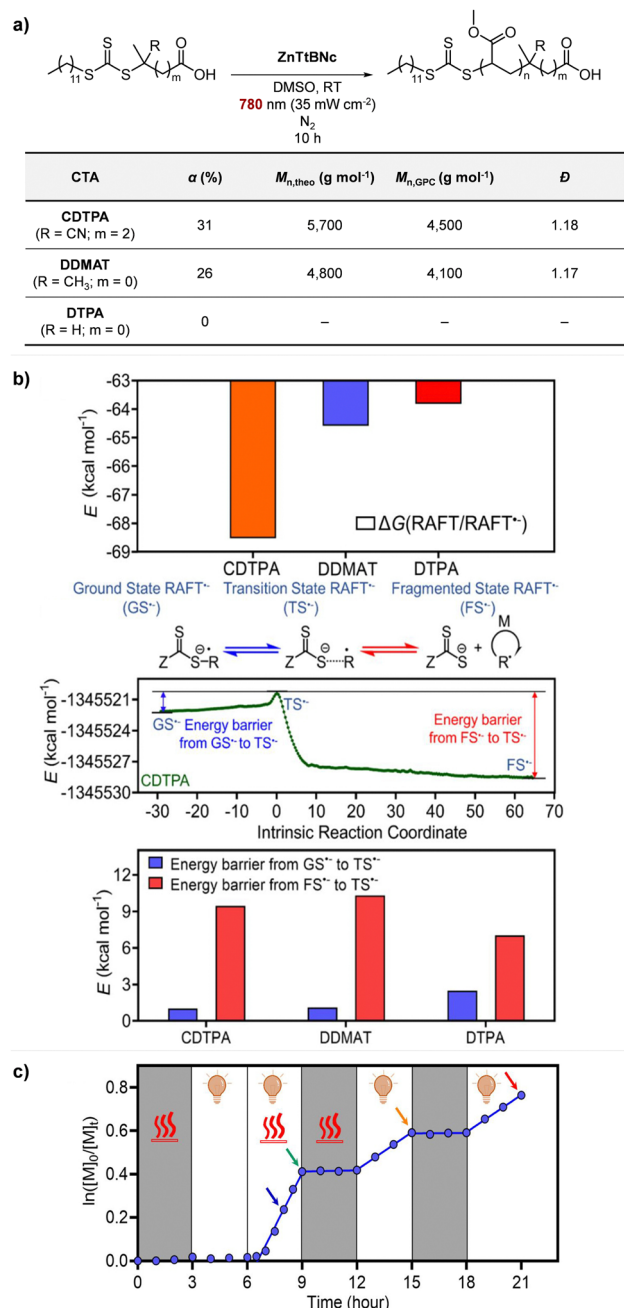


for propagation. By changing the irradiation wavelength from green (520 nm, 4.25 mW cm<sup>-2</sup>) to blue (465 nm, 6.5 mW cm<sup>-2</sup>), the remaining intact BTPA could be consumed for polymerization of MA or *N,N*-dimethyl acrylamide (DMAM) in which both the R group of the CTA and the monomer generated secondary R groups (Scheme 10b).

As it is the change in C–S bond stability and balance among the various possible reactions (*e.g.*, chain transfer, dissociation, propagation, and recombination) within the RAFT equilibrium that dictate the selectivity in the activation of the CTA to add a monomer, the existence of a PC is not necessary for the selective activation of the CTA and subsequent polymerization; nevertheless, the PC facilitates the reaction or allows upscale of the reaction system because of oxygen tolerance. For further discussion on SUMI and utilization of the unique selectivity of photocontrolled RAFT polymerization to confer polymers with complex architectures, please see Sections 4.3.1.2 and 4.3.2, respectively.

**3.2.3. Overcoming the selectivity issue by heat.** Very recently, Boyer, Liu, and coworkers reported that the selectivity issue could be overcome by heat.<sup>64</sup> In PET-RAFT polymerization of (meth)acrylates under NIR light irradiation (780 nm), MNCs selectively activated TTCs with tertiary R groups over TTCs with secondary R groups (Fig. 6a). Computational chemistry suggested that the oxidation capabilities of MNCs in their excited states were too low to transfer an electron to DTPA, a model CTA with the secondary R group. The leaving ability of the R group depends on bond dissociation energy and RSE. From intrinsic reaction coordinate (IRC) simulation to compare the energy barrier between either before or after the fragmentation of the CTA radical anion, and the transition state, DTPA, compared to CDTPA and DDMAT with the tertiary R group, was unlikely to favor the formation of the transition state and thus the fragmentation to initiate the polymerization (Fig. 6b). In contrast, poly(MA)<sub>59</sub>-DTPA prepared by thermally initiated RAFT polymerization successfully underwent PET-RAFT polymerization along with a decrease in the Gibbs free energy of ~1 kcal mol<sup>-1</sup> during one-electron reduction of the CTA, as the inserted monomer units did decrease the effect of the original R group. The authors further postulated that this energy barrier could be overcome by increasing the reaction temperature by 15 °C using a hot plate. The MNC-catalyzed PET-RAFT polymerization of MA from DTPA, which could not be realized, was achieved only after the heat-promoted photoactivation of DTPA in the initial state (Fig. 6c). It is noted that the revealed mechanistic origin of the unique selectivity of MNCs to a certain CTA would help overcome the abovementioned energy barrier, and consequently expand the applicability of PCs *via* the combined use of light and thermal energy.

**3.2.4. Overcoming the selectivity issue by oxygen.** Likewise, the energy barrier and thermodynamic constraints within the photocatalytic cycle limit the applicability of a certain PC for successful polymerization. PCs that absorb at long wavelengths particularly suffer from weak excited-state redox properties which thermodynamically restricts PET-RAFT polymerization *via* OQP or RQP. Therefore, it has been difficult to find



**Fig. 6** (a) PET-RAFT polymerization of MA. (b) Comparison of Gibbs free energy change, reaction path calculated by the IRC method, and energy barriers in CTA<sup>-</sup> fragmentation. (c) Heat-assisted photoactivation (at 52 °C) of DTPA for PET-RAFT polymerization of MA. Adapted with permission from ref. 64 (Copyright 2022 American Chemical Society).

appropriate PC candidates for polymerization under NIR light irradiation. In this regard, Boyer, Liu, and coworkers proposed a new oxygen-mediated pathway for PET-RAFT polymerization using NIR-light-absorbing (metallo)porphyrin and phthalocyanines as a PC, where the PC, oxygen, and triethylamine (TEA) synergistically provide thermodynamically favored electron transfer for one-electron-reduction of the CTA and subsequent polymerization.<sup>111</sup> This necessity of oxygen for successful and



well-controlled polymerization was contradictory to the conventional role of oxygen in inhibiting the reaction (for a detailed explanation, please see Section 3.4.3).

### 3.3. Orthogonality

Multiple reactions that can occur either individually or simultaneously in one pot without interfering with each other are said to be orthogonal. For example, in terms of the type of reactive species, PET-RAFT or photoiniferter polymerization with radical intermediates is orthogonal to the reactions, including (photomediated) cationic RAFT or anionic or cationic ring-opening polymerization (ROP), involving ionic intermediates. In terms of the energy source, light can be turned on and off without interrupting other stimuli. Moreover, light at certain wavelengths that can selectively activate one of the several combined organic photochemical reactions has paved the way for efficient synthesis of advanced functional materials through, for example, formation and post-modification of the polymer network and programmed patterning of given surfaces.<sup>112–114</sup> Therefore, researchers either orthogonally turned on and off the photomediated reversible (de)activation of the radicals produced from the PC and/or CTA to ionic polymerizations mediated by other stimuli (e.g., heat,<sup>115</sup> electricity,<sup>116,117</sup> and the presence of specific reagents<sup>118–122</sup>) or selectively activated two photomediated polymerizations *via* irradiation at disparate wavelengths.<sup>123–126</sup>

This orthogonality that allows on-demand control of each polymerization system has been applied to the one-pot synthesis of polymers with complex architectures and compositions as discussed in Sections 4.3.1.1 and 4.3.2. By combining two orthogonal polymerizations, the scope of the monomers incorporated along the single backbone has widened. The microstructure of multiblock copolymers (e.g., order, length, and number of blocks) could also be facily manipulated by tuning the order and length of the applied external stimuli, and the number of switching between two polymerizations.

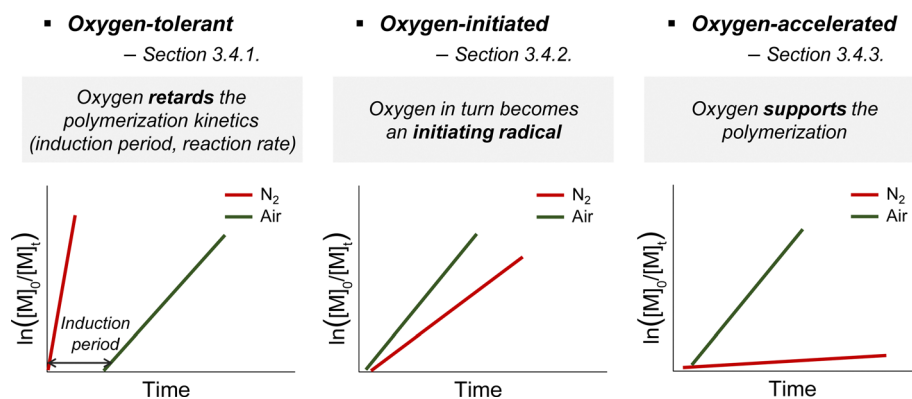
### 3.4. Oxygen tolerance

Due to its radical scavenging effect, oxygen is detrimental to radical polymerization and thus needs to be removed before the reaction. To conduct the reaction in the presence of oxygen,

oxygen tolerance is of significant interest as the degassing process is time-consuming and limits the practicability of polymerization from both biological and industrial perspectives. Among the various photomediated RAFT polymerizations discussed herein, oxygen tolerance of PET-RAFT polymerization has been extensively recognized,<sup>49,127</sup> as compared to the cases of photoiniferter and photomediated cationic RAFT polymerizations. It is because inactivation of oxygen occurs *via* a photoinduced electron or energy transfer mechanism in the presence of the PC and/or any additives that play a supporting role (Section 3.4.1.1). In contrast, photoiniferter polymerization involving direct photolysis of the CTA lacks the ability to consume oxygen, and thus is intrinsically sensitive to oxygen. Therefore, in the reported studies, alternative approaches such as not stirring the reaction mixture or use of solvent with high viscosity and low oxygen solubility, to physically block the diffusion of oxygen into the polymerization mixture, or additives were employed. Every reported photomediated cationic RAFT polymerization has been performed in deoxygenated media, providing no hint towards oxygen tolerance of the reaction system. As cationic reaction intermediates are not affected by radical-scavenging oxygen, cationic polymerization is known to be insensitive to oxygen;<sup>22,128</sup> nevertheless, the impact of oxygen on photocatalytic systems needs to be investigated.

Meanwhile, in some cases, oxygen could in turn be transformed into an initiating source or even facilitate the activation of the CTA, which contradicts its known inhibitory role. These examples of oxygen-initiated or -accelerated polymerizations are discussed in Section 3.4.2. This section describes the three categories of oxygen tolerance reported to date in various polymerization reactions (Scheme 11).

It should be noted that, regardless of the type of mechanism, ‘the presence of oxygen’ can refer to the reaction being performed in either a completely ‘open-to-air’, ‘sealed but not degassed’ container or other containers where the volume of the remaining head space substantially affects the amount of oxygen and controllability of polymerization. In any case, oxygen tolerance has extended the applications of photocontrolled RAFT polymerization to 3D/4D printing or surface functionalization of given surfaces or biomolecules in which the deoxygenation



**Scheme 11** Three categories of oxygen tolerance. Schematic representation of the kinetic plot of  $\ln([M]_0/[M]_t)$  vs. reaction time in (a) oxygen-tolerant, (b) oxygen-initiated, and (c) oxygen-accelerated PET-RAFT polymerizations.



process can be time-consuming, cumbersome, or harsh to the substrate.

### 3.4.1. Oxygen-tolerant polymerization

**3.4.1.1. PET-RAFT polymerization.** Although the consumption of oxygen accompanies the induction period or slower polymerization kinetics as compared to the case in the absence of oxygen, the polymerization reaction would eventually proceed. Thus, well-defined polymers with high end-group fidelity in the presence of oxygen could be realized. The mechanism to achieve oxygen tolerance depends on the reaction system composition and the concomitant role of the excited-state PC as a reductant (*via* OQP) or an oxidant (*via* RQP). In brief, oxygen is reduced by the excited-state PC in OQP and by the ground-state anion of the PC in RQP. Photoinduced energy transfer from the triplet excited-state PC to triplet oxygen is another route for oxygen tolerance (Scheme 12).

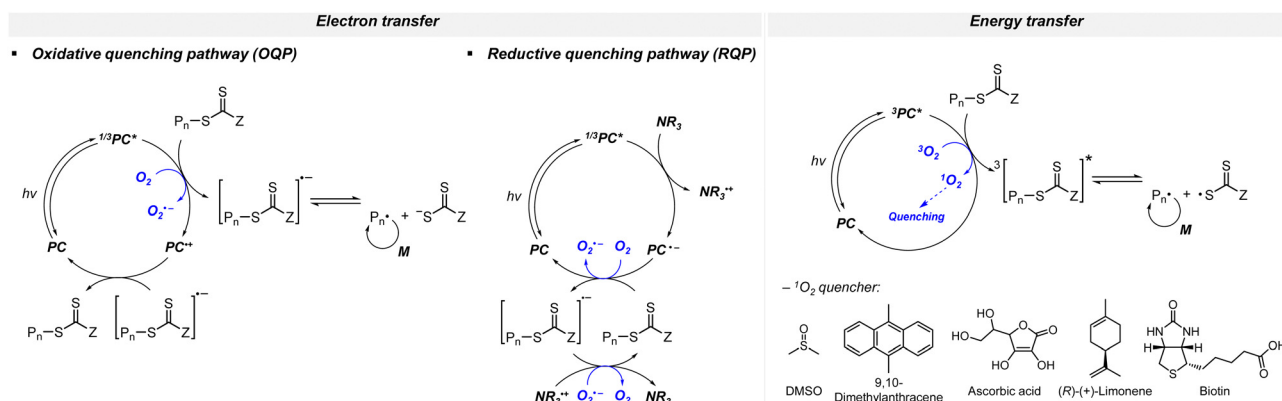
**Electron transfer: oxidative quenching pathway (OQP).** Oxygen tolerance of PET-RAFT polymerization was discovered by Boyer and coworkers in 2014 in their first study of PET-RAFT polymerization using Ir(ppy)<sub>3</sub> as a PC.<sup>31</sup> Strongly reducing excited-state Ir(ppy)<sub>3</sub> was expected to reduce oxygen into a superoxide radical anion, which allows the polymerization in a non-degassed sealed vessel. The kinetics of the polymerization of MMA and MA in DMSO were almost identical to that in a degassed vessel after the induction period to consume oxygen, indicating no degradation of the PC or CTA. With the preserved photocatalytic activity and chain ends, a di- or tri-block copolymer was successfully synthesized by simply adding the monomer and solvent to the reaction mixture. Ru(bpy)<sub>3</sub>Cl<sub>2</sub> with reducing property ( $E_{\text{ox}}^* = -0.81$  V vs. SCE) similar to that of Ir(ppy)<sub>3</sub> ( $E_{\text{ox}}^* = -1.73$  V vs. SCE) also exhibited oxygen tolerance for the polymerization of MA and DMAM in DMSO despite the retardation in polymerization kinetics in the presence of air.<sup>129</sup> It was attributed to the sluggish consumption of oxygen by the PC. Whereas the induction period was decreased with an increase in the catalyst loading, the polymerization rate was not significantly affected.

**Electron transfer: reductive quenching pathway (RQP).** In their first study of PET-RAFT polymerization using organic

dyes, Boyer and coworkers observed that EY and fluorescein with lower  $E_{\text{ox}}^*$  (PC<sup>\*</sup>/PC<sup>•+</sup>) than  $E_{\text{red}}^0$  (CTA/CTA<sup>•-</sup>) and sufficiently low  $\Phi_{\text{FL}}$  allowed effective PET and polymerization of methacrylates in DMSO under blue light irradiation.<sup>66</sup> The apparent propagation rate ( $k_{\text{p}}^{\text{app}}$ ) which was lowered by oxygen was restored by adding TEA. The shortened inhibition period suggested that *via* RQP, the one-electron-reduced EY, generated by the reduction of excited-state EY by TEA, concurrently reduced oxygen to a superoxide radical anion and activated the CTA to allow polymerization without degassing. TEA of at least one equivalent to the CTA was required to completely reduce dissolved oxygen in the reaction vessel. The concentrations of TEA and EY were also important as the highly increased polymerization rate (*i.e.*, high radical flux and high catalyst turnover) led to an increase in polymer dispersity ( $D = 1.4$ ).<sup>130</sup> In addition to the tertiary amine, ascorbic acid (or ascorbate)<sup>131–133</sup> was added to the reaction system to induce reductive quenching of other PCs including ZnTPPS<sub>4</sub><sup>−</sup><sup>131,133</sup> and poly(boron dipyrromethene-*alt*-fluorene),<sup>132</sup> and concomitant oxygen tolerance in the reaction system.

The study of the effect of tertiary amines on PET-RAFT polymerization using EY by Ferji and coworkers revealed that the stability of the amine radical cation impacted the efficiency of the reduction of excited-state EY, subsequent reduction of the CTA, and polymerization in DMSO in the presence of air.<sup>73</sup> Herein, the authors concluded that (i) oxygen tolerance originated from photoinduced conversion of oxygen to inactive singlet oxygen rather than from the reduction of oxygen to the superoxide radical anion and (ii) the tertiary amine facilitated the reduction of the CTA by preferably generating the EY radical anion. Among five amines (TEA, triethanolamine (TEOA), tributylamine, *N,N,N',N',N'*-pentamethyldiethylenetriamine (PMDETA), and 4-(dimethylamino)pyridine (DMAP)), tributylamine and DMAP increased the amine radical stability and conferred oxygen tolerance because of the long alkyl chain and  $\pi$ -bond conjugation, respectively, whereas TEOA in combination with EY produced an initiating radical even in the absence of a CTA to provide polymers with high dispersity.

To date, a variety of amines such as TEA,<sup>134</sup> TEOA,<sup>67,135–140</sup> *N,N,N',N'*-tetramethylethylenediamine (TEMED)<sup>141</sup> and PMDETA<sup>68–70</sup> have been employed as cocatalysts with EY in various solvents for 3D printing resin, surface-initiated polymerization from proteins



Scheme 12 Mechanisms of the three categories of oxygen tolerance in PET-RAFT polymerization.





and DNA, and polymerization in continuous flow reactors, where oxygen tolerance and accelerated polymerization kinetics are highly advantageous. Another xanthene-based organic PC EB/TEOA system was also employed for 3D printing in aqueous solutions without prior deoxygenation.<sup>142</sup> However, some reaction systems were still degassed despite the use of amines, and the reason for degassing and the results of negative controls such as polymerization without a PC, amine, or CTA were not provided, which hampered the elucidation of the exact role of an amine additive. Moreover, Boyer, Sumerlin and coworkers reported that the reaction mechanism became complicated depending on the reaction conditions (*e.g.*, irradiation wavelength, reagents, concentration, and solution pH) and concomitantly generated different reaction intermediates.<sup>57</sup>

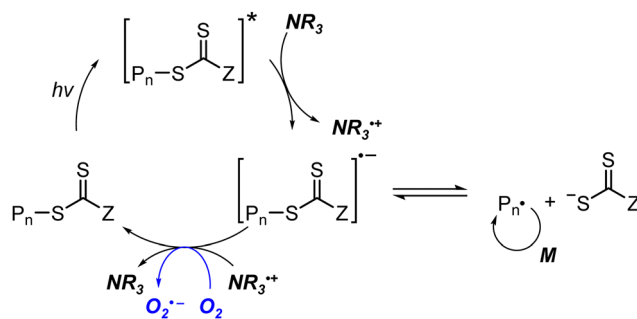
Amine-facilitated reduction of oxygen was also reported for graphitic carbon nitride (g-C<sub>3</sub>N<sub>4</sub>).<sup>143,144</sup> Qiao and coworkers observed a significant decrease in the inhibition period (from 3 hours to 30 minutes) after the addition of TEOA into PET-RAFT polymerization of MA under UV light irradiation (365 nm, 3.5 mW cm<sup>-2</sup>).<sup>143</sup> The efficient deoxygenation was ascribed to an additional pathway to reduce dissolved oxygen *via* g-C<sub>3</sub>N<sub>4</sub>-mediated electron transfer from TEA. Ferji and coworkers again examined the influence of the amount of amine on polymerization control.<sup>144</sup> In g-C<sub>3</sub>N<sub>4</sub>-catalyzed PET-RAFT polymerization of MMA as a model monomer in the presence of tributylamine under irradiation at 405 nm (60 mW cm<sup>-2</sup>), loss of polymerization control was noticed when five equivalents of tributylamine relative to TTC were added. It was attributed to the production of species that could initiate free radical polymerization *via* the interaction of the oxidized amine with another amine. The authors thus set the appropriate molar ratio of amine to CTA as one.

**Energy transfer.** Oxygen can also be inactivated *via* the photoinduced energy transfer mechanism. Owing to the excitation of triplet oxygen to the singlet state *via* triplet-triplet annihilation with excited-state ZnTPP and subsequent consumption of singlet oxygen by DMSO to form dimethyl sulfone, the concentration of dissolved oxygen was kept sufficiently low to continue the polymerization of DMAM even under fully open conditions.<sup>145</sup> However, in other solvents with properties (*i.e.*, boiling point, molecular weight, and dielectric constant) similar to those of DMSO, polymerization became considerably slower with longer inhibition time, implying the intrinsic role of DMSO in the consumption of singlet oxygen. Therefore, to realize oxygen tolerance in other solvents, additives as singlet oxygen quenchers were necessary.<sup>146</sup> Among 9,10-dimethylantracene, ascorbic acid, and (*R*)-(+)-limonene, 9,10-dimethylantracene was the most effective additive, demonstrating similar kinetics to the polymerization with deoxygenation, a very short inhibition period, and excellent temporal control. ZnTMPyP, another water-soluble analogue of ZnTPP, with biotin was employed in the oxygen-tolerant aqueous dispersion polymerization of hydroxypropyl methacrylate (HPMA) for photoinitiated polymerization-induced self-assembly (photo-PISA) in a 96-well plate without deoxygenation.<sup>147</sup> Herein, the thioether group of biotin was

oxidized to sulfoxide upon trapping of singlet oxygen. When the thioether group was a part of the monomer, polymerization of 2-(methylthio)ethyl methacrylate (MTEMA) bearing the thioether group using ZnTPP was oxygen-tolerant without any additives.<sup>148</sup> This oxygen tolerance of ZnTPP was also retained when embedded in 2D metal-organic framework (MOF) nanosheets.<sup>149</sup> Similarly, sodium ascorbate significantly reduced singlet oxygen in Ru(bpy)<sub>3</sub>Cl<sub>2</sub>-catalyzed rapid and controlled polymerization of acrylamides in water and enabled the facile preparation of triblock copolymers within an hour without deoxygenation.<sup>150</sup>

**3.4.1.2. Photoiniferter polymerization.** In the abovementioned mechanisms of conferring oxygen tolerance to PET-RAFT polymerization, oxygen is commonly consumed and inactivated *via* additional reaction pathways mediated by a PC with or without additives. In contrast, photoiniferter polymerization in which a reactive radical can only be generated by direct photolysis of the CTA innately suffers from rather slow reaction kinetics and is not tolerant to oxygen. Thus, oxygen tolerance has rarely been achieved.

For instance, TTC-based CTAs in the presence of tertiary amines could mediate polymerization under UV<sup>71</sup> or blue light irradiation<sup>151,152</sup> to prepare polymers in the absence of a PC. Energetically favored photoinduced electron transfer from the amine to the excited-state CTA and then from the resulting CTA anion to oxygen led to *in situ* removal of oxygen such that polymerization without prior deoxygenation proceeded after the induction period (Scheme 13).<sup>151</sup> Regarding the mechanistic origin of oxygen tolerance, photoinduced energy transfer (*i.e.*, generation of singlet oxygen) was excluded by the similar monomer conversions of MA in DMSO and in toluene despite the different abilities of the solvents to scavenge singlet oxygen. Very recently, Zhang, Weng, and coworkers reported an oxygen-tolerant polymerization system using CPADB under irradiation with a household lamp (14 W, 2.4 mW cm<sup>-2</sup>) where the amine was incorporated as a part of 2-(dimethylamino)-, 2-(diethylamino)-, or 1-(dipropylamino)ethyl methacrylate monomers.<sup>153</sup> However, with a target degree of polymerization (DP) of 400, the relatively high dispersity (1.42–2.12), deviation of molecular weight from theoretical values, and/or the color change of solution from red to yellow (*i.e.*, degradation of CPADB) suggested the need for further optimization of reaction conditions. Gibson and coworkers disregarded the high dispersities of



**Scheme 13** Tertiary amine-assisted oxygen-tolerant polymerization in the absence of a PC.



polymers synthesized *via* amine-catalyzed photolysis of TTC and only focused on the quick preparation of large libraries of polymers *via* high-throughput (HTP) synthesis in a 96-well plate. Dioxane with degassing ability inferior to that of DMSO was thus used as a solvent owing to the ease of purification of polymers by simple evaporation of solvent under vacuum.<sup>152</sup> It has to be noted that categorizing these reports which harnessed amine additives as photoiniferter polymerization might be controversial because herein amine-catalyzed electron transfer instead of the direct photolysis of the CTA initiated the polymerization, which was similar to PC-catalyzed electron transfer in PET-RAFT polymerization. Meanwhile, Chen and coworkers introduced  $\text{Zn}_{0.64}\text{Fe}_{2.36}\text{O}_4$  into DMSO<sup>154,155</sup> or ZnO NPs into aqueous medium<sup>156</sup> to reduce oxygen to a hydroxyl radical *via* photoinduced generation of electron-hole pairs under sunlight irradiation, and enabled open-to-air photoiniferter polymerization from various CTAs despite the poor controllability ( $\bar{D} = 1.35\text{--}1.56$ ).

Oxygen tolerance was also achieved without additives. The so-called “polymerization through oxygen” was reported by Johnson and coworkers even in a completely open vial, where the diffusion of oxygen into the polymerization site was substantially restricted by the high viscosity and low solubility of oxygen in DMSO and not stirring the reaction mixture.<sup>157</sup> Polymerization of acrylates and acrylamides from TTCs was thus conducted at the bottom of the reaction vessel directly above the high-intensity irradiation source (450 nm,  $\geq 503\text{ mW cm}^{-2}$ ) to ensure a high radical flux and a short inhibition period arising from high light intensity. Although this oxygen-tolerant and rapid polymerization retained the controlled and living nature, the molecular weight of the polymer was larger than the theoretical value due to partial degradation of the CTA located near the solution/air interface. The use of deep eutectic solvents (DES) instead of DMSO improved the “polymerization through oxygen” approach.<sup>158</sup> DES, composed of hydrogen-bonding-accepting tetrabutylammonium chloride and hydrogen-bonding-donating ethylene glycol, provided an enhanced polymerization rate and higher stability of the end group of TTCs and DTBs against photodegradation under 465 nm irradiation (0.7 or  $3.1\text{ mW cm}^{-2}$ ). In addition, oxygen tolerance behavior was more pronounced such that stirring the reaction mixture in an open vial did not affect the polymerization rate. Similar results were observed with PET-RAFT polymerization using  $\text{Ir}(\text{ppy})_3$ , EY, and  $\text{ZnTPP}$  as a PC, although the exact role of DES needs to be elucidated. The effects of composition of DES, solubility of monomers and polymers in DES, and propagation rate constants ( $k_p$ s) of monomers in DES should also be considered.

Meanwhile, oxidative decomposition of xanthates and concomitant molecular weight discrepancy were also observed during additive-free polymerization of *n*-butyl acrylate (*n*-BA) under violet light irradiation in a closed non-degassed reaction vessel.<sup>159</sup> Subsequently, Konkolewicz and coworkers filled the remaining headspace in the reaction vessel with an inert solvent rather than air to block the diffusion of oxygen.<sup>160</sup> The combination of two immiscible liquids (water and mineral oil)

allowed the preparation of aqueous- or organic-soluble polymers after the induction period to consume the already dissolved oxygen.

Benefitting from the simple system composition, photoiniferter polymerization has recently been applied to 3D printing where rapidness and efficiency of polymerization may have higher significances than precise controllability of polymerization. Zhu, Li, and coworkers conducted open-to-air rapid 3D printing using a commercial digital light processing (DLP) technique-based 3D printer, where the oxygen was consumed by the radicals generated after the photolysis of xanthate EXEP under violet light irradiation (405 nm,  $2.0\text{ mW cm}^{-2}$ ).<sup>161</sup> Herein, xanthate was employed because of its favored photolysis due to lower stability of the intermediate radical and the weaker C–S bond as compared to those of TTCs. The radicals generated after photolysis consumed oxygen thereby affording oxygen tolerance to the reaction system. It is noted that in the preparation of a linear polymer under blue light irradiation (460–470 nm), deviation of molecular weight because of the oxidation of some portion of EXEP was observed with a long induction period.<sup>162</sup>

**3.4.1.3. Photomediated cationic RAFT polymerization and others.** Oxygen tolerance in PET-RAFT and photoiniferter polymerization is achieved by converting oxygen to reactive oxygen species which is then trapped or deactivating oxygen by coupling with excess radicals. For example, DMSO acts as both a solvent and a singlet oxygen quencher, and thus it is extensively used for oxygen-tolerant polymerization. In contrast, oxygen tolerance of photomediated cationic RAFT polymerization remains elusive presumably because cationic propagating species cannot capture oxygen and this polymerization method is not compatible with DMSO due to the high Lewis basicity of DMSO.<sup>121</sup> Cationic reaction intermediates are insensitive to oxygen, but oxygen tolerance of photomediated cationic RAFT polymerization has not been studied.

In other polymerizations, enzymes are utilized. This enzymatic degassing strategy harnesses the intrinsic enzymatic activity to reduce oxygen, so the oxygen tolerance is achieved regardless of irradiation and decoupled from light. Glucose oxidase (GOx) or pyranose oxidase (P2Ox) in the presence of glucose reduces oxygen to hydrogen peroxide. Thus, *in situ* removal of oxygen was leveraged for EY-catalyzed surface-initiated PET-RAFT polymerization from CTA-tethered substrates under ambient conditions.<sup>163</sup> Nanopure water had to be used as a solvent as the enzymatic stability of GOx and the polymerization rate could be influenced by residual minerals and salts in deionized water. Flavin adenine dinucleotide (FAD), a cofactor within GOx, was reduced to  $\text{FADH}^-$  by glucose. Upon violet light irradiation (405 nm,  $11.5\text{ W}$ ),  $\text{FADH}^-$  was excited, became a highly reducing state, and initiated polymerization by transferring an electron to a monomer or CTA. In addition to the deoxygenation capability by GOx, oxygen was consumed by  $\text{FADH}^-$  regenerating FAD. Therefore, an excess of glucose was necessary initially for GOx and then for FAD to continuously generate  $\text{FADH}^-$  that played a catalytic role. This photoenzymatic RAFT polymerization was employed for ultrahigh-molecular-weight (UHMW) polymer synthesis in an



aqueous solution from *N*-vinylcaprolactam,<sup>164</sup> oligo(ethylene glycol) methyl ether methacrylate (OEGMA), and other monomers.<sup>165</sup>

In conventional photomediated radical polymerization based on Type II visible-light-sensitive photoinitiating systems, oxygen tolerance is achieved by coinitiators and additives (e.g., amine, thiol, silane, germane, borane, phosphine, and phosphite).<sup>128,166,167</sup> These hydrogen donors quench inactive peroxy radicals by hydrogen abstraction and generate new initiating radicals. Page and coworkers recently reported rapid visible-light-driven thiol-ene reaction-based 3D printing of acrylic resin under ambient conditions using a three-component photoinitiating system (ZnTPP as a PC, and electron-donating and electron-accepting coinitiators) (Scheme 14).<sup>168,169</sup> The thiol quenched a peroxy radical which was formed by the addition of oxygen to the propagating radical. The resulting thiyl radical was substantially reactive than the peroxy radical, so consequently decreased the oxygen inhibition period and continued the polymer network formation. Moreover, the thiol reduced excited-state ZnTPP to yield a thiyl radical which in turn was incorporated as a thioether within the network. The thioether also contributed to oxygen tolerance by scavenging singlet oxygen which was generated by TTA between excited-state ZnTPP and triplet oxygen. Only 1 wt% thiol was sufficient to achieve oxygen tolerance, and the mechanical properties of the printed objects were adjustable by the thiol content.

**3.4.2. Oxygen-initiated polymerization.** As mentioned above, oxygen acts as an inhibitor or a scavenger of propagating radicals, so it needs to be physically removed or inactivated

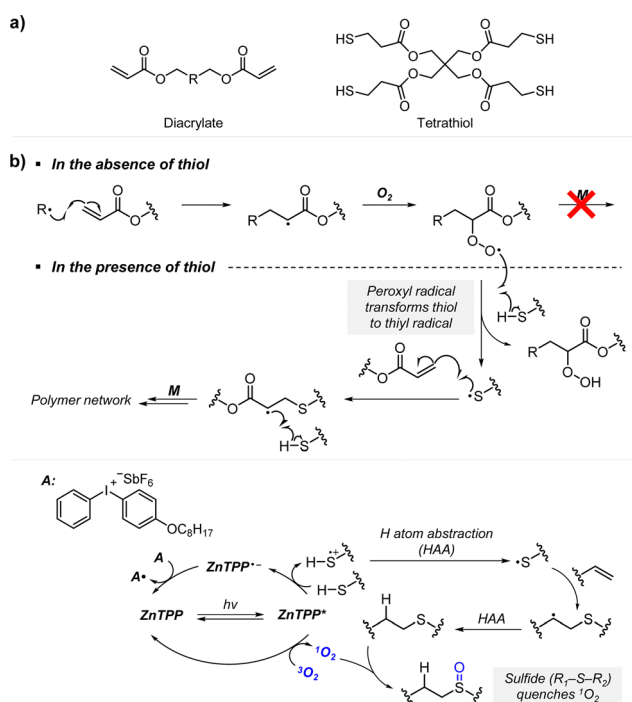
using PCs or additives for successful polymerization. However, if oxygen in turn could become an initiating species (*i.e.*, hydroxyl radical), the reaction would proceed without prior deoxygenation; however, the reaction can be accompanied by imperfect temporal control due to latent radical generation. Hydroxyl radicals are generated from oxygen in the presence of ascorbic acid or water.

Ascorbic acid converts singlet oxygen into hydrogen peroxide and then reduces hydrogen peroxide into hydroxyl radicals. Hydroxyl radicals enable polymerization in ultralow volumes ( $\mu\text{L}$  scale) where deoxygenation is difficult.<sup>170</sup> On the other hand, hydroxyl radical-initiated polymerization could also proceed in the dark *via* the hydroxyl radicals after a brief irradiation period.<sup>93</sup> Hydrogen peroxide, a precursor of hydroxyl radicals, was generated during irradiation. Under near neutral and basic conditions where hydrogen peroxide remained stable, the temporal control was restored as in the case of  $\text{ZnTPPS}_4^-$ /ascorbic acid-catalyzed PET-RAFT polymerization of DMAM in water.<sup>131</sup> Inferior temporal control of polymerization was also observed for a fluorescein/ascorbic acid system.<sup>171</sup> Only the prior deoxygenation prevented the generation of the latent radicals and stopped the reaction in the dark, but the polymerization rate accordingly decreased owing to lowered amount of radicals.

Oxygen in the presence of water can also generate hydroxyl radicals. Very recently, Hou, Xiao, Zhao, and coworkers reported that 1,3,6,8-tetrakis(4-formylphenyl)pyrene (TFPPy)-azine based covalent organic frameworks (COFs) generated initiating hydroxyl radicals from water and atmospheric air under white light irradiation ( $15 \text{ mW cm}^{-2}$ ).<sup>172</sup> Photoinduced production of the superoxide radical anion followed by reaction with water generated hydroxyl radicals. Thus, in a completely open vial, the polymerization rate increased with an increase in the volumetric ratio of water to dioxane, whereas polymerization did not proceed in the absence of water. Nonpolar solvents were not appropriate reaction media due to inefficient stabilization of photogenerated carriers. Adding methylene blue or benzoquinone to scavenge the hydroxyl radical or superoxide radical anion, respectively, led to no polymerization, supporting the initiation mechanism. TEA promoted polymerization by enhancing charge separation in the COF and the capability to transform singlet oxygen into a superoxide radical anion.

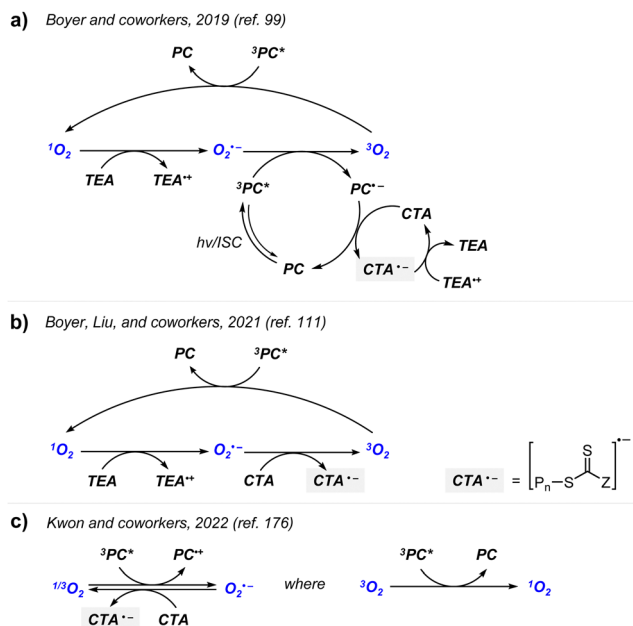
**3.4.3. Oxygen-accelerated polymerization.** Even the peculiar role of oxygen in supporting and accelerating the PET-RAFT polymerization was observed very recently in several reports. Herein, oxygen is directly involved in the photocatalytic cycle for activation of the CTA (Scheme 15). In the examples discussed below, the significantly improved polymerization kinetics were ascribed to the reduction of the CTA by the superoxide radical anion. The superoxide radical anion was generated either in the presence or absence of a tertiary amine.

Boyer and coworkers firstly reported the surprisingly supportive role of oxygen in ZnOETPP/TEA-catalyzed PET-RAFT polymerization under far-red light irradiation ( $690 \text{ nm}$ ,  $3.0 \text{ mW cm}^{-2}$ ).<sup>99</sup> DMAM and MA could be polymerized in the presence of PC, TEA, and oxygen. “On/off” switchability of the



**Scheme 14** Oxygen-tolerant thiol-ene reaction-based visible-light-driven 3D printing of acrylic resin.<sup>169</sup> (a) Structure of diacrylate and tetrathiol monomers. (b) Mechanism of oxygen tolerance in the presence of ZnTPP and thiol.

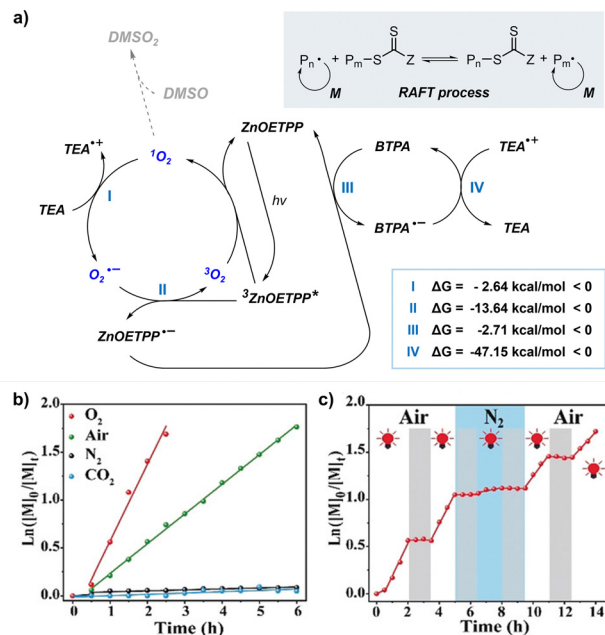




**Scheme 15** Three distinct mechanisms proposed for oxygen-accelerated PET-RAFT polymerization. Generation of the superoxide radical anion to reduce the CTA was achieved as described in (a) ref. 99 and (b) ref. 111 in the presence or (c) absence of TEA as an additive.<sup>176</sup> It is noted that to emphasize the participation of oxygen, the complete catalytic cycles of reagents are not described for clarity.

reaction by the introduction and removal of oxygen combined with a constant polymerization rate in the “on” state implied the essential role of oxygen as a catalyst. Moreover, pure oxygen, when compared to atmospheric air, further increased the polymerization kinetics. Based on the experimental investigation and DFT calculations of the formation of singlet oxygen and the superoxide radical anion, the authors proposed the mechanism of oxygen-catalyzed PET-RAFT polymerization. The superoxide radical anion, which was generated *via* the reduction of singlet oxygen by TEA, reduced excited-state ZnOETPP to proceed PET-RAFT polymerization *via* RQP (Scheme 15a and Fig. 7).

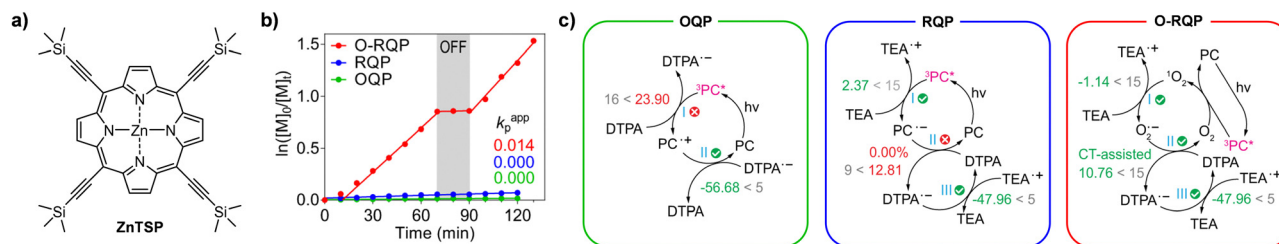
The peculiar role of oxygen, namely the ‘oxygen-mediated reductive quenching pathway (O-RQP)’, was also reported by Boyer, Liu, and coworkers.<sup>111</sup> Herein, oxygen allowed the activation of the CTA, which otherwise was restricted by the unfavorable thermodynamics of the PC exhibiting long wavelength absorption either *via* conventional OQP or RQP. The excited-state PC generates singlet oxygen, which is reduced to a superoxide radical anion by TEA. It was this superoxide radical anion that directly activated the CTA *via* single-electron transfer and activated the polymerization (Scheme 15b and Fig. 8). Combined experimental and theoretical investigations of the PET-RAFT polymerization of MA in DMSO using four model (metallo)porphyrin-based PCs revealed that the thermodynamic viability of O-RQP predominantly depended on the singlet oxygen generation ability of the PC, rather than the electron transfer ability. In particular, *via* O-RQP in the presence of oxygen, the fastest kinetics was achieved as compared to that *via* other pathways. Finally, as expected, four phthalocyanines that were previously considered



**Fig. 7** (a) The proposed mechanism of ZnOETPP/TEA-catalyzed PET-RAFT polymerization accelerated by oxygen. Kinetic plots of  $\ln([M]_0/[M]_t)$  vs. reaction time (b) under different atmospheres and (c) in gas and light dual-gated polymerization. Monomer: MA; CTA: BTPA; additive: TEA (one equivalent relative to the CTA). Adapted with permission from ref. 99 (Copyright 2019 John Wiley & Sons, Inc.).

inactive for PET-RAFT polymerization *via* the conventional mechanisms became successful PC candidates for well-controlled PET-RAFT polymerization under red to NIR light irradiation (590, 660, 730, and 780 nm depending on PCs,  $10 \text{ mW cm}^{-2}$ ) *via* the newly proposed O-RQP (Scheme 16a). This mechanism was partially valid for aqueous polymerization in water using a water-soluble phthalocyanine  $\text{ZnPCS}_4^-$  (Scheme 16b).<sup>173</sup> Herein, reactive oxygen species did not directly activate the CTA, but participated in the generation of other initiating radicals. Water as a hydrogen donor transformed the superoxide radical anion into a hydrogen peroxy radical, which is a precursor of hydrogen peroxide. Hydrogen peroxide was then activated by excited-state  $\text{ZnPCS}_4^-$  to form an initiating hydroxyl radical. Based on experimental and DFT calculations, this proposed pathway was more favored than OQP and RQP, leading to successful demonstration of polymerization in water under NIR irradiation (730 nm,  $12 \text{ mW cm}^{-2}$ ). Another water-soluble phthalocyanine possessing several ethylene glycol units could also catalyze PET-RAFT polymerization under NIR irradiation (730 nm,  $75.7 \text{ mW cm}^{-2}$ ) only in the presence of hydrogen peroxide under a  $\text{N}_2$  atmosphere,<sup>174</sup> supporting the proposed mechanism for initiation. This newly proposed O-RQP is thus promising to widen the scope of PCs in catalyzing PET-RAFT polymerization at longer wavelengths; nevertheless, the stability of PC candidates in the presence of reactive oxygen species must be considered. Hou, Xiao, and coworkers reported a similar system for heterogeneous PCs involving porphyrins.<sup>175</sup> As the head space or amount of oxygen in the sealed reaction vessel increased, the polymerization rate was accelerated albeit with the lengthened induction period. TEA-catalyzed depletion of





**Fig. 8** (a) Chemical structure of ZnTSP. (b) Kinetic plot of  $\ln([M]_0/[M]_t)$  vs. reaction time and temporal control of model PET-RAFT polymerization via OQP (green), RQP (blue), and O-RQP (red). (c) Schematic representation of thermodynamic viability (denoted by Gibbs free energy change [kcal mol<sup>-1</sup>]) for each mechanism. Written in grey are threshold values for each step. Monomer: MA; CTA: DTPA; additive: TEA (0.5 equivalent relative to the CTA). Adapted with permission from ref. 111 (open access).

singlet oxygen and the formation of the superoxide radical anion were experimentally confirmed by UV/Vis and electron spin resonance (ESR) spectroscopy.

Very recently, Kwon and coworkers in collaboration with Gierschner and Koo reported 3DP-MSDP-IPN as a novel organic PC for additive-free oxygen-accelerated polymerization in ambient and aqueous environments.<sup>176</sup> The mechanism was similar to O-RQP<sup>111</sup> in terms of generation of singlet oxygen by the excited-state PC and activation of the CTA by the superoxide radical anion. However, Stern–Volmer analysis suggested that the excited-state PC was likely to be quenched by oxygen rather than by the CTA, which means that in the presence of a PC possessing a suitable redox potential, the superoxide radical anion could be generated without an external reductant (Scheme 15c). Ag<sub>2</sub>S NCs also exhibited a similar phenomenon.<sup>65</sup> Using potassium superoxide as a source of the superoxide radical anion, the polymerization still proceeded in the absence of Ag<sub>2</sub>S NCs, confirming the proposed mechanism for oxygen-accelerated polymerization.

Nevertheless, it should be noted that the abovementioned oxygen-accelerated polymerization, such as *via* O-RQP, is mechanically distinct from the previously reported oxygen-demanding polymerization using alkylborane (complex) as a precursor of the initiating radical. For example, triethylborane reacts with oxygen to liberate an ethyl radical, which reacts with another oxygen to generate a peroxy radical. The peroxy radical then reacts with triethylborane to generate an ethyl radical as an initiating species (Scheme 17a). Therefore, polymerization can be initiated and externally regulated by the presence of oxygen.<sup>177</sup> If alkylboranes are complexed, the complex first needs to be decomplexed for further processes.<sup>178</sup> Wu and coworkers

reported both oxygen-demanding and photocontrolled polymerization based on light-induced decomplexation of the alkylborane complex.<sup>179</sup> Upon UV light irradiation, the photoacid in the triethylborane-amine/photoacid complex 1,3-diaminopropane-triethylborane (DAPTb)/Ph<sub>2</sub>I<sup>+</sup> generated a proton which subsequently released ethylborane to consecutively initiate polymerization (Scheme 17b).

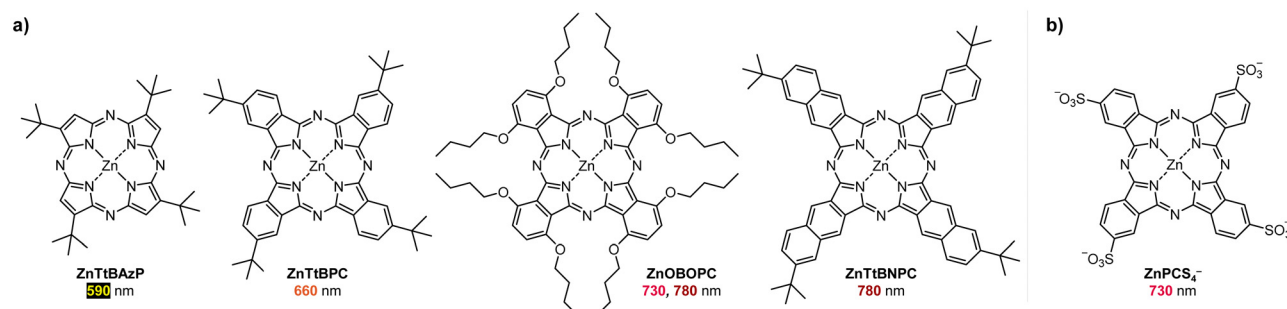
## 4. PET-RAFT polymerization

### 4.1. Overview

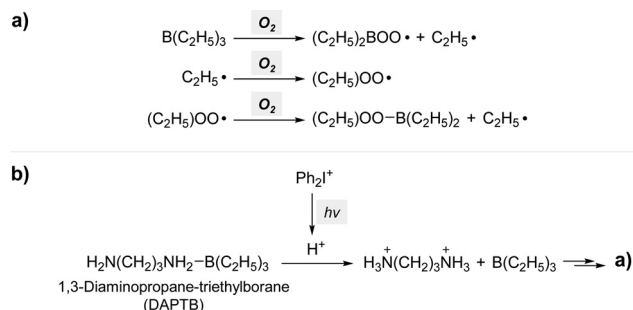
This section aims to summarize the research on PET-RAFT polymerization. First of all, the reported PCs are outlined in Section 4.2. The next sections summarize the applications of PET-RAFT polymerization such as for preparation of polymers with precise control over their characteristics (*e.g.*, sequence, architecture, polymer tacticity, and dispersity). PET-RAFT polymerization has been widely applied to various applications owing to its uniquely distinct features in contrast to the conventional RAFT polymerization. In particular, surface-initiated polymerization to functionalize a given surface, 3D/4D printing technologies, and stereolithography along with the advent of advanced techniques, such as flow chemistry and high-throughput (HTP) synthesis, would pave the way to the industrial applications. If worth mentioning, the newly designed functional monomers are also introduced.

### 4.2. PCs for polymerization

Since the first employment of Ir(ppy)<sub>3</sub> as a PC in 2014,<sup>31</sup> along with the increasing number of applications, the scope of PCs has



**Scheme 16** Chemical structures of the phthalocyanines discovered for PET-RAFT polymerization at longer wavelengths (> 590 nm) *via* O-RQP.<sup>111</sup>



**Scheme 17** Mechanism of (a) oxygen-mediated generation of an initiating radical from triethylborane<sup>177</sup> and (b) photomediated decomplexation of 1,3-diaminopropane-triethylborane (DAPT B) to triethylborane.<sup>179</sup>

been accordingly widened to realize PET-RAFT polymerization of various monomers under a wide range of wavelengths. In brief, the development of PCs has been directed as follows. Concerns regarding environmental issues of transition metals have led to development of metal-free (in)organic alternatives, which increased the environmental compatibility of PCs and eliminated the potential harm in applying the prepared polymeric materials in electronic and/or biomedical fields.<sup>180,181</sup> In the case of biomedical applications, PCs that can be activated under irradiation at longer wavelengths are desired as deeper penetration length and lower energy would allow polymerization in the presence of biomolecules and eventually enable *in vivo* polymerization in the near future. Last but not least, heterogeneous PCs that can be easily purified and reused for the next polymerizations have also gained interest. In any case, highly efficient photocatalytic performance of a PC that realizes polymerization at low catalytic loading and/or endows the reaction system with oxygen tolerance is desired.

During the search of PCs, researchers initially adapted PCs that were efficient for other types of visible-light-driven organic transformations including RDRPs, solar energy conversion, or water splitting, and successfully demonstrated PET-RAFT polymerization using a wide range of PCs. Apart from these trial-and-error strategies, recently emerging approaches are based on investigation of the structure–property/performance relationship of conventional PCs and computer-guided design of novel PCs.<sup>96,182</sup> These general design strategies have been quite well established and allow efficient, systematic, and rational design of novel PCs. For details on the rational design of PCs, please refer to the review articles by Boyer, Miyake, Liu, and coworkers, who have summarized the effects of the structures of PCs on their photocatalytic activities (light absorption, quantum yield, and redox properties) in various photo-controlled polymerizations (including PET-RAFT and photomediated cationic RAFT polymerizations),<sup>183</sup> and Kwon and coworkers, who have particularly focused on the recently emerged purely organic PCs since 2016.<sup>184</sup>

In the following sections, the reported PCs are categorized into metal-based, organic, inorganic, and modified PCs. The types of PCs are briefly described, while the detailed applications are mentioned throughout Sections 4.3 and 4.4. For representative PCs, structures of the PCs are provided with

the used wavelengths and monomers reported for polymerization (Table 1). It is noted that PET-RAFT polymerization provided high tolerance of functional groups incorporated into monomers (Scheme 18). For example, by PET-RAFT polymerization using Ir(ppy)<sub>3</sub><sup>100</sup> or EY,<sup>185</sup> macrocyclic allylic sulfones, which introduce degradable ester bonds along the polymer backbone, could be evenly distributed within a nearly ideal random copolymer of macrocyclic allylic sulfones and acrylic monomers, which otherwise is not achieved by thermally initiated RAFT polymerization. The even distribution of degradable moieties along the copolymers led to significantly improved degradation behaviors.

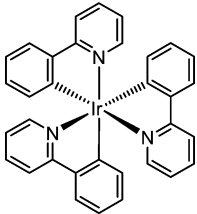
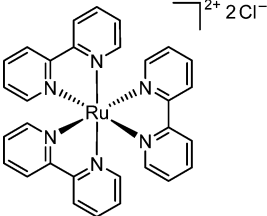
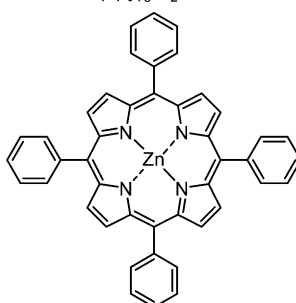
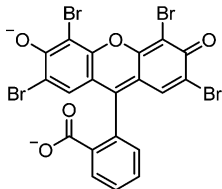
**4.2.1. Metal-based PCs.** Ir(ppy)<sub>3</sub>, as the PC employed for PET-RAFT polymerization for the first time,<sup>31</sup> is one of the most extensively applied PCs. A wide range of monomers ranging from challenging unconjugated monomers (*i.e.*, vinyl acetate (VAc), *N*-vinylpyrrolidinone (NVP), and vinyl benzoate (VBz)),<sup>31,186</sup> vinyl ketones,<sup>130,187</sup> to monomers bearing various functional groups (*e.g.*, metallocene,<sup>188</sup> amino acids,<sup>189</sup> and fluorine<sup>190,191</sup>) were successfully polymerized. Another transition metal-based Ru(bpy)<sub>3</sub>Cl<sub>2</sub> exhibited less efficient photocatalytic performance than Ir(ppy)<sub>3</sub>,<sup>129</sup> but expanded the scope of solvent of PET-RAFT polymerization to alcoholic dispersion<sup>192</sup> and aqueous systems<sup>129,193</sup> owing to its water-solubility. Moreover, owing to its traditional usage as an electrochemiluminescence (ECL) probe, after the Ru(bpy)<sub>3</sub>Cl<sub>2</sub>-catalyzed polymerization to synthesize surface-modified gold NPs as a solid substrate of ECL sensors, Ru(bpy)<sub>3</sub>Cl<sub>2</sub> need not be purified. Based on these wide utilities, Ir(ppy)<sub>3</sub><sup>84,85</sup> and Ru(bpy)<sub>3</sub>Cl<sub>2</sub><sup>83,84</sup> have been a model PC in the recently emerging field of systematic investigation of the PET-RAFT polymerization mechanism.

Chlorophyll a, a naturally occurring visible-light-absorbing PC for photosynthesis in green plants, is considered the first non-transition metal-based PC and it allowed utilization of low-energy red light (635 nm) for PET-RAFT polymerization for the first time.<sup>194,195</sup> Bacteriochlorophyll a, which is present in purple bacteria and absorbs at even longer wavelength (>900 nm), further expanded the wavelength range of PET-RAFT polymerization to the far-red (780 nm) and NIR region (850 nm).<sup>196</sup> Metalloporphyrins were also effective under red light irradiation (635 nm).<sup>105</sup> Among the metalloporphyrins embedded with different core metals (Zn<sup>2+</sup>, Ni<sup>2+</sup>, Co<sup>2+</sup>, and Fe<sup>3+</sup>), only ZnTPP catalyzed the polymerization as its high triplet state quantum yield (0.88) and low  $\Phi_{\text{FL}}$  (0.04) increased the probability of photoinduced electron transfer at the triplet excited state. Aluminum (Al<sup>3+</sup>) porphyrin complexes were recently discovered for polymerization under blue light irradiation (460 nm, 5 mW cm<sup>-2</sup>).<sup>197</sup> On the other hand, free base porphyrin without the core metal still retained photocatalytic ability albeit with a slow polymerization rate, owing to ineffective collision between free base porphyrin and CTA.<sup>198</sup> The polymerization rate was significantly enhanced by covalently tethering the CTA to free base porphyrin.

ZnTPP demonstrated a wide absorption profile, so PET-RAFT polymerization could be performed under blue, green,



Table 1 Representative PCs employed for PET-RAFT polymerization

PC	Irradiation wavelengths	CTA–monomer pair		
		Dithiobenzoates	Trithiocarbonates	Xanthates
<b>Metal-based PCs – Section 4.2.1</b>				
 Ir(ppy) <sub>3</sub>	Blue (435–470 nm)	MMA, OEGMA, TFEMA HPMAm (Others)→	CoAEMA, MAEFe <i>t</i> -BA, BzA, MA, OEGA, TFEA DEAm, DMAm, NAM, NIPAm, <i>N</i> -acryloyl amino acids Isoprene, St, VAc, vinyl ketones, macrocyclic allylic sulfone Fluorinated monomers	←(Methacrylates) ←(Acrylates) ←(Methacrylamides) ←(Acrylamides)
	White			DVP, NVP, VAc, VBz, VCz, VP VDF
 Ru(bpy) <sub>3</sub> Cl <sub>2</sub>	Blue (435–470 nm)	BzMA, MMA, OEGMA	HPMA, MAA DEGA, MA, NASS, OEGA  DEAm, DMAm, NAM, NIPAm St	
 ZnTPP	Red (635 nm) Yellow (560 nm) Green (530 nm)  White		BzMA, DMAPS-MA, GMA, HEMA, HPMA, MMA, MPC, MTEMA, NBMA, NHSMA, OEGMA, TFEMA <i>n</i> -BA, <i>t</i> -BA, Boc-AEA, BzA, CHA, DEGA, DMAEA, EA, EHA, <i>n</i> -HA, HEA, HPA, IBOA, MA, MSEA, OEGA, TEGDA, TFEA  AAm, AAPTAC, <i>t</i> -BA, Boc-AEAm, Cp-DIBAC, DAAm, DEAm, DMAm, HEAm, NAM, NIPAm, PEAm St, VBA DEAm, DMAm, HEAm, NAM	
<b>Organic PCs – Section 4.2.2</b>				
 Eosin Y	Blue (450–483 nm) Green (520–530 nm)	BzMA, DMAEMA, GMA, HEMA, MAA, MMA, OEGMA, PFPMA CBMAm, HPMAm	HFBMA, MMA  <i>n</i> -BA, <i>t</i> -BA, HEA, MA, OEGA, PEGDA  AMPS, DAAm, DEAm, DMAm, FSAm, HEAm, NAM, NIPAm, PEG-based monomers, saccharide- and peptide-based monomers BTP, NaSS, St, vinyl ketones, macrocyclic allylic sulfone	

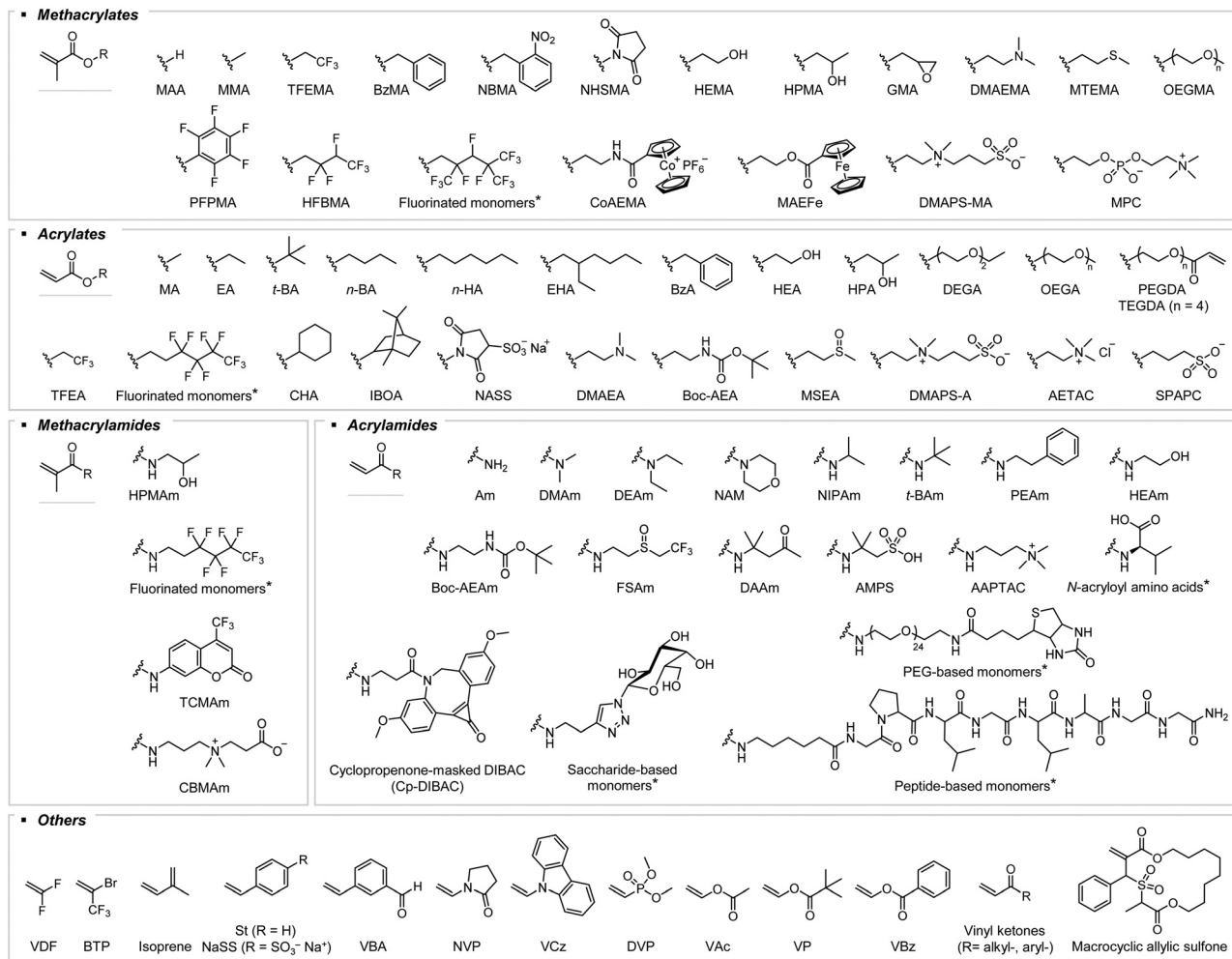
yellow, orange, and red light irradiation (460, 522, 565, 595, and 635 nm, respectively).<sup>105</sup> Nevertheless, red light has been typically used in subsequent studies. Several ZnTPP derivatives were employed as well. Water-soluble analogues including ZnTPPS<sub>4</sub><sup>−98,131,133,199</sup> and ZnTMPyP<sup>147,200,201</sup> or supramolecular ZnTPOR/cucurbit[7]uril which exhibited improved water-solubility compared to ZnTPOR<sup>202</sup> catalyzed polymerization in aqueous systems. In the case of supramolecular ZnTPOR/cucurbit[7]uril, host–guest complexation between cucurbit[7]uril and TPOR also prevented self-aggregation-induced quenching of excited-state ZnTPOR in water and reduction of photocatalytic performance. Similarly, self-aggregation of ZnTPP at high concentration in DMSO was reduced by linking polyhedral oligomeric silsesquioxane (POSS) to ZnTPP.<sup>203</sup> ZnOETPP could absorb far-red light

(690 nm), but could catalyze polymerization only in the presence of oxygen and TEA, which is contradictory to the common role of oxygen in inhibiting the polymerization<sup>99</sup>

Very recently, phthalocyanines were discovered for PET-RAFT polymerization under red to NIR light irradiation (Scheme 16).<sup>111,173</sup> These molecules exhibiting long wavelength absorption were inactive for polymerization *via* OQP and RQP owing to the unfavorable thermodynamics, but became active for polymerization *via* O-RQP in the presence of oxygen and tertiary amines. For a detailed explanation on the role of oxygen in the case of ZnOETPP and phthalocyanines, please see Section 3.4.2.2.

**4.2.2. Organic PCs.** Organic PCs reduce the potential negative impacts of residual transition metal components on polymeric materials for electronic and biological applications.<sup>36,180,181</sup>





**Scheme 18** Chemical structures and abbreviations of monomers employed for PET-RAFT polymerization. The asterisk denotes that only a selected monomer is shown.

In the initial investigations of the photocatalytic capabilities of commercially available and non-toxic organic dyes (*i.e.*, EY, fluorescein, methylene blue, Nile red, and rhodamine 6G) in PET-RAFT polymerization, EY and fluorescein were found to be efficient.<sup>66</sup> Since then, EY has been extensively utilized as a PC under green and blue light irradiation, owing to its adequate catalytic efficiency and water-solubility. Later studies revealed that Rose Bengal,<sup>93</sup> EB,<sup>204</sup> and Phloxine B,<sup>204</sup> which share the common fluorescein scaffolds (Scheme 19), could also catalyze the polymerization.

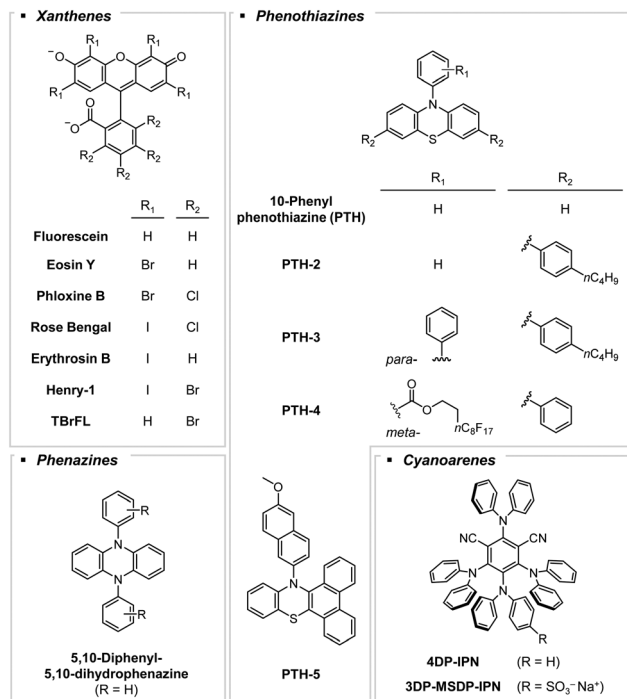
EY has been widely applied as a PC in various organic transformation reactions *via* photoredox catalysis.<sup>205</sup> In this regard, researchers have employed other classes of previously reported organic PCs (*e.g.*, phenothiazines, phenazines, and cyanoarenes) for PET-RAFT polymerization (Scheme 19). For example, PTH, which realized photoinduced organocatalyzed ATRP (O-ATRP) for the first time,<sup>206</sup> promoted the PET-RAFT polymerization of acrylates and acrylamides under irradiation using a CFL<sup>207</sup> or at 400 nm.<sup>208</sup> Incorporation of electron withdrawing groups (*i.e.*, *n*-butylphenyl and hydrofluorocarbons) into PTH caused a red-shift in absorption profiles, and thus enhanced

visible-light-absorbing abilities in the case of PTH-2,<sup>209</sup> PTH-3,<sup>210,211</sup> and PTH-4.<sup>212</sup> Moreover, fluorinated PTH-4 provided better control over the polymerization of fluorinated polymers as compared to non-fluorinated PTH-3, owing to the fluorine-fluorine interaction between the PC and the propagating chain-end.<sup>212</sup> PTH-5 with the extended conjugation exhibited lower  $E_{\text{red}}^*$  and higher  $E_{\text{ox}}^0$  than PTH-3, which led to favored initial electron transfer from the excited-state PC to xanthate and subsequent electron transfer from the xanthate anion to the one-electron-oxidized PC.<sup>213</sup> A series of phenazine-based PCs developed by structural modification of 5,10-diphenyl-5,10-dihydrophenazine exhibited disparate photocatalytic activities in PET-RAFT polymerization under blue light irradiation (460 nm).<sup>125</sup> Likewise, covalent structural modification of the known PC scaffolds, including extension of the conjugated structure or change of substituents, has been widely applied to modulate the performance of PCs in polymerization under desired reaction conditions (*e.g.*, irradiation wavelengths and chemical properties of reagents).

As the structures of PCs affect their catalytic abilities for PET-RAFT polymerization, a comprehensive investigation of commercial fluorescein derivatives guided the development of







Scheme 19 Four representative scaffolds of organic PCs discovered for PET-RAFT polymerization.

a novel PC Henry-1.<sup>214</sup> Herein, the photophysical properties studied by DFT calculations were compared with the experimental results of the polymerization. On the other hand, the discovery of TBrFL was fully guided by DFT calculations.<sup>96</sup> In a similar vein, *via* a synthetic platform proposed for the design of organic PCs based on strongly twisted donor-acceptor scaffolds,<sup>182</sup> a combination of various donors and acceptors provided a large number of PC candidates with predictable photophysical and electrochemical characteristics. Thus, highly efficient cyanoarene derivatives 4DP-IPN<sup>215</sup> and 3DP-MSDP-IPN<sup>176</sup> were newly designed for PET-RAFT polymerization in an organic and aqueous system, respectively. The outstanding photocatalytic performances of all systematically designed PCs (*i.e.*, Henry-1, TBrFL, 4DP-IPN, and 3DP-MSDP-IPN) were ascribed to efficient generation of a triplet excited state and appropriate excited-state redox potentials, proposing the key design principle of next-generation PCs for PET-RAFT polymerization.

Thus far, perylene,<sup>216</sup> benzaldehyde,<sup>217–219</sup> benzothiadiazole,<sup>220</sup> PheoA,<sup>106</sup> reduced free base porphyrin,<sup>221</sup> fluorophenyl bac-

teriochlorin,<sup>222</sup> self-assembled carboxylated porphyrin (SA-TCPP),<sup>223</sup> g-C<sub>3</sub>N<sub>4</sub>,<sup>143,144,224,225</sup> poly(1,4-diphenylbutadiene)-nanofibers (PDNB-NF),<sup>226</sup> imine-based COFs,<sup>227</sup> and (heteroatom-doped) carbon dots<sup>228</sup> have been reported as organic PCs. Among them, SA-TCPP, g-C<sub>3</sub>N<sub>4</sub>, imine-based COFs, and PDPB-NF were heterogeneous, so they can be separated after the polymerization and reused several times. Moreover, biomolecules such as flavin mononucleotide<sup>229</sup> and FAD cofactor<sup>164,165</sup> were employed. FAD is a cofactor of GOx and is reduced to FADH<sup>−</sup> in the presence of glucose. FADH<sup>−</sup> exhibits a high excited-state reducing power, so could catalyze photoenzymatic RAFT polymerization under violet light irradiation (405 nm).

**4.2.3. Inorganic PCs.** Numerous inorganic materials including Ag<sub>3</sub>PO<sub>4</sub>,<sup>230</sup> Ag<sub>2</sub>S NCs,<sup>65</sup> semi-conducting nanomaterials (*i.e.*, ZnO,<sup>231</sup> Zn<sub>0.64</sub>Fe<sub>2.36</sub>O<sub>4</sub>,<sup>154,155</sup> Bi<sub>2</sub>O<sub>3</sub>,<sup>232</sup> and CdSe<sup>233–235</sup> and Si-based quantum dots (QDs)<sup>236</sup>), and upconversion nanoparticles (UCNPs) (*i.e.*, CsPbBr<sub>x</sub>I<sub>3–x</sub> perovskite NCs<sup>237</sup> and NaYF<sub>4</sub>:Yb<sup>3+</sup>/Tm<sup>3+</sup> and NaYF<sub>4</sub>:Yb<sup>3+</sup>/Er<sup>3+</sup> NPs<sup>238</sup>) have been employed for PET-RAFT polymerization (Table 2).<sup>239</sup> Several studies showed that the catalytic performance of PCs was affected by size<sup>234</sup> and morphology<sup>230</sup> of the prepared PCs.

It is noted that Ag<sub>3</sub>PO<sub>4</sub> could be activated in the NIR region (940 nm) owing to the localized surface plasmon resonance effect.<sup>230</sup> NaYF<sub>4</sub>:Yb<sup>3+</sup>/Tm<sup>3+</sup> and NaYF<sub>4</sub>:Yb<sup>3+</sup>/Er<sup>3+</sup> NPs,<sup>238</sup> and CsPbBr<sub>x</sub>I<sub>3–x</sub> perovskite NCs<sup>237</sup> could also utilize NIR light owing to their upconversion properties and an extremely large two-photon absorption cross-section, respectively. NaYF<sub>4</sub>:Yb<sup>3+</sup>/Tm<sup>3+</sup> and NaYF<sub>4</sub>:Yb<sup>3+</sup>/Er<sup>3+</sup> NPs absorbed NIR light (980 nm) and emitted light at 325–380 and 425–500 nm *via* upconversion.<sup>238</sup>

Moreover, based on the heterogeneity of inorganic PCs, recovery and reusability of the used PCs for the next polymerizations were demonstrated for several PCs such as CdSe-based QDs,<sup>233</sup> Zn<sub>0.64</sub>Fe<sub>2.36</sub>O<sub>4</sub>,<sup>154</sup> and Bi<sub>2</sub>O<sub>3</sub>.<sup>232</sup> These PCs were typically retrieved by simple centrifugation, whereas magnetic Zn<sub>0.64</sub>Fe<sub>2.36</sub>O<sub>4</sub> could be recovered with a magnet.

**4.2.4. Modified PCs.** Besides the structural modification strategies, small molecule PCs have been modified by their immobilization on heterogeneous supports. The resulting PCs became heterogeneous, allowing the simple catalyst recovery from the polymerization mixtures through centrifugation or filtration. For example, free base porphyrin and ZnTPP were immobilized onto cotton thread (Fig. 9a),<sup>240</sup> sponges,<sup>241</sup> and silica microspheres.<sup>242</sup> EY was conjugated to cotton thread<sup>243</sup> and silica NPs.<sup>244</sup> Surface-initiated copolymerization of acrylate-

Table 2 Operational irradiation wavelengths of reported inorganic PCs for PET-RAFT polymerization

PC	Irradiation wavelengths				
Ag <sub>3</sub> PO <sub>4</sub>	Blue (465 nm)	Green (525 nm)	Red (625 nm)	NIR (780, 940 nm)	Sunlight
Ag <sub>2</sub> S NCs	Blue (455 nm)	Green (515 nm)	Red (630 nm)		Sunlight
Zn <sub>0.64</sub> Fe <sub>2.36</sub> O <sub>4</sub>					Sunlight
Bi <sub>2</sub> O <sub>3</sub>					White
CdSe QDs	Blue (465 nm)	Green (532 nm)			White, sunlight
Si QDs	Blue (460 nm)				White
CsPbBr <sub>x</sub> I <sub>3–x</sub> NCs	Blue (460 nm)	Green (535 nm)	Red (635 nm)		
NaYF <sub>4</sub> :Yb <sup>3+</sup> /Tm <sup>3+</sup> and NaYF <sub>4</sub> :Yb <sup>3+</sup> /Er <sup>3+</sup> NPs				NIR (980 nm)	



functionalized fluorescein with MA from glass beads provided fluorescein-immobilized glass beads (Fig. 9b).<sup>245,246</sup> The catalytic performance was comparable to that of their small molecule counterparts and was preserved after repeated recoveries. Moreover, after its conjugation to silica NPs, the stability of EY against photodegradation was enhanced.<sup>244</sup> Immobilization of Ir(ppy)<sub>3</sub>,<sup>101</sup> ZnTPP,<sup>102</sup> and carbon dots<sup>103</sup> on functional materials such as magnetic nanocomposites led to switchable catalytic performance in response to an external magnetic field. Agglomeration of the modified PCs limited the access and electron transfer between PC and CTA, and subsequent polymerization.

PCs can be covalently incorporated into a macromolecular network. *Via* the introduction of polymerizable vinyl moieties into PCs, followed by copolymerization with different monomers, macromolecular versions of PTH<sup>94</sup> and EY<sup>247,248</sup> were prepared. Copolymerization with NIPAm resulted in PC-embedded poly-(NIPAm)s with thermoresponsive behavior, allowing the purification of macromolecular PCs by heating the reaction mixture at temperatures above the LCST (Fig. 9c).<sup>94,247</sup> Amine-functionalized EY served as a monomer for ROP between diglycidyl and diamine monomers for the preparation of an interpenetrating polymer network.<sup>249</sup> The prepared PC-based copolymers could be grafted onto the commercial ultrafiltration

membranes.<sup>250,251</sup> These PC-tethered membranes served as an integrated synthesis-separation system by catalyzing the polymerization and efficiently filtering unreacted monomers and other reagents after the polymerization. On the other hand, Sonogashira–Hagihara reactions between halogen substituents of xanthene dyes (*i.e.*, EB and Rose Bengal) and dialkynes<sup>97</sup> and Debus–Radziszewski reactions between amine-terminated porphyrins and imidazolium bromides<sup>252</sup> generated PC-conjugated porous polymer frameworks. Cross-linking between hydroxy-terminated porphyrins and dichlorodimethylsilanes provided twisted 3D structures with open catalytic sites.<sup>253,254</sup> The effective catalytic performance was ascribed to the large surface area of catalytically active sites, prevention of aggregation of porphyrins and concomitant reduction of quenching of excited-state porphyrins.

COFs or MOFs also served as heterogeneous platforms. 2D porphyrinic COFs were synthesized through polycondensation reactions between amine-terminated porphyrins and multivalent aldehydes.<sup>255,256</sup> 3D MOFs synthesized from zirconium-based clusters and porphyrins showed catalytic activities dependent on their crystal structures (Fig. 9d).<sup>257</sup> During the synthesis of 3D MOFs from free base- or zinc-embedded porphyrins as organic ligands and zinc-based clusters as metal

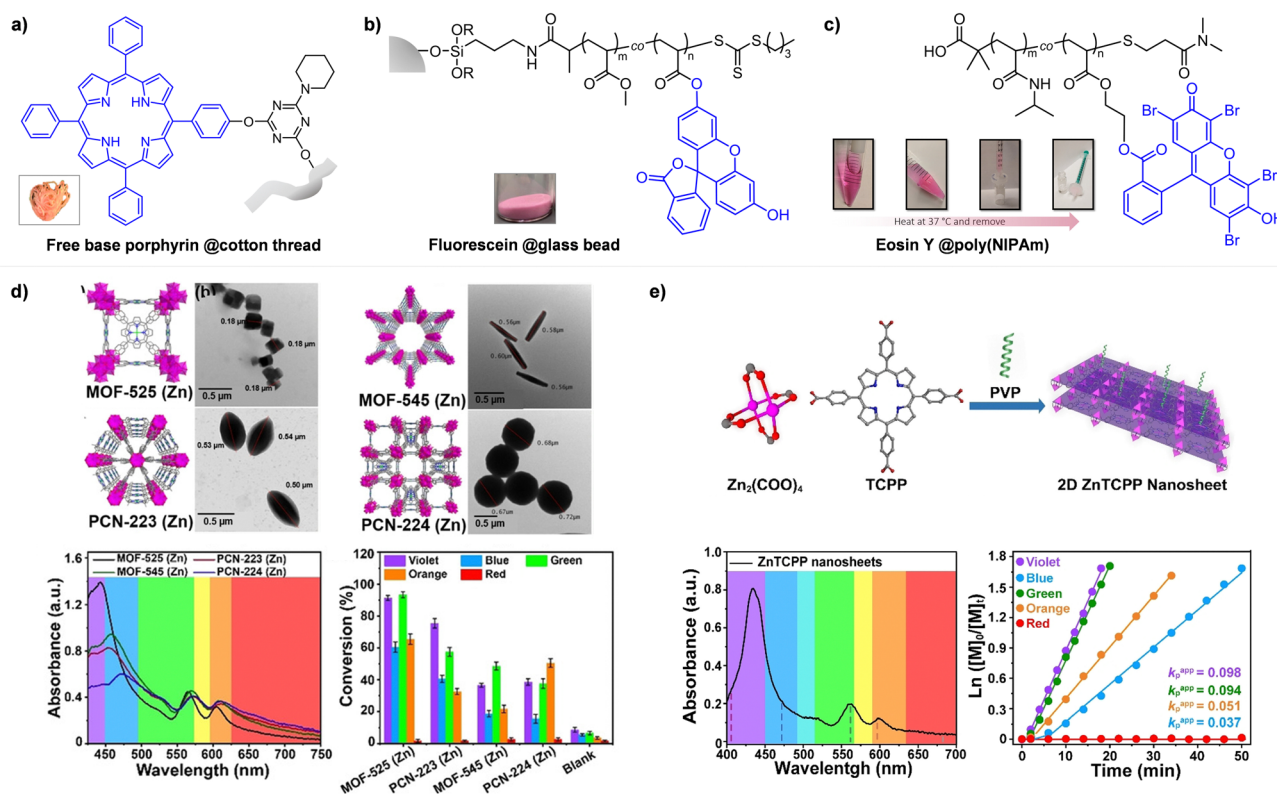


Fig. 9 Chemical structures and photographs of (a) free base porphyrin, (b) fluorescein, and (c) EY immobilized on heterogeneous supports or polymers. (d) Crystal structures, TEM images (top) and UV/Vis absorption spectra of 3D zinc porphyrinic MOFs, and monomer conversions in the polymerization of MA from BTPA using various 3D zinc porphyrinic MOFs under irradiation (9 mW cm<sup>-2</sup>) (bottom). (e) Schematic representation and UV/Vis absorption spectrum of the 2D zinc porphyrinic MOF, and kinetic plots of  $\ln([M]_0/[M]_t)$  vs. reaction time in the polymerization of MA from BTPA using the 2D zinc porphyrinic MOF under irradiation (10 mW cm<sup>-2</sup>). Adapted with permission from (a) ref. 240 (Copyright 2018 American Chemical Society), (b) ref. 245 (Copyright 2022 The Royal Society of Chemistry), (c) ref. 247 (Copyright 2021 American Chemical Society), (d) ref. 257 (Copyright 2020 John Wiley & Sons, Inc.), and (e) ref. 258 (Copyright 2021 John Wiley & Sons, Inc.).

nodes, addition of polyvinylpyrrolidone (PVP) induced anisotropic growth of the frameworks and generation of ultrathin 2D nanosheets (Fig. 9e).<sup>258</sup> Ultrathin 2D nanosheets demonstrated more rapid polymerization kinetics than 3D MOFs owing to the higher aspect ratio, larger surface area, and more accessible catalytically active sites.<sup>149,258,259</sup>

### 4.3. Applications

High end-group fidelity in PET-RAFT polymerization allows the one-pot synthesis of multiblock copolymers comprised of vinyl monomers with various side chains *via* chain extension with subsequently added monomers. Multiple extensions technically would lead to the preparation of (ultra)high-molecular-weight polymers (Section 4.3.5). Vinyl ethers and cyclic monomers (*e.g.*, cyclic esters, thiiranes, and epoxides) which are ionically (not radically) polymerized can also be manually incorporated into the polymers at the designated positions with tunable lengths and numbers of blocks. This is owing to the orthogonality and compatibility of PET-RAFT polymerization with other polymerizations (Section 4.3.1.2). Moreover, by introducing specially designed monomers, CTA, or any additives, the control of architecture (Section 4.3.2), stereochemistry (Section 4.3.3), and dispersity (Section 4.3.4) has been achieved. It is noted that to fully demonstrate the versatility of PET-RAFT polymerization, strategies that include “click” reactions to synthesize structurally diverse polymers by linking multiple polymers possessing pre- or post-functionalized chain ends into a single chain are not discussed here. Becer and coworkers described various methodologies for multiblock copolymer synthesis.<sup>260</sup>

#### 4.3.1. Sequence control

**4.3.1.1. Multiblock copolymer synthesis.** Multiblock copolymers are synthesized by a number of successful chain extensions. After each step, end-group fidelity should remain high, and the

reactivity of the PC should be retained to restart polymerization reaction upon addition of new monomers. In their first discovery of PET-RAFT polymerization using Ir(ppy)<sub>3</sub> as a PC in 2014, Boyer and coworkers leveraged the effective retention of the DTB end group of the polymer to demonstrate whether chain extension could yield di-, tri-, or even deca-block copolymers.<sup>31</sup> The decablock copolymer of MA ([poly(MA)]<sub>10</sub>,  $M_{n, GPC} = \sim 82\,000\text{ g mol}^{-1}$  and  $D = \sim 1.40$ ) was synthesized from BTPA by ten repeated quantitative polymerizations of MA (58–144 equivalents to the macroinitiator) dissolved in degassed DMSO as the viscosity of the reaction mixture increased with the number of polymerizations. Neither isolation of the macroinitiators nor an additional amount of PC was required. The tailing of GPC traces at the low molecular weight region was attributed to dead polymers and the gradual decrease in end-group fidelity (Fig. 10a). The final end-group fidelity after the tenth polymerization was calculated to be 68% from the deconvolution of the MWD. Similarly, the pentablock copolymer of five different monomers (methyl, ethyl, *n*-propyl, *n*-butyl, and *n*-pentyl acrylate) with the target DP of 50 for each monomer was synthesized from BSTP ( $M_{n, GPC} = 28\,390\text{ g mol}^{-1}$ ,  $D = 1.14$ , and end-group fidelity =  $\sim 80\%$ ).<sup>261</sup> By adding Ir(ppy)<sub>3</sub> of 10 ppm relative to the monomer in the polymerization of the first monomer,  $>89\%$  monomer conversion was achieved in 24 hours and 48 hours for the first three and rest two reactions, respectively. The authors decided to increase the reaction time instead of the catalytic loading to avoid the loss of the end group which appeared in the GPC traces. A functional triblock copolymer of the monomers possessing ketone and trimethylsilyl-protected alkynes could also be synthesized although the fast reactivity of the latter monomer was considered to increase the dispersity to 1.24.

Ru(bpy)<sub>3</sub>Cl<sub>2</sub> was the first reported PC that enabled the synthesis of [poly(MA)<sub>70</sub>]<sub>10</sub>-*b*-poly(MA)<sub>90</sub> and [poly(DMAm)<sub>60</sub>]<sub>5</sub>-

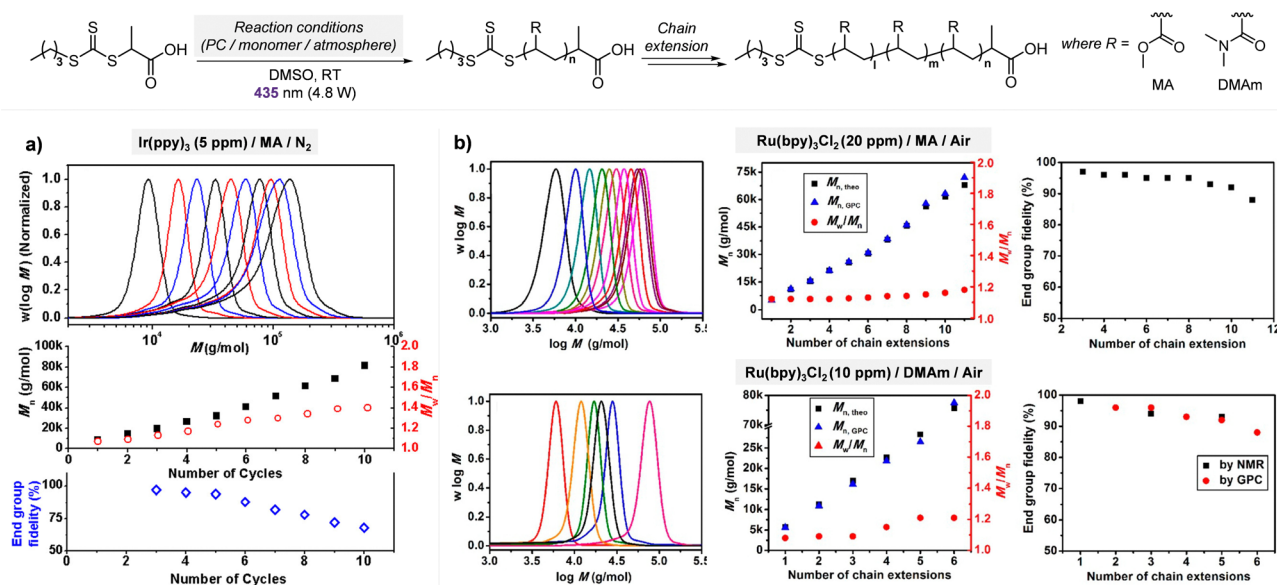


Fig. 10 Multiblock polymers of MA and DMAm obtained by PET-RAFT polymerization. Evolution of MWDs,  $M_n$ ,  $M_w/M_n$ , and end-group fidelity vs. number of cycles of chain extensions for (a) Ir(ppy)<sub>3</sub>- and (b) Ru(bpy)<sub>3</sub>Cl<sub>2</sub>-catalyzed reactions. Adapted with permission from (a) ref. 31 (Copyright 2014 American Chemical Society) and (b) ref. 129 (Copyright 2014 American Chemical Society).



*b*-poly(DMAm)<sub>300</sub> in DMSO in the presence of oxygen when used at 20 ppm and 10 ppm, respectively, under blue light irradiation (435 nm, 4.8 W) (Fig. 10b).<sup>129</sup> Herein, neither the reaction vessel nor the monomer solution was degassed, but polymerization was controlled such that the end-group fidelity determined by GPC remained higher than 86% and dispersity did not exceed 1.2. Owing to its aqueous solubility, Ru(bpy)<sub>3</sub>Cl<sub>2</sub> was also employed for the oxygen-tolerant and rapid synthesis of a water-soluble triblock copolymer.<sup>150</sup> Ru(bpy)<sub>3</sub>Cl<sub>2</sub> (25 ppm relative to the monomer) with ascorbate (two equivalents relative to BTPA) was employed to prepare poly(*N*-acryloylmorpholine (NAM))<sub>40</sub>-*b*-poly(*N,N*-diethylacrylamide (DEAm))<sub>40</sub>-*b*-poly(DMAm)<sub>40</sub> in water within an hour under blue light irradiation (470 nm, 26 mW cm<sup>-2</sup>). Employment of a continuous flow reactor further enhanced the polymerization kinetics. EY disodium salt in combination with TEOA (0.01 and one equivalent relative to the CTA, respectively) allowed the rapid oxygen-tolerant synthesis of the triblock copolymer poly(DMAm)<sub>100</sub>-*b*-poly(DMAm)<sub>50</sub>-*b*-poly(DMAm)<sub>50</sub> (*D* = 1.39) and [poly(DMAm)<sub>10</sub>]<sub>3</sub> (*D* = 1.24) within 15 minutes without prior deoxygenation.<sup>136</sup> Meanwhile, ZnTPP that could achieve oxygen tolerance in DMSO without any additives solely pushed the limit to HTP polymerization in a 96-well plate. At diluted monomer concentration (1.0 M), 400 ppm of ZnTPP under yellow light irradiation (560 nm, 9.7 mW cm<sup>-2</sup>) provided [poly(NAM)<sub>25</sub>]<sub>6</sub> (*M*<sub>n,GPC</sub> = 20 900 g mol<sup>-1</sup> and *D* = 1.19) with low molecular weight tailing.<sup>262</sup> This simple and efficient ZnTPP-catalyzed HTP polymerization has enabled the simple and efficient synthesis of high-order block copolymers to construct a library of polymers with varying sequences, compositions, molar ratios between different monomer functionalities (e.g., cationic, hydrophobic, and hydrophilic), or structures, which revealed the relationship between the structures and properties of polymers in antimicrobial activities<sup>263,264</sup> and polymer-protein binding interactions.<sup>265,266</sup>

Liao, Lalevée, and coworkers developed a novel organic PC oxygen-doped anthanthrene (ODA) for metal-free synthesis of [poly(*n*-BA)]<sub>10</sub> (*M*<sub>n,GPC</sub> = ~143.2 kg mol<sup>-1</sup> and *D* = ~1.31) (Fig. 11).<sup>267</sup> The polymerization of the first block with ODA (5 ppm), BTPA as the CTA, and *n*-BA as the monomer (100 equivalents relative to BTPA) under blue light irradiation (455 nm, 3 mW cm<sup>-2</sup>) was followed by multiple chain extensions with degassed *n*-BA (100 equivalents relative to the macroinitiator) for four hours per step.

**4.3.1.2. Incorporation of various monomers into a single polymer chain.** PET-RAFT polymerization with radical intermediates is orthogonal to other polymerizations with ionic intermediates. Moreover, the use of light as an energy source allows selective activation of PET-RAFT polymerization and consumption of radically polymerizable vinyl monomers (e.g., (meth)acrylates and (meth)acrylamides) from the reaction mixture in which ionically polymerizable monomers (e.g., vinyl ether and cyclic monomers) also exist. The remaining monomers can be independently polymerized in the presence of corresponding initiators. Therefore, using appropriately designed initiators, various monomers can be incorporated into a single polymer chain *via* dual polymerization processes.

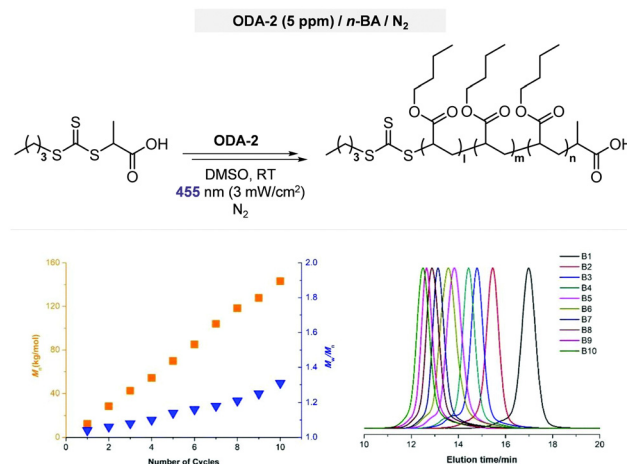


Fig. 11 Multiblock polymers of *n*-BA obtained by ODA-2-catalyzed PET-RAFT polymerization. Evolution of *M*<sub>n</sub>, *M*<sub>w</sub>/*M*<sub>n</sub>, and MWDs vs. number of cycles of chain extensions. Adapted with permission from ref. 267 (Copyright 2022 The Royal Society of Chemistry).

First of all, the same dormant TTC can be activated to undergo either PET-RAFT or (photomediated) cationic RAFT polymerization. Fors and coworkers, for the first time, reported wavelength-dependent activation of Ir(ppy)<sub>3</sub> at 450 nm for PET-RAFT polymerization of MA and of pyrylium tetrafluoroborate salt at 520 nm for photomediated cationic RAFT polymerization of iBVE (Table 3, entry 1).<sup>124</sup> However, as the pyrylium salt also exhibited absorption at 450 nm, the catalyst loading had to be regulated to selectively activate PET-RAFT polymerization and avoid the synthesis of tapered block copolymers. On the other hand, cationic RAFT polymerization could be activated by (electro)chemical means which are completely orthogonal to light stimuli. The CTA was oxidized by adding ferrocenium tetrafluoroborate salt and deactivated by adding one equivalent of DTC anion into the reaction mixture to cap the propagating cations and reduce the ferrocenium salt (Table 3, entry 2).<sup>119</sup> In the electrochemical activation, the CTA was oxidized by anodic oxidation of ferrocene (as a redox mediator) to ferrocenium and deactivated by applying cathodic current, and the concentration of ferrocene should be kept low to prevent the quenching of the triplet excited-state of Ir(ppy)<sub>3</sub> and block the PET-RAFT polymerization (Table 3, entry 3).<sup>116</sup> Instead, Alaniz, Sepunaru, and coworkers utilized PTH as the redox mediator (Table 3, entry 4).<sup>117</sup> As PTH catalyzed the PET-RAFT polymerization of MA (380 nm, 3 mW cm<sup>-2</sup>), switching between two polymerizations by toggling two corresponding external stimuli successfully generated block copolymers of vinyl ether and acrylate up to tetrablocks. Meanwhile, Satoh and coworkers reported that the change of irradiation wavelength could affect the ratio of the two monomers separately incorporated by two orthogonal processes and the number of interconversions (Table 3, entry 5).<sup>121</sup> Herein, cationic RAFT polymerization was kept constantly “on” by the presence of Lewis acid B(C<sub>6</sub>F<sub>5</sub>)<sub>3</sub> and only ZnTPP-catalyzed PET-RAFT polymerization could be reversibly activated. Under red light irradiation (630 nm, 45 mW), both MA and iBVE participated in polymerization. The diad sequence of iBVE in <sup>13</sup>C NMR







**Table 3** Reported polymerization methods that can be combined with PET-RAFT polymerization for multiblock copolymer synthesis

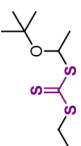
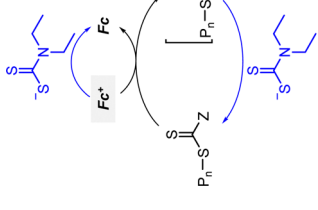
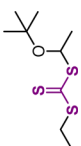
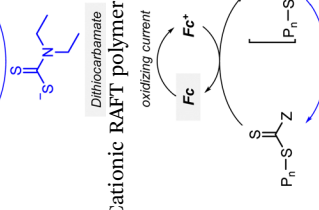
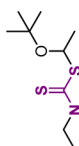
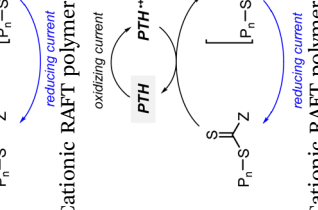
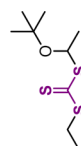
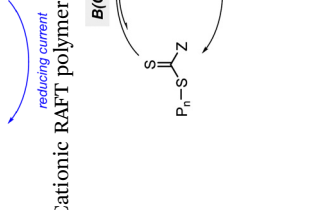
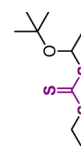

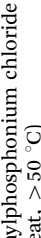
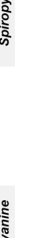
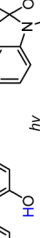
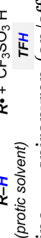
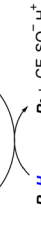
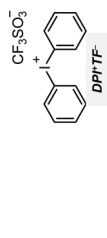
PET-RAFT polymerization			Combined polymerization		
Entry	PC (stimuli)	Monomer	Initiator	Mechanism	Reagents (stimuli)
1	Ir(ppy) <sub>3</sub> (on/off: light, 450 nm)	MA		Cationic RAFT polymerization 	Pyrylium salt (on/off: light, 520 nm)
2	Ir(ppy) <sub>3</sub> (on/off: light, 450 nm)	MA		Cationic RAFT polymerization 	Ferrocenium tetrafluoroborate salt (FcBF <sub>4</sub> )/ dithiocarbamate (on/off: chemical redox reaction)
3	Ir(ppy) <sub>3</sub> (on/off: light, 455 nm)	MA		Cationic RAFT polymerization 	Ferrocene (Fc) (on/off: electrical redox reaction)
4	10-phenyl phenothiazine (PTH) (on/off: light, 380 nm)	MA		Cationic RAFT polymerization 	PTH (on/off: electrical redox reaction)
5	ZnTPP (on/off: light, 630 nm)	MA		Cationic RAFT polymerization 	B(C <sub>6</sub> F <sub>5</sub> ) <sub>3</sub> (only on)



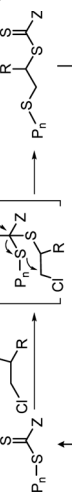
Table 3 (continued)

PET-RAFT polymerization			Combined polymerization		Monomer	Ref.
Entry	PC (stimuli)	Monomer	Initiator	Mechanism		
6	Ir(ppy) <sub>3</sub> (on/off: light, 460 nm)	MA		Cationic ring-opening polymerization	ε-Caprolactone	123
7	Ir(ppy) <sub>3</sub> (on/off: light, blue)	MA		Cationic ring-opening polymerization	δ-Valerolactone	120
8	ZnTPP (on/off: light, 635 nm)	MA		Cationic ring-opening polymerization	δ-Valerolactone	118
9	Ir(ppy) <sub>3</sub> (on/off: light, blue)	DMAM, NIPAM		Anionic ring-opening polymerization	Thiiranes	115

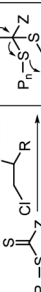
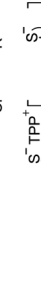
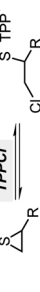
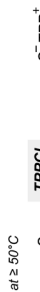
Diphenyl phosphate (on)  
Diphenyliodonium triflate (DPI+TF-) + Ir(ppy)<sub>3</sub>  
(on/off: light, blue)



Tetraphenylphosphonium chloride (TPPCL)  
(on/off: heat, > 50 °C)



Anionic ring-opening polymerization  
at ≥ 50 °C



spectra, which was not observed in the PET-RAFT polymerization of MA and iBVE, confirmed that the Lewis acid-catalyzed cationic RAFT and ZnTPP-catalyzed PET-RAFT polymerization from the common CTA were interconvertible. Under green light irradiation (525 nm, 20 mW), the contribution of PET-RAFT polymerization was higher and the consumption of iBVE was lower than that under red light irradiation owing to more active generation of the TTC anion.

Other monomers including cyclic monomers (*e.g.*, cyclic esters and epoxides) can be incorporated into a single polymer chain using a bifunctional initiator prepared by the functionalization of the CTA with a hydroxyl group, for example, *via* the esterification of the carboxylic acid moiety in the R group. Boyer and coworkers firstly reported the one-pot synthesis of block copolymers by a combination of PET-RAFT polymerization and another polymerization method (Table 3, entry 6).<sup>123</sup> The block copolymer of  $\epsilon$ -caprolactone and MA was synthesized using diphenyl phosphate and Ir(ppy)<sub>3</sub> and the ratio of the length of each block was simply controlled *via* the temporal control of PET-RAFT polymerization (460 nm, 0.7 mW cm<sup>-2</sup>). You and coworkers employed diphenyliodonium triflate that only generated photoacid in the presence of Ir(ppy)<sub>3</sub> under blue light irradiation (10 W) and then catalyzed the cationic ROP of  $\delta$ -valerolactone (Table 3, entry 7).<sup>120</sup> Ir(ppy)<sub>3</sub> could still catalyze PET-RAFT polymerization after the addition of MA to the reaction mixture. In this case, both processes required irradiation such that only diblock copolymers with defined orders could be obtained. Boyer and coworkers reported the generation of photoacid *via* intramolecular cyclization of merocyanine to spiropyran followed by dissociation of the proton under blue light irradiation (460 nm, 0.7 mW cm<sup>-2</sup>) (Table 3, entry 8).<sup>118</sup> ZnTPP that absorbs at 635 nm afforded orthogonality in wavelength and thus selective activation of two polymerizations. However, upon changing the light source from blue to red, the ROP of  $\delta$ -valerolactone was not completely inactivated due to slow inactivation of the photoacid molecule. Effective switching between anionic ROP and PET-RAFT polymerization was realized using a combination of heat and light as two external stimuli (Table 3, entry 9).<sup>115</sup> Herein, the anionic ROP of the cyclic thiirane monomer using quaternary onium salts (tetraphenylphosphonium chloride) and TTC only proceeded at >50 °C due to the energy barrier to open the ring such that PET-RAFT polymerization of acrylamides under blue light irradiation (5 W) was orthogonally conducted at room temperature. As the reaction temperature and irradiation wavelength were easily switched in an orthogonal manner, interconversion of two polymerizations five times from symmetric TTC provided an undecablock copolymer (Fig. 12). Programmed heating and/or irradiation, such as intermittent irradiation during heating, enabled precise insertion of the DMA block at any position within the homopolymer of thiiranes, which would otherwise require careful consideration of the reactivities of monomers.

Lastly, in addition to ionic polymerization, radical-mediated O-ATRP was selectively activated with PET-RAFT polymerization. Boyer, Miyake, and coworkers reported that *N,N*-diaryl dihydrophenazine could catalyze not only O-ATRP but also PET-

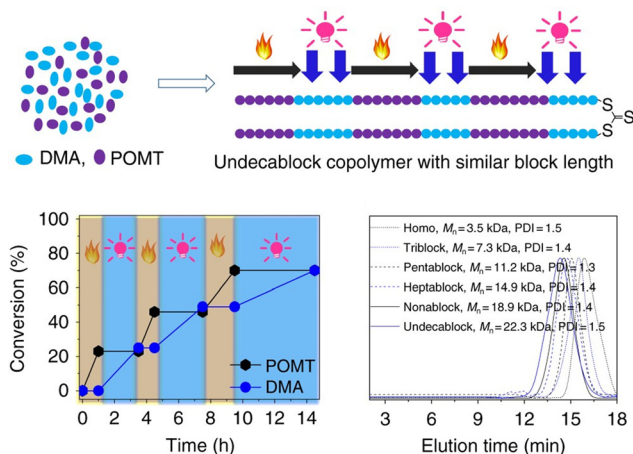


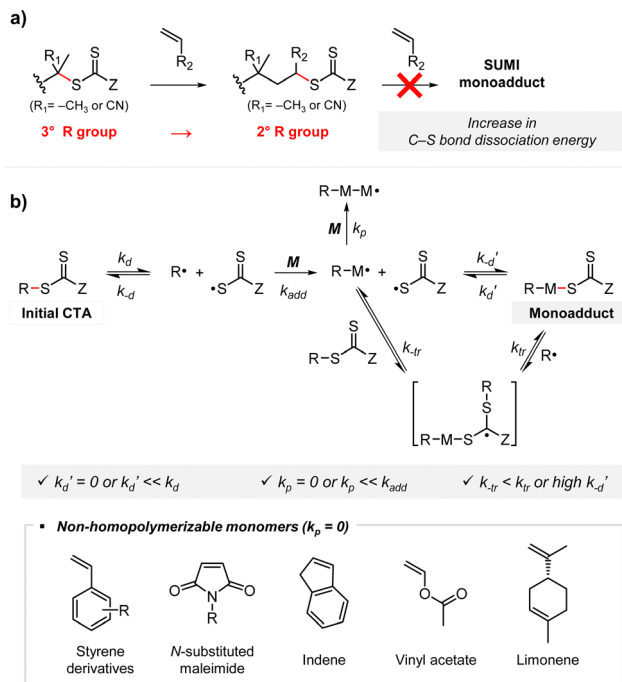
Fig. 12 Synthesis of an undecablock copolymer by multiple cycles of heating and irradiation. Under heating, 2-(phenoxymethyl) thiirane (POMT) was selectively consumed by TTC-mediated anionic ROP whereas under irradiation DMAm was consumed by PET-RAFT polymerization. Adapted with permission from ref. 115 (open access).

RAFT polymerization, based on the similarity between two reaction mechanisms and hence the required catalytic properties.<sup>125</sup> Interestingly, PET-RAFT polymerization required less amount of PC as compared to O-ATRP of MMA. Therefore, using alkyl bromide-functionalized CTA and by increasing the loading of PC from 50 to 500 ppm, diblock copolymers could be obtained *via* PET-RAFT polymerization of MA followed by O-ATRP of MMA.

**4.3.1.3. Single unit monomer insertion (SUMI).** SUMI refers to selective insertion of a single unit monomer at a time.<sup>268</sup> As the stability of the C–S bond changes after the insertion of a certain monomer, carefully designed reaction conditions (the combination of CTA, monomer, and PC) can only activate the initial CTA to which the monomer is added.<sup>109</sup> The monoadduct can be isolated and its synthesis can be confirmed by NMR, mass spectrometry, and gel permeation chromatography. Sequential SUMI of a series of monomers leads to discrete oligomers with known monomer sequences, which would pave the way for synthetic polymer chemistry to reach DNA or proteins possessing a high precision in the monomer sequence and the resulting functionalities. For example, the well-defined oligomers can be the building blocks for higher-order polymers or can provide a hint at the stereochemical effect on the activation of the diastereomeric oligomeric CTA, which has been challenged by the difficulties in the preparation of appropriate materials.<sup>269–271</sup> Visible-light-driven RAFT polymerization under mild reaction conditions in the absence of exogenous radical initiators is advantageous to prepare polymers with high end-group fidelity and prevent the formation of initiator-derived byproducts, when compared to conventional thermally initiated polymerizations.

For successful SUMI (*i.e.*, to limit multiple additions of monomers), dissociation of the initial CTA should be preferred compared to that of the monoadduct *via* the increase in C–S bond dissociation energy along with the insertion of a monomer with a less stable R group (Scheme 20a). If the monoadduct

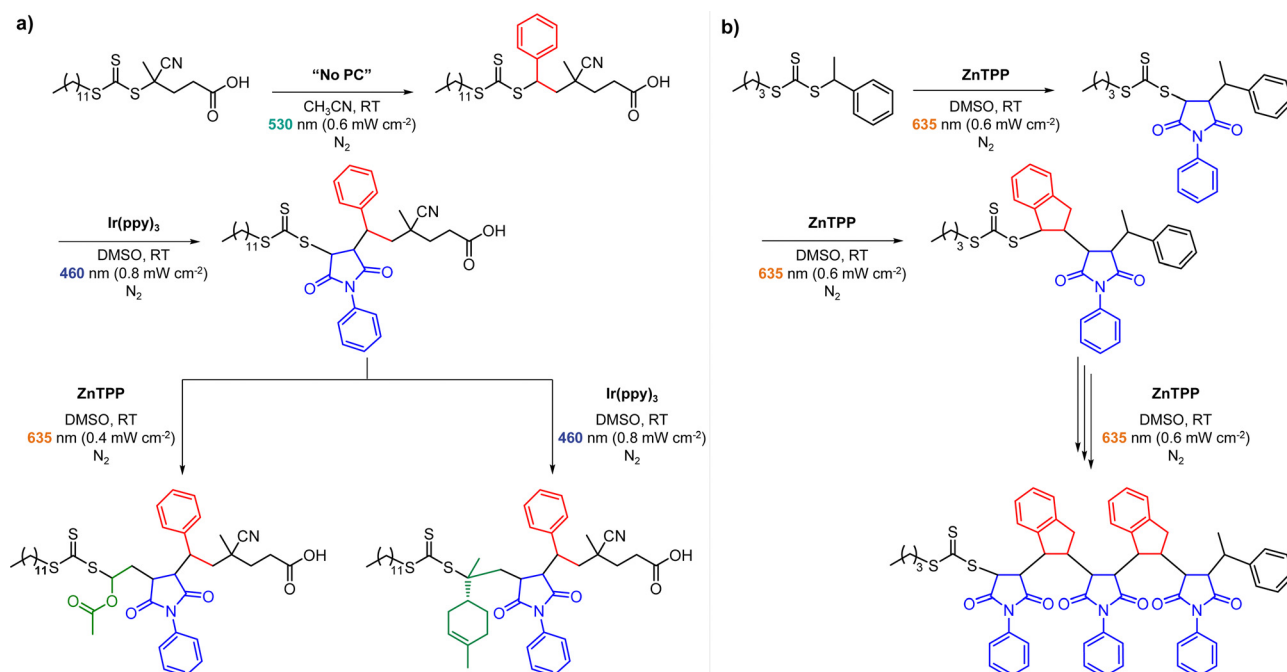




**Scheme 20** (a) Mechanism and (b) requirements for SUMI, where  $k_d$  ( $k_{-d}$ ) is the decomposition (recombination) rate constant of the initial CTA under irradiation,  $k_{add}$  is the addition rate constant of a monomer to the R group radical of the initial CTA,  $k_p$  is the propagation rate constant of the second monomer to the R group radical of the SUMI monoadduct,  $k_{tr}$  is the chain transfer rate constant of the R group radical of the initial CTA to the SUMI monoadduct,  $k_{tr}'$  is the chain transfer rate constant of the R group radical of the SUMI monoadduct to the initial CTA, and  $k_d'$  ( $k_{-d}'$ ) is the decomposition (recombination) rate constant of the SUMI monoadduct under irradiation.

decomposes, deactivation of the propagating radical instead of propagation by either recombination or chain transfer to the initial CTA is required (Scheme 20b). The use of non-homopolymerizable monomers, such as styrene, *N*-substituted maleimide, VAc, limonene, and indene, with low  $k_p$  is also helpful. The blue shift of the UV absorption band of the monoadduct to lower wavelengths as compared to that of the initial CTA enabled selective and efficient activation of the initial CTA by light.<sup>272</sup> However, in cases where the selected monomers were purposely inserted in desired sequences *via* success SUMI, PCs such as PheoA,<sup>106</sup> Ir(ppy)<sub>3</sub>,<sup>89</sup> and/or ZnTPP<sup>89,269,270,273,274</sup> were necessary to achieve reasonably high reaction efficiencies under mild reaction conditions. Using ZnTPPS<sub>4</sub><sup>−</sup>, a water-soluble analogue of ZnTPP, Moad and coworkers observed the significant enhancement of reaction kinetics in SUMI of DMAM as a model monomer in water.<sup>199</sup>

For example, in the first report of the synthesis of trimers by Boyer, Moad, Hawker, Xu, and coworkers, the insertion of the first monomer styrene into CDTA under green light irradiation (530 nm, 0.6 mW cm<sup>−2</sup>) was followed by the Ir(ppy)<sub>3</sub>-catalyzed PET-RAFT polymerization of the second monomer *N*-substituted maleimide under blue light irradiation (460 nm, 0.8 mW cm<sup>−2</sup>) (Scheme 21a).<sup>89</sup> The combination of styrene and maleimides is well-known for alternative copolymerization due to the formation of donor-acceptor pairs. The last third monomer VAc or limonene was inserted using ZnTPP under red light irradiation (635 nm, 0.4 mW cm<sup>−2</sup>) or Ir(ppy)<sub>3</sub>, respectively, because Ir(ppy)<sub>3</sub> resulted in multiple addition of VAc. Further functionalization of the trimers provided a new methacrylate monomer possessing a precisely defined side chain of hexamer as a potential building block for periodic polymers. Later, Boyer and coworkers



**Scheme 21** Synthetic scheme for a discrete (a) trimer<sup>89</sup> and (b) pentamer.<sup>273</sup>



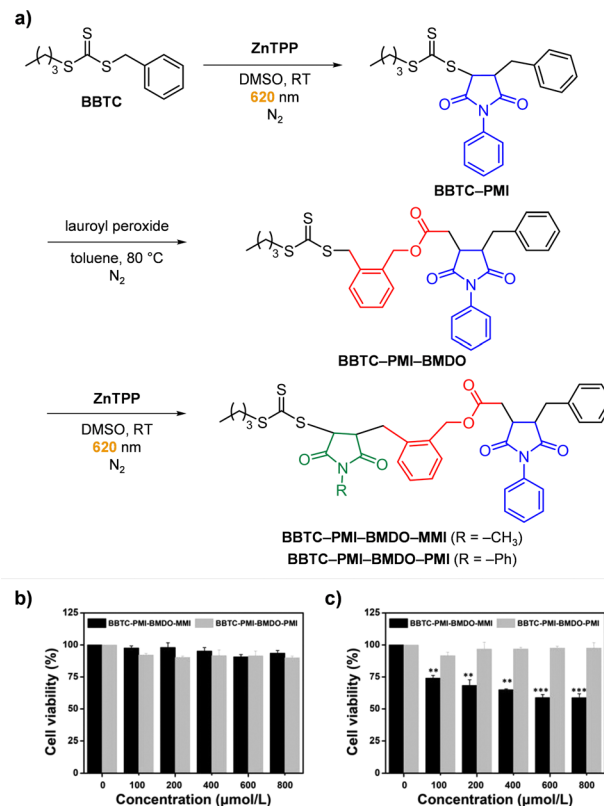


conducted sequential SUMI of up to five monomers in the gram scale while addressing scalability problems by the use of flow reactors for reaction and automated flash chromatography for purification.<sup>273</sup> ZnTPP in DMSO imparted oxygen tolerance and non-homopolymerizable electron-donating indene and electron-accepting *N*-substituted maleimide derivatives were alternatively polymerized (Scheme 21b).

Meanwhile, discrete oligomeric CTAs have aided the investigation of the stereochemical effect on photoactivation, copolymerization kinetics of a certain monomer in the RAFT process, and the influence of precisely designed sequences on polymeric properties. Into the pool of pairs of electron-donating (*e.g.*, indenenes and ( $\beta$ -methyl)styrene derivatives) and electron-accepting monomers (*e.g.*, *N*-substituted maleimides), various functionalities can be introduced as their substituents. Initially, SUMI of various  $\alpha,\beta$ -disubstituted vinyl monomers led to the synthesis of a stereospecific discrete oligomeric CTA.<sup>269,270</sup> Insertions of the examined cyclic *N*-substituted maleimides in *trans*-configurations were preferred owing to steric hindrances and restricted rotations of cyclic monomers, as combinedly evidenced by structural analysis by single-crystal X-ray diffraction and QC calculations.<sup>269</sup>

Xu and coworkers reported that for the successful SUMI of  $\beta$ -methylstyrene derivatives, careful selection of the CTA was required.<sup>275</sup> When  $\beta$ -methylstyrene derivatives were inserted next to maleimide into TTCs with different R groups using ZnTPP, the dimer was formed in 50% yield despite the complete conversion of the starting monoadduct of maleimide due to the degradation of the desired dimer after a certain reaction time. The proposed degradation mechanism was based on the  $\beta$ -methylstyrenenic carbon radical, which when fragmented abstracts hydrogen from an excess of  $\beta$ -methylstyrene derivatives and can no longer participate in the RAFT process (*i.e.*, chain transfer or recombination). Therefore, the authors postulated that to prevent the degradation of the product, (i) chain transfer of the fragmented  $\beta$ -methylstyrenenic carbon radical should occur faster than the hydrogen abstraction and (ii) the starting monoadduct should possess a better leaving R group than  $\beta$ -methylstyrenes. As expected, quantitative formation of the dimer was achieved when the first monomer was changed from maleimide to acrylonitrile (AN).

Xiao, Lai, and coworkers synthesized trimers consisting of two *N*-substituted maleimides and 5,6-benzo-2-methylene-1,3-dioxepane (BMDO) in between from *n*-butyl benzyl TTC (BBTC).<sup>274</sup> BMDO is a cyclic ketene acetal monomer whose radical ROP affords a polymer with a degradable ester bond in the backbone. Contrary to the successful insertion of *N*-substituted maleimide into BBTC using ZnTPP in DMSO under red light irradiation (620 nm), the use of thermal initiator lauroyl peroxide in toluene was required for the insertion of BMDO due to hydrolysis of BMDO in hygroscopic DMSO and poor solubility of ZnTPP in toluene (Scheme 22a). Two model trimers, BBTC-*N*-phenyl maleimide (PMI)-BMDO-*N*-methyl maleimide (MMI) and BBTC-PMI-BMDO-PMI, were degradable under basic conditions and cytocompatible with the human normal cell line (HUVEC) at up to 600  $\mu\text{mol L}^{-1}$  concentration (Scheme 22b), but only BBTC-PMI-BMDO-MMI was cytotoxic to the human cancer cell line



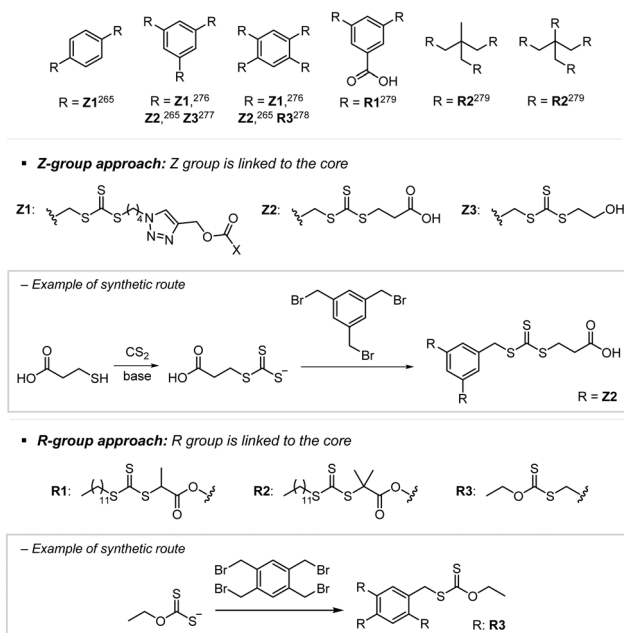
**Scheme 22** (a) Synthetic scheme for the trimers BBTC-PMI-BMDO-MMI and BBTC-PMI-BMDO-PMI. Cell viability of the two trimers against (b) human normal cell line (HUVEC) and (c) human cancer cell line (MCF-7) after 24 hours of incubation. Adapted with permission from (b) and (c) ref. 274 (Copyright 2021 American Chemical Society).

(MCF-7) (Scheme 22c) implying the potential of sequence-defined oligomers for biological applications.

#### 4.3.2. Architecture control

**4.3.2.1. Design of the CTA.** Designing an appropriate initiator is one of the simplest ways to obtain polymers with complex architectures (Scheme 23). For example, star or multi-arm polymers have been synthesized from multi-arm CTAs.<sup>265,276–279</sup> Multi-arm TTCs were prepared from thiols, carbon disulfide, and scaffold molecules with multiple bromines which underwent substitution reactions, whereas multi-arm xanthates were prepared using xanthogenate instead of thiol and carbon disulfide. Multi-arm polymers have been examined for various applications. Chapman, Boyer, and coworkers prepared a series of star polymers from two, three, or four-arm CTAs to investigate the relationship between the structures and binding affinities of polymers to protein.<sup>265</sup> Gormley, Chapman, and coworkers employed simple and oxygen-tolerant HTP polymerization to build a library of multivalent polymers possessing a strained alkyne at each arm end, which may be useful for conjugating biomolecules *via* strain-promoted azide-alkyne cycloaddition (SPAAC).<sup>276</sup> Boyer, Corrigan, Zhang, and coworkers controlled the mechanical properties of 3D printed objects in a broad range by optimizing the compositions (*i.e.*, the ratio and concentrations of multi-arm CTAs possessing different number of arms) of





**Scheme 23** Examples of multi-arm CTAs and the corresponding synthetic routes.

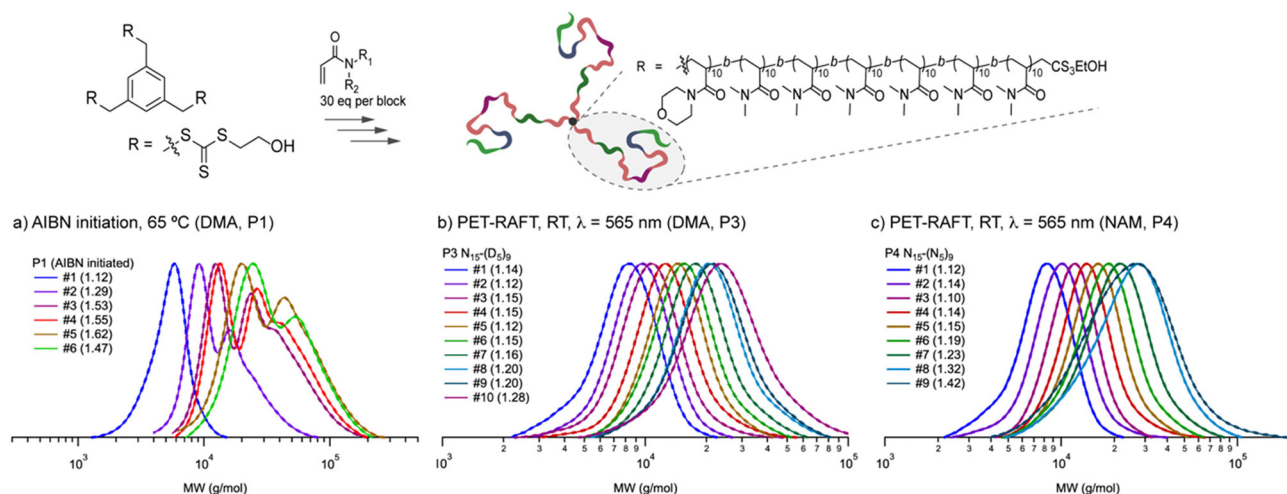
3D printable resins.<sup>279</sup> Finally, Chapman and coworkers analyzed the effects of the type of monomers (hydrophobic, hydrophilic, and charged) and their order of arrangements on the sizes and assemblies of multiblock star polymers in solution.<sup>277</sup>

It is noted that the core of star polymers can be linked to either the R or Z group of the CTA (Scheme 23). In the Z-group approach, the polymers grow from the fragmented R group liberated from the core, whereas in the R-group approach, the polymers grow from the core. For controlled polymerization, the Z-group approach is suitable to attach short arms at low grafting density because steric hindrance limits reattachment and chain transfer of propagating chains to the core Z group. The R-group approach suffers from biomolecular radical

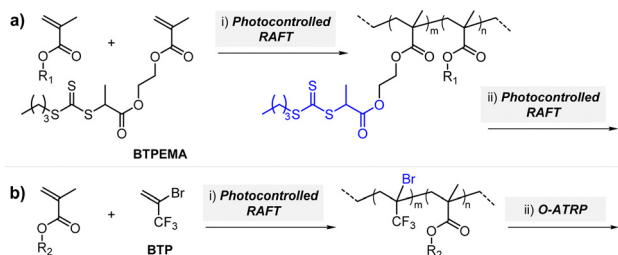
termination between either two star polymers (star–star coupling) or a star polymer and an exogenous macroradical rather than from the steric hindrance. Star–star coupling results in higher molecular weight byproducts, and reattachment of the exogenous macroradical instead of the Z group leads to the loss of CTA functionality and livingness, preventing further polymerization from dead chains to broaden the dispersity. Therefore, the synthesis of well-defined star polymers with (ultra)high molecular weights or multiple blocks with preserved end-group fidelity has particularly been challenging. Photocontrolled RAFT polymerization in the absence of exogenous initiating radicals thus emerged as a successful solution to the abovementioned problem as observed for photoiniferter polymerization by Qiao and coworkers<sup>278</sup> and PET-RAFT polymerization by Chapman and coworkers (Fig. 13).<sup>277</sup>

**4.3.2.2. Design of the monomer.** Other unique advantages of photocontrolled RAFT polymerization include spatiotemporal control, selectivity (which needs to be satisfied for the productive activation of the RAFT process), and orthogonality (to other polymerization methods). Carefully designed reaction conditions or systems along with properly functionalized monomers have enabled the preparation of complex polymeric architectures such as graft, comb-like, bottlebrush, and (hyper)branched polymers. For example, so-called “inimer” contains initiating moieties for two polymerizations, which can be activated selectively and in series (Scheme 24). Initially, as a mono“mer” for RAFT polymerization, the vinyl moiety comprises a polymer backbone while the other initiating moiety remains unreacted in the side chain. By changing the reaction conditions (*e.g.*, irradiation wavelength) or adding different types of monomers, the remaining “ini”tiator is then activated for another polymerization to transform the linear polymer into polymers with grafting chains or other high complexities.

Boyer, Xu, and coworkers synthesized graft copolymers *via* two selectively activated PET-RAFT polymerizations (Scheme 8 and 24a).<sup>106</sup> The reaction mixture contained two pairs of PC



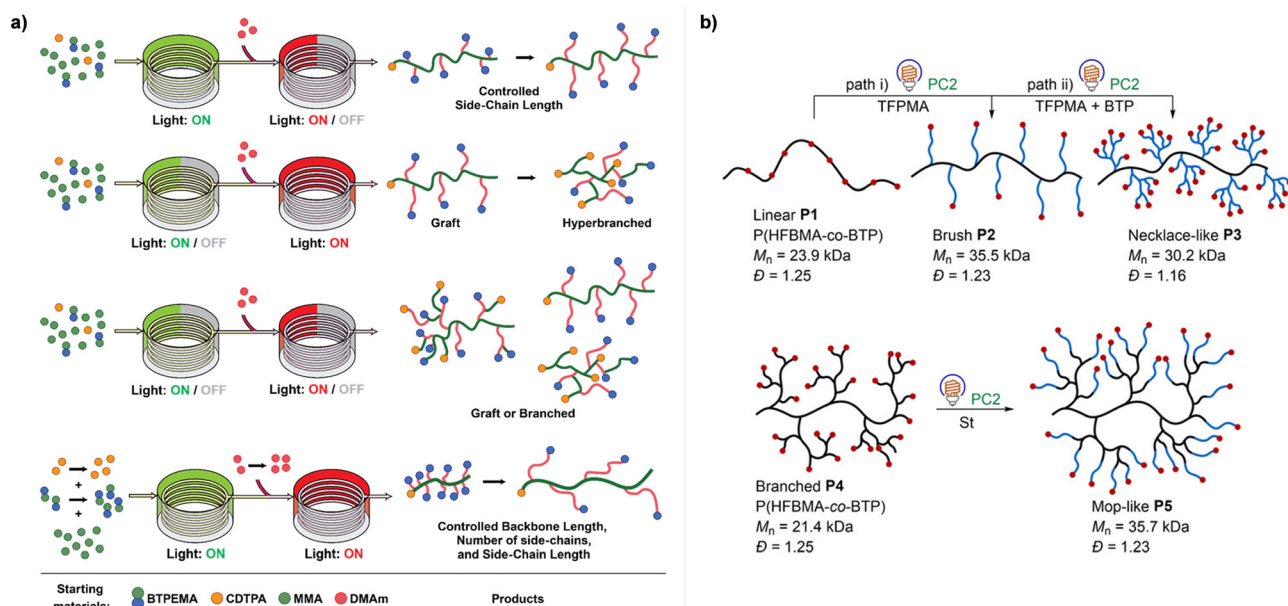
**Fig. 13** Synthesis of multiblock star polymers by thermal and ZnH<sub>2</sub>PP-catalyzed PET-RAFT polymerization. MWDs after each chain extension are shown below. Adapted with permission from ref. 277 (Copyright 2022 American Chemical Society).



**Scheme 24** Example of functionalized monomers and their stepwise activation to control polymer architectures.<sup>106,211</sup>

and CTA. The methacrylic polymer backbone was synthesized by the PheoA-catalyzed PET-RAFT polymerization of MMA and another methacrylate embedded with a TTC (BTPEMA) from CPADB under red light irradiation (690 nm, 2 mW cm<sup>-2</sup>). Then, MA was added to the reaction mixture for the ZnTPP-catalyzed PET-RAFT polymerization from the TTCs under green light irradiation (530 nm, 0.6 mW cm<sup>-2</sup>) to graft acrylic chains along the backbone. Herein, selective activation was possible as (i) the irradiation wavelengths were carefully set to avoid overlap in the absorption profiles of the two PCs PheoA and ZnTPP, and (ii) the pair of PheoA-CPADB and ZnTPP-TTC exhibited specific PC-CTA interaction. Selective excitation of one PC led to concomitant selective activation of one CTA within the reaction mixture. Switching the irradiation wavelength enabled sequential two-step polymerization in one-pot. However, it is noted that the second monomer MA should be added after the polymerization of MMA from CPADB because otherwise the insertion of MA into CPADB would block further propagation due to the change in C-S bond dissociation energy. Boyer, Hawker, Moad, and coworkers coupled PET-RAFT polymerization with photoiniferter polymerization

(Fig. 14a).<sup>280</sup> At first, the methacrylic backbone of MMA and BTPEMA was prepared from CDTPA via green light-mediated photoiniferter polymerization (520 nm, 4.4 W m<sup>-2</sup>) at 60 °C. Model polymerization of MMA confirmed that after the addition of MMA into CDTPA or BTPA, fragmentation of the RAFT intermediate was only favored for CDTPA owing to higher C-S bond dissociation energy. Subsequently, the unreacted BTPA moieties in the side chains were polymerized with DMAM. In this step, despite the increase in reaction temperature and/or irradiation at shorter wavelengths (*i.e.*, with higher energy), the rate of polymerization was not sufficiently high. Thus, PET-RAFT polymerization using ZnTPP was conducted instead. This one-pot approach could be operated even in one-pass using a flow reactor. In a one-pass reaction system, the solution of DMAM and ZnTPP for the second reaction was easily added before the reaction mixture flows to the second batch, and irradiation of each batch was separately turned on and off. Moreover, by simply varying the injection volume, concentration, flow rate, and/or irradiation time, the synthesis of diverse graft and branched copolymers possessing backbones and/or side chains with different lengths and backbones with different numbers of grafted chains was achieved. Matyjaszewski and coworkers utilized two sequential photoiniferter polymerizations for the synthesis of comb-like and bottlebrush polymers.<sup>110</sup> The polymerization of the methacrylic backbone from CDTPA under green light irradiation (520 nm, 4.25 mW cm<sup>-2</sup>) was followed by the polymerization of MA or DMAM from pendant BTPA of polymerized BTPEMA under blue light irradiation (465 nm, 6.5 mW cm<sup>-2</sup>). Depending on the MMA/BTPEMA ratio in the first polymerization, the grafting density of acrylic side chains in the resulting polymer was facily controlled so that the homopolymer of “inimer” was transformed into a bottlebrush polymer.

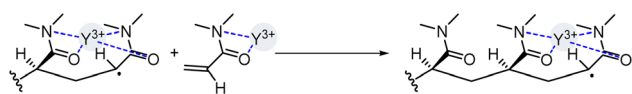


**Fig. 14** Diverse polymer architectures obtained by (a) switching each reactor on and off or manipulating the parameters (*e.g.*, flow rate and injection volume) in flow chemistry and (b) combination of different photomediated RDRP processes. Adapted with permission from (a) ref. 280 (Copyright 2021 American Chemical Society) and (b) ref. 211 (Copyright 2020 John Wiley & Sons, Inc.).



The second polymerization from the initiating moiety of the inimer after the first polymerization of vinyl moieties need not be limited to visible-light-driven RAFT polymerization. The orthogonality of visible-light-driven RAFT polymerization to other polymerization methods and the accompanying ability to interconvert two orthogonal processes for the facile synthesis of multiblock copolymers possessing various (non)vinyl monomers has been discussed in Section 4.3.1.2. Chen and coworkers designed an inimer containing both vinyl and alkyl bromide functionalities for photocontrolled divergent synthesis of polymers with a wide variety of topologies (Scheme 24b).<sup>211</sup> The reaction system comprised two PCs (EY and a phenothiazine derivative), fluorinated-TTC, methacrylate monomers bearing different numbers of fluorine atoms, and 2-bromo-trifluoropropene (BTP) as an inimer (Fig. 14b). Owing to the different excited-state redox potentials, reduction of bromine for O-ATRP after the polymerization of BTP could only be achieved using the phenothiazine-derived PC, whereas TTC could be reduced by both PCs for PET-RAFT polymerization. Therefore, EY-catalyzed PET-RAFT polymerization of the linear copolymer of BTP and other monomers followed by phenothiazine derivative-catalyzed O-ATRP afforded branched polymers in which bromine at any location served as a branching point. Variation in the ratio of BTP and other monomers in copolymerization, target DP, and/or location of bromine led to various polymer topologies such as linear, brush, necklace-like, branched, and mop-like.

**4.3.3. Stereochemistry control.** Control over stereochemistry during polymerization or tacticity of polymers is known to critically affect the thermomechanical properties of polymeric materials. However, stereocontrolled polymerization of vinyl monomers has been challenged by the generation of a planar  $sp^2$ -hybridized propagating radical with no facial preference for the addition of monomer.<sup>281</sup> Selective addition of the monomer to one face can be achieved in the presence of auxiliary additives that confine the propagating radical. Boyer and coworkers added rare earth triflate  $Y(OTf)_3$  into the stereocontrolled  $Ir(ppy)_3$ -catalyzed PET-RAFT polymerization of DMAM in a methanol/toluene mixture under blue light irradiation (460 nm, 0.7 mW  $cm^{-2}$ ).<sup>282</sup> Coordination of the Lewis acid  $Y(OTf)_3$  to the amide functionalities of the monomer during polymerization allowed good control over the tacticity of polymers (Scheme 25). Although the weaker yet possible coordination of  $Y(OTf)_3$  to TTCs slightly increased the dispersity, control over the molecular weight or livingness was not influenced so that a stereoblock or stereogradient copolymer of atactic and isotactic blocks could be prepared. The authors modulated the tacticity of polymers by using DMSO which tightly complexes with  $Y(OTf)_3$  to weaken the complexation between  $Y(OTf)_3$  and DMAM and thereby offers stereochemistry control. Nevertheless, the reaction system could



Scheme 25 Coordination of  $Y(OTf)_3$  to the amide functionality to increase the isotacticity of poly(DMAM).<sup>282</sup>

not be expanded to another PC (*i.e.*,  $Ru(bpy)_3Cl_2$ ) presumably due to unfavorable interaction between the bipyridine ligand and  $Y(OTf)_3$ . Substitution of  $Ir(ppy)_3$  for  $Ru(bpy)_3Cl_2$  resulted in no or poorly controlled polymerization. On the other hand, for photoiniferter polymerization in the absence of a PC, Zhu, Boyer, and coworkers employed the fluoroalcohol 1,1,1,3,3,3-hexafluoro-2-propanol (HFIP) to control the stereochemistry of poly(VAc).<sup>283</sup> Interaction of fluoroalcohol with vinyl monomers introduced steric hindrance and improved stereospecificity during propagation. These interactions enhanced at low temperatures, so syndiotacticity of the polymer was controlled by temperature and the choice of solvent. The highest syndiotacticity diad (62%) for polymerization in HFIP as a solvent at  $-20\text{ }^\circ\text{C}$  was decreased to 59 and 56% along with an increase in the polymerization temperature to 0 and  $25\text{ }^\circ\text{C}$ , respectively, whereas the change of solvent to isopropyl alcohol or bulk polymerization led to 52 or 53%. The dependencies of stereospecificity on the polymerization temperature and solvent were consistent with those reported by Kwarck and coworkers for the preparation of syndiotactic-rich poly(VAc) using fluoroalcohols.<sup>284</sup> Herein, the polymerization was initiated by photoinitiator BAPO.

**4.3.4. Dispersity control.** Apart from the main challenge and aim of RDRP to synthesize nearly monodisperse polymers, the usefulness to tailor the dispersity and shape (*e.g.*, breadth, skewness, and kurtosis) of MWD has been revealed to be important for controlling the physical, thermal, and rheological properties of polymers.<sup>53,285,286</sup> Synthetic strategies reported thus far include physical blending of polymers with a range of dispersities, temporally regulated initiation to prepare polymers with different lengths, and tailoring catalyst concentration.<sup>287</sup>

Boyer and coworkers introduced flow chemistry in combination with the use of ZnTPP as a PC.<sup>288–290</sup> In PET-RAFT polymerization of acrylamides in a continuous flow reactor, polymers of different molecular weights were generated by simply adjusting the flow rates, concentration of the CTA, and intensity or wavelength of the light source (blue, green, or red).<sup>288</sup> Blending of the prepared polymers resulted in the target MWD as per the calculated theoretical curves (Fig. 15a)<sup>288</sup> or the mathematically modelled fitting which is the so called computer-guided approach.<sup>290</sup> The polymer retained high end-group fidelity so that polymerization from the blended poly(DMAM) led to successful copolymerization with NAM or benzyl acrylate (BzA) and yielded a block copolymer with tailored compositional gradients (Fig. 15b).<sup>289</sup> The second monomer was easily added from a separated line (pump) in the flow setup. However, to fully utilize the aforementioned simplicity and robustness of the flow chemistry technique for dispersity control, fluid dynamics or profiles and parameters such as tube diameter, volume, flow rate, and reactant volume have to be carefully investigated and optimized.<sup>290</sup>

In the case of PET-RAFT polymerization in batch, Anastasaki and coworkers mixed two CTAs at varying ratio,<sup>291</sup> as previously applied for AIBN-initiated conventional RAFT polymerization by the same research group.<sup>292</sup> In EY-catalyzed PET-RAFT polymerization in DMSO under blue light irradiation (465 nm, 12 W), two CTAs possessing different transfer constants or reactivities





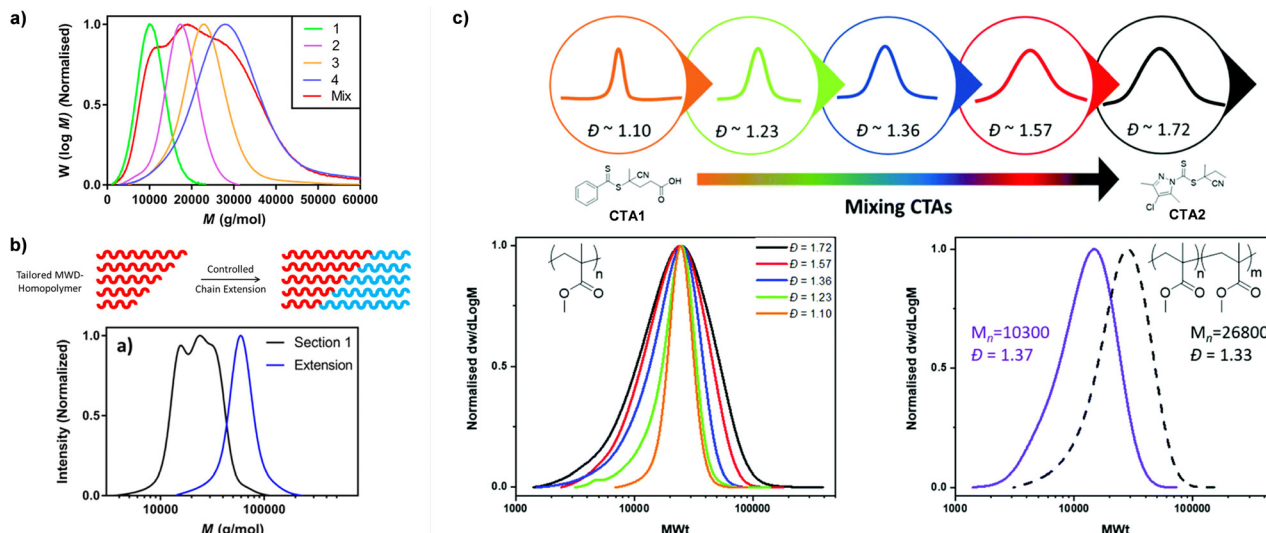


Fig. 15 (a) MWDs for monomodal poly(DMAM)s (1–4) and their blended mixture. (b) Narrowing the initially broad MWD through chain extensions. (c) The variation in dispersity as two CTAs were mixed in different ratios (aligned by the peak molecular weight value). Poly(MMA) prepared from 10 mol% CTA1 and 90 mol% CTA2 was successfully extended with MMA. Adapted with permission from (a) ref. 288 (Copyright 2017 American Chemical Society), (b) ref. 289 (Copyright 2018 American Chemical Society), and (c) ref. 292 (Copyright 2020 The Royal Society of Chemistry).

(dictated by R and mostly Z group) were mixed at varying ratios to obtain polymers with any intermediate targeted value of dispersity (Fig. 15c). One CTA with the higher transfer constant afforded polymers with low dispersity (as the lower limit), whereas another CTA with the lower transfer constant afforded polymers with high dispersity (as the higher limit). Apart from the discrepancy in reactivities, two CTAs should separately provide monomodal MWD, high end-group fidelity, and agreement between theoretical and experimental molecular weights for polymerization of a given monomer. The method was effective for MMA, MA, and DMAM in which dispersity was tunable across a wide range (1.08–1.82). Konkolewicz and coworkers expanded the abovementioned method to poly(vinyl ketone)s.<sup>293</sup> Herein, after the generation of initiating radicals through Norrish chemistry of vinyl ketone monomers under blue light irradiation (450 nm, 7.9 mW cm<sup>-2</sup>), either homopolymers of phenyl or methyl vinyl ketone or copolymers of ethyl acrylate were synthesized from the mixture of TTC (higher activity) and xanthate (lower activity). Dispersity was increased with the ratio of xanthate and was able to be modulated further owing to the photodegradable nature of vinyl ketone under UV light irradiation.

Anastasaki and coworkers also utilized their strategy of mixing CTAs to prepare two homopolymers each possessing a wide range of dispersities and blended them to provide polymers with unrivalled precise control of both dispersity and MWD shape.<sup>294</sup> Moreover, the strategy was still valid for a single CTA with switchable reactivity, rather than the mixture of two CTAs.<sup>295</sup> Herein, the reactivity of the CTA (methyl 2-[methyl(4-pyridinyl)-carbamothioylthio]propionate) was *in situ* switched back and forth by the addition of acid and base to the reaction mixture. It was still only reported for VA-044 initiated thermal RAFT polymerization; nevertheless, it is notable that on-demand control over dispersity of the sequence-defined multiblock copolymer of acrylamides was accomplished by simply

adjusting acidic and basic conditions along with the subsequent monomer addition.

**4.3.5. Ultrahigh-molecular-weight (UHMW) polymer synthesis.** Synthesis of UHMW polymers, with molecular weights over 10<sup>6</sup> g mol<sup>-1</sup>, requires fast and efficient generation of propagating radicals and monomers with a high propagation rate, while minimizing the probability of side reactions (*i.e.*, chain transfer and termination).<sup>296</sup> As neither PET-RAFT nor photoiniferter polymerization uses external initiators, the reaction becomes free of the initiator-derived radicals and side reactions therefrom. Acrylamide monomers possessing high  $k_p$  in high polarity solvents (mostly water) coupled with efficiently photolyzable CTAs (mostly xanthate) thus has been extensively employed for UHMW polymer synthesis. Radical influx should be kept high enough for fast and efficient propagation but should be (re)generated in a controlled manner, which could be achieved under visible light irradiation exclusively by the use of a highly efficient PC in the case of PET-RAFT polymerization.

Supramolecular perylene diimide/cucurbit[7]uril complex/TEOA under green light irradiation (535 nm, 5 W) induced aqueous polymerization of DMAM from TTC with molecular weight up to 1.04 × 10<sup>6</sup> g mol<sup>-1</sup> and a dispersity of 1.33 after 8 hours.<sup>297</sup> This photoinitiating system was so efficient that only 1 ppm was required, but the role of TEOA was claimed to be rather complex, including initiation of RAFT polymerization after its single-electron oxidation by excited-state perylene diimide. Photoenzymatic RAFT polymerization enabled the synthesis of UHMW polymers of unconjugated NVP, *N*-vinylcaprolactam with rather narrow dispersity ( $\bar{D}$  = ~1.39)<sup>164</sup> and of monomers with low  $k_p$  (*e.g.*, OEGMA)<sup>165</sup> under violet light irradiation (405 nm, 11.5 W). These exceptional reactivities were attributed to the generation of stable radicals in low concentration by GOx/glucose as the PC, and the high reducing

power of excited-state  $\text{FADH}^-$  to efficiently conduct the polymerization process.

On the other hand, Chen and coworkers reported a mechanically distinct strategy for the synthesis of UHMW fluoropolymers from TTCs (up to  $3.05 \times 10^6 \text{ g mol}^{-1}$  and  $D \leq 1.12$  after 2–8 hours) using  $\text{Ir}(\text{ppy})_3$  in DMSO under white light irradiation ( $33 \text{ mW cm}^{-2}$ ) (Fig. 16a).<sup>190</sup> Fluoropolymers from a polymer chemistry perspective have been appreciated due to their functionally diverse properties,<sup>298</sup> but here strong and selective fluorine–fluorine interaction also played a key role in excellent regulation over propagation (Fig. 16b). As depicted, at first, the CTA with a lipophilic DMAM block as the R group (denoted as R2) and an alkyl chain as the Z group (denoted as R1) stabilized the resulting emulsion with a fluorophilic interior where fluoromonomers were located. As some portions of the CTA (propagating group, PG) participated in polymerization, fluorine–fluorine interaction between the grown polymers and the monomers resulted in phase separation. The remaining intact CTA (supporting group, SG) residing in the outer solvent phase had no access to the monomer but to RAFT equilibrium, providing the polymerization of fluoromonomers from PG with the additional control and livingness. Replacing  $\text{Ir}(\text{ppy})_3$  with a PC possessing a fluoro-substituent significantly reduced monomer conversion, evidencing that single-electron transfer between the excited-state PC and CTA and subsequent polymerization occurred in the outer solvent phase. This distinctive spatial confinement strategy for the preparation of well-defined UHMW fluoropolymers was compatible with fluorinated (meth)acrylates and methacrylamides as well.

**4.3.6. Photoinitiated polymerization-induced self-assembly (photo-PISA).** Visible-light-driven RAFT polymerization has been applied to polymerization-induced self-assembly (PISA) to construct nano-sized assemblies with various morphologies including

worms, vesicles, and micelles. These assemblies are used for nanocomposite fabrication or the encapsulation of hydrophobic drugs or proteins in vesicles. As the solvophobic block is extended from a macro-CTA with a solvophilic block, the resulting morphologies depend on the target DP or length of the solvophobic block, composition of the copolymer, and solid content. Compared to the case of the conventional thermally initiated RAFT polymerization, visible-light-driven RAFT polymerization has offered better control over particle size and expanded the available morphologies. In addition to the absence of exogenous radicals, the ability to maintain the reaction temperature throughout the entire process (from polymerization to phase separation-induced morphological transition) reduced the influence of high temperature on both the polymerization kinetics and morphology and allowed deriving an isothermal phase diagram. As not all thermal initiators require severe heating (typically above  $70^\circ\text{C}$ ), O'Reilly and coworkers could examine the influence of the initiation method on end-group fidelities of polymers and the resulting morphological transitions. In the case of photo-PISA under violet light irradiation (405 nm, 800 mW) based on the photoiniferter process, further irradiation of the synthesized polymer assemblies (post-synthetic irradiation) removed the end group of polymers and transformed their morphologies.<sup>299</sup> In contrast, *via* an identical process under lower irradiation power (160 mW) either in the presence or absence of VAZO-44 which decomposes at  $37^\circ\text{C}$ , stable aggregates were formed irrespective of the initiation mechanism. Type I and II photoinitiators that produce free radicals under irradiation *via* homolytic cleavage or hydrogen abstraction have also been widely employed; however, in this section, we focus on the use of PCs. For the current status and future directions of RAFT-mediated PISA initiated by various means including visible light, please refer to the very recent review article reported by Thang, Fan, and coworkers.<sup>300</sup>

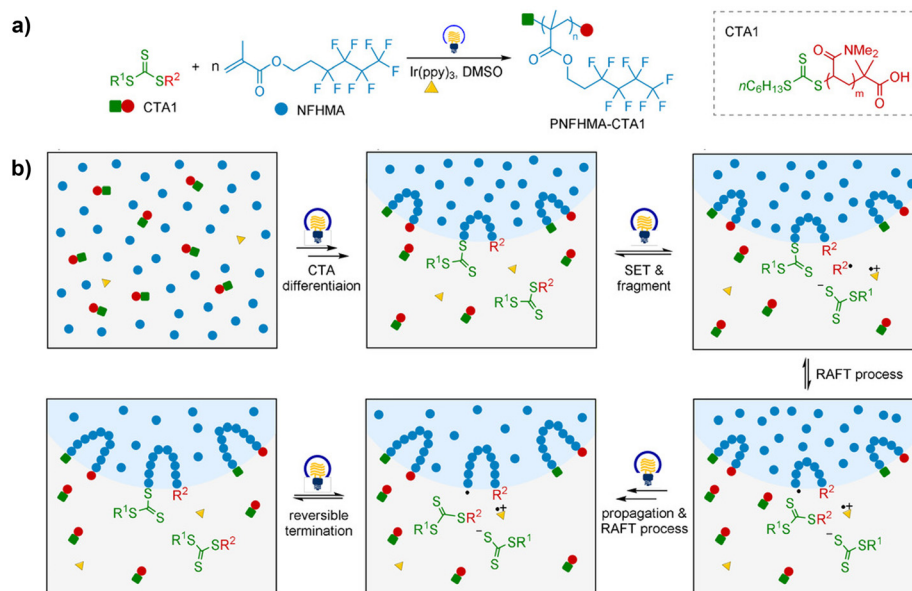


Fig. 16 (a) Synthetic scheme of UHMW fluoropolymers and (b) mechanistic concept for CTA differentiation for regulation over propagation. Adapted with permission from ref. 190 (Copyright 2020 John Wiley & Sons, Inc.).



Boyer and coworkers reported the first photo-PISA that was mediated by  $\text{Ru}(\text{bpy})_3\text{Cl}_2$  under blue light irradiation (460 nm,  $0.7 \text{ mW cm}^{-2}$ ).<sup>192</sup> Up to 100 ppm of  $\text{Ru}(\text{bpy})_3\text{Cl}_2$  was loaded for the dispersion polymerization of solvophobic benzyl methacrylate (BzMA) from the solvophilic poly(OEGMA)-based macro-CTA. The dispersity of the polymer was maintained at lower than 1.3 despite the presence of unreacted or dead chains with lower molecular weight than the theoretical values and increase in the viscosity of the solution. ZnTPP was the very first PC for oxygen-tolerant photo-PISA and under red or yellow light irradiation at longer wavelength (635 and 560 nm, respectively).<sup>301</sup> Oxygen tolerance was achieved by the combination of ZnTPP as a singlet oxygen generator and ascorbic acid<sup>301</sup> or 9,10-dimethylanthracene<sup>146</sup> as a singlet oxygen quencher, so as to conduct the reaction in an open vessel at ultralow volumes (40  $\mu\text{L}$  scale) without prior deoxygenation. However, only in the presence of 9,10-dimethylanthracene, perfect temporal control of polymerization was observed. Furthermore, ascorbic acid in larger amount seemed to affect self-assembly behavior. Very recently, Boyer and coworkers for the first time reported oxygen-tolerant photo-PISA under NIR irradiation (730 nm,  $12 \text{ mW cm}^{-2}$ ) using  $\text{ZnPCS}_4^-$  in combination with TEOA.<sup>173</sup>

Meanwhile, ZnTPP could still generate singlet oxygen after its encapsulation in the hydrophobic core of the vesicle *via* dialysis of the reaction mixture into water, implying the potential use of the resulting vesicle as a photodynamic therapeutic agent.<sup>301</sup> It was insolubility of ZnTPP in water that enabled the encapsulation. Similarly, doxorubicin, a hydrophobic antitumor drug, was encapsulated in spherical polymeric NPs.<sup>302</sup> Herein, doxorubicin was added into the reaction mixture from the beginning of the polymerization. While the polymerization process did not significantly affect the bioactivity of doxorubicin, the polymerization kinetics were improved, implying the potential photocatalytic capability of doxorubicin for photomediated polymerization.

ZnTMPyP, as a water-soluble analogue of ZnTPP, allowed aqueous dispersion polymerization,<sup>147</sup> and simplified photo-PISA by eliminating the preparation of solvophilic macro-CTAs which undergo chain extension with solvophobic monomers.<sup>200,201</sup> Instead, hydrophilic OEGMA and hydrophobic core-forming diacetone acrylamide (DAAm) were put together for gradient copolymerization based on preferential incorporation of OEGMA over DAAm owing to different reactivities of methacrylates and acrylamides for polymerization.<sup>201</sup> If both solvophilic and solvophobic blocks are prepared from the same monomer families, slow injection of solvophobic monomers into the reaction mixture gradually changed the ratio of the solvophobic- to solvophilic block length within a polymer chain, which led to PISA.<sup>200</sup> Lastly, Chen and coworkers controlled the size of raspberry-like NPs with a poly(pentafluorostyrene) core by light intensity.<sup>303</sup> At around 330 ppm of  $\text{Ir}(\text{ppy})_3$  and the same target DP, strong irradiation ( $33 \text{ W cm}^{-2}$ ) as compared to weak light irradiation ( $0.56 \text{ W cm}^{-2}$ ) activated more CTAs to decrease the polymer molecular weight at the same monomer conversion, and then to reduce the size of NPs. The effect of intensity and wavelength of light irradiated on

polymerization control (*e.g.*, molecular weight and end group fidelity) and thus the morphologies of synthesized NPs has been reported for several cases.<sup>301,303</sup>

Organic PCs such as PTH,<sup>304</sup> EY,<sup>135,170,305</sup> Rose Bengal,<sup>306</sup> and Rhodamine 6G<sup>307</sup> have also been employed but mostly in combination of tertiary amines to achieve oxygen-tolerant reaction systems and enhance the reaction rate. Oxygen tolerance in photo-PISA particularly allows one to conduct the reaction in a continuous flow reactor with simple optimization of reaction parameters.<sup>135,305,308</sup>

**4.3.7. Bioapplications.** For the successful preparation of hybrid biomaterials composed of natural biomolecules (*e.g.*, DNA, cells, and proteins) and synthetic polymers, deoxygenation processes (*e.g.*, freeze-pump-thaw method and  $\text{N}_2$  purging process) and harsh reaction conditions that would affect the integrity of biomolecules should be avoided. In this regard, PET-RAFT polymerization has been widely applied for bioapplications because it is rapid, oxygen-tolerant and can be conducted in biologically relevant media under mild reaction conditions without heating.<sup>309,310</sup>

Soh, Hawker and coworkers reported *in situ* grafting-to conjugation of poly(acrylamide)s onto several biomolecules (L-phenylalanine, 5-[(2-aminoethyl)amino]-naphthalene-1-sulfonic acid sodium salt (EDANS), and bovine serum albumin (BSA)) *via*  $\text{Ru}(\text{bpy})_3\text{Cl}_2$ /sodium ascorbate-catalyzed PET-RAFT polymerization under blue light irradiation (470 nm,  $80 \text{ mW cm}^{-2}$ ).<sup>150</sup> The copolymerization of NAM and *N*-acryoylsulfosuccinimide (NASS) with the target DP of 40 reached 95% conversion after 15 minutes even without prior deoxygenation. This short reaction time minimized the hydrolysis of succinimides and allowed *in situ* preparation of bioconjugates *via* the addition of biomolecules to the polymerization mixture.

To functionalize the surface of live cells, more rapid kinetics under milder reaction conditions are required to reduce the potential harm to the cells. Soh, Hawker and coworkers employed EY/TEA-catalyzed PET-RAFT polymerization under blue light irradiation (465 nm,  $5.0 \text{ mW cm}^{-2}$ ) for grafting-from functionalization of live yeast and mammalian cells.<sup>67</sup> After 10 minutes of Ar purging and 5 minutes of irradiation, the cell surface was successfully functionalized with polyacrylamides bearing poly(ethylene glycol) (PEG) side chains while maintaining both high control over polymerization and high cell viability. Copolymerization with azido- or biotin-incorporated monomers allowed post-polymerization functionalization of the cells *via* copper-free SPAAC or streptavidin conjugation chemistry, respectively, which is promising to manipulate the cell surface and regulate cell-cell interactions. Although this early demonstration required Ar purging and the use of blue light, the recently reported examples with novel modified PCs have improved the reaction system toward a wide range of irradiation wavelengths. Qiao, Tang, Fu, and coworkers synthesized SA-TCPP for TEOA-cocatalyzed PET-RAFT polymerization of OEGMA ( $M_n = 480 \text{ g mol}^{-1}$ ) in the presence of mouse fibroblast cells (NIH 3T3) in a 96-well plate.<sup>223</sup> After 45 minutes of red light irradiation, the monomer conversion and cell viability were 11 and 46%, respectively. Subsequently, a ZnTPP-derived 2D nanosheet





reported by Cai, Li, and coworkers was employed for the ascorbic acid-cocatalyzed PET-RAFT polymerization of OEGA ( $M_n = 480 \text{ g mol}^{-1}$ ) in the presence of human embryonic kidney 293 cells.<sup>149</sup> The monomer conversion was 60.8–73.2% resulting in polymers with a rather broad dispersity (1.21–1.32) without negatively impacting the cell viability after two hours of irradiation under red light (635 nm,  $3.6 \text{ mW cm}^{-2}$ ). Although the reaction conditions have to be further optimized, these preliminary studies suggested that PET-RAFT polymerization is suitable for cytocompatible *in vivo* polymerization in cellular applications.

Barner-Kowollik, Ng, Weil, and coworkers synthesized DNA-polymer conjugates from CTA-terminated single-stranded DNA (ssDNA) (Fig. 17a).<sup>311</sup> EY with the aid of ascorbic acid as a singlet oxygen quencher under blue light irradiation (470 nm,  $4.0 \text{ mW cm}^{-2}$ ) was employed to avoid problematic deoxygenation at ultralow reaction volumes (20  $\mu\text{L}$ ). However, good control over dispersity could only be achieved after the freeze-pump-thaw process despite the use of ascorbic acid. The synthesized ssDNA-polymer conjugates could be hybridized with complementary ssDNA, and the size of the hybridized structure was increased with the size of the conjugated

polymer. Lipid-polymer conjugates, prepared from CTA-terminated lipid using EY under blue light irradiation (465 nm,  $5.0 \text{ mW cm}^{-2}$ ), could self-assemble and were used to mediate assemblies of gold NPs.<sup>312</sup>

Lastly, proteins are also of great interest. Once a polymer is conjugated to a protein, the properties of the protein would be influenced as in the case of a protein attached to PEG, being widely used in the clinic worldwide.<sup>313,314</sup> PEG enhances the pharmacokinetic/dynamic properties while reducing the immunogenicity of therapeutic proteins.<sup>315</sup> Therefore, owing to the large diversity of polymers and the increasing desire to utilize proteins for the degradation of plastics,<sup>316</sup> for capture of heavy metal ions,<sup>317,318</sup> and as catalysts in organic chemical synthesis,<sup>319</sup> researchers are attracted to develop novel protein-polymer conjugates (PPCs). To reduce the potential harm to the structural integrity of proteins and preserve their enzymatic activities after polymerization, PET-RAFT polymerization that operates under mild reaction conditions and offers oxygen tolerance has been particularly recognized as a promising method.

Averick and coworkers studied the effects of the hydrophobicity and molecular weight of grafted acrylamide polymers on the enzymatic activities of two lipases (*Candida antarctica* lipase B and *Thermomyces lanuginosus* lipase).<sup>141</sup> EY/TEMED-catalyzed PET-RAFT polymerization from the grafted TTC in DMF was performed. Hydrophobic polyacrylamides led to a molecular weight-dependent increase in the activities and stability of lipases, so that the resulting hydrophobic hybrids could be immobilized on a glass slide while retaining the enzymatic activities. Whittaker and coworkers utilized EY with a tertiary amine to attach hydrophilic and low-fouling fluoropolymers to BSA as a model protein for *in vivo* quantitative tracking of polymer-conjugated therapeutics by  $^{19}\text{F}$  magnetic resonance imaging (MRI) and extending the pharmacokinetics (e.g., blood circulation time) (Fig. 17b).<sup>70</sup> Another hydrophilic sulfoxide-containing polymer improved the pharmacokinetics of lysozymes by reducing macrophage cellular uptake.<sup>320</sup> Although the listed applications of PPCs still have been mainly limited to therapeutics, many researchers focused on how to use PET-RAFT polymerization as a more efficient platform for preparation of PPCs, which would allow extension of the diversity of protein-based functional materials in the near future. For example, macromolecular and heterogeneous PCs for their facile purification after the reaction,<sup>247,321,322</sup> or PCs operating under irradiation at longer wavelength (*i.e.*, with lower energy) were developed.

Ever since Boyer and coworkers employed  $\text{Ru}(\text{bpy})_3\text{Cl}_2$  under blue light irradiation for PET-RAFT polymerization from BSA macroinitiator which was chemically modified to possess TTC moieties,<sup>193</sup>  $\text{Ru}(\text{bpy})_3\text{Cl}_2$ ,<sup>323</sup> EY and its derivatives,<sup>68,70,141,247,249,320,321</sup> ZnTPP derivative,<sup>322</sup> and a novel purely organic PC<sup>176</sup> have been discovered and utilized. Although EY is biocompatible and has facilitated the use of green LEDs as an irradiation source, tertiary amines<sup>68,70,141,247,320</sup> and/or ascorbic acid<sup>247,321</sup> need to be added to achieve oxygen tolerance. Photodegradation of EY is another issue.<sup>141,247,324</sup> Averick and coworkers observed photodegradation of EY in the presence of TEMED as an amine cocatalyst in DMF after up to 60 min of irradiation at

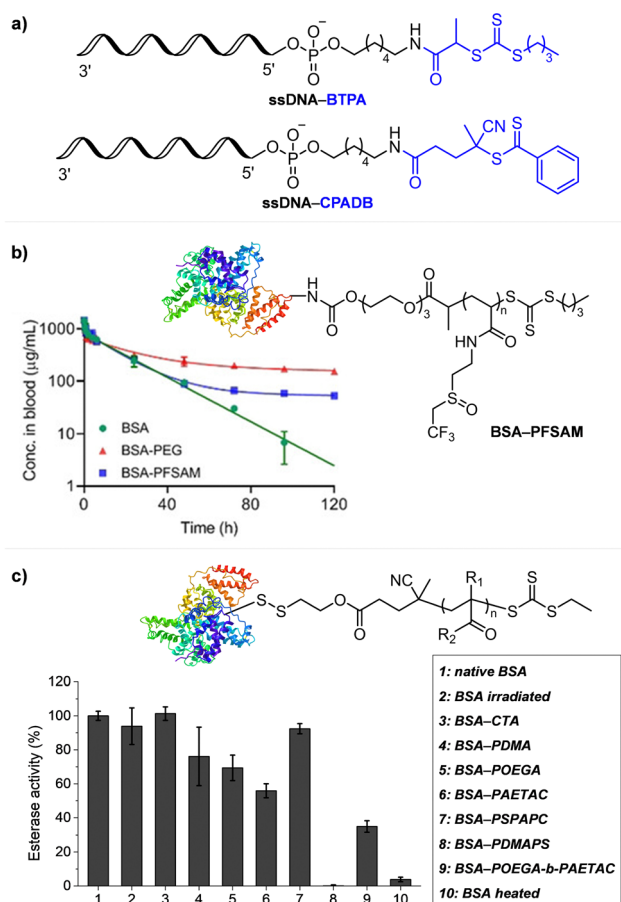


Fig. 17 (a) Schematic representation of ssDNA-CTA conjugates for synthesis of ssDNA-polymer conjugates.<sup>311</sup> (b) Pharmacokinetics and (c) enzymatic activities of BSA and various BSA-polymer conjugates. Adapted with permission from (b) ref. 70 (Copyright 2020 John Wiley & Sons, Inc.) and (c) ref. 176 (Copyright 2022 John Wiley & Sons, Inc.).





460 nm.<sup>141</sup> Sumerlin and coworkers observed photobleaching of EY under irradiation at 458 nm ( $0.6 \text{ mW cm}^{-2}$ ) and 515 nm ( $0.5 \text{ mW cm}^{-2}$ ), which was attributed to one of the possible side reactions caused by ascorbic acid at high concentration.<sup>247</sup> Due to the lack of singlet oxygen quenchers under aqueous conditions, the ZnTPP derivative where zinc porphyrin was integrated into a MOF (MOF-525-Zn) required purging with Ar, in contrast to the excellent oxygen tolerance of ZnTPP observed in the presence DMSO which acted as both a solvent and a singlet oxygen quencher.<sup>322</sup> Although these water-insoluble and heterogeneous PCs can be easily purified after the reaction and even reused, a water-soluble PC that enables oxygen-tolerant polymerization without additives is also beneficial; nevertheless, it has been limited to Ru(bpy)<sub>3</sub>Cl<sub>2</sub>. In this regard, Kwon and coworkers in collaboration with Gierschner and Koo developed a highly efficient water-soluble purely organic PC 3DP-MSDP-IPN.<sup>176</sup> Efficient generation of triplet excited states, substantially negative  $E_{\text{ox}}^*$  ( $-1.56 \text{ V vs. Ag/AgCl}$ ), and highly stable radical cation of the PC synergetically afforded oxygen tolerance (or even acceleration of polymerization kinetics by oxygen present at limited concentration; for a detailed explanation, please see Section 3.4). Thus, polymerization was conducted using the BSA macroinitiator in ambient and aqueous environments without additives under green light irradiation (515 nm,  $10 \text{ mW cm}^{-2}$ ). A variety of acrylamide/acrylate monomers, including hydrophilic and ionic (cationic, anionic, and zwitterionic) monomers, were polymerized from the protein macroinitiator to affect the enzymatic activities to varying degrees as compared to native BSA (Fig. 17c). However, the authors observed that the molecular weights of the polymers cleaved from the protein were smaller than the corresponding theoretical values and presumed that *via* reactions between the excited-state PC and disulfide bonds of BSA, thiyl radicals might be generated and became additional reaction sites for the propagating radical intermediates. Although the formation of thiyl radicals has not yet been detected, the selectivity issue for the PC, by PET, to selectively activate the CTA over other reactive groups within proteins (*e.g.*, TTCs over disulfide bonds) needs to be further investigated to design better photocatalytic systems for future bioapplications. Development of novel PCs and expansion of the available water-soluble and/or biocompatible PCs, rather than Ru(bpy)<sub>3</sub>Cl<sub>2</sub> and EY, would stimulate related research and allow the synthesis of polymers comprising various monomers rather than acrylamide monomers which are extensively preferred because of their more rapid polymerization kinetics than those of other monomer families.

Meanwhile, without grafting and conjugation, polymers can also affect biomolecules. In polymer-protein hybrids, certain polymers could be hybridized with certain proteins, thereby helping to maintain the protein activities in non-native environments such as organic solvents<sup>316,325,326</sup> and thermal denaturing conditions.<sup>266</sup> Synthetic antimicrobial polymers that mimic the peptides with antimicrobial activities were discovered by investigating the structure-activity relationships of a large library of polymers composed of different categories of monomers (*e.g.*, hydrophobic, hydrophilic, and cationic) with varying compositions<sup>263,327</sup> and compositional drifts along the

polymer backbone,<sup>264</sup> or by incorporating additional functional monomers into the polymers.<sup>328</sup> Wong, Boyer and coworkers synthesized a novel monomer (acrylated ZnTPP) that not only self-catalyzed the oxygen-tolerant PET-RAFT polymerization of monomers, but also enhanced the production of reactive oxygen species to promote antimicrobial activities.<sup>328</sup> Gianneschi and coworkers synthesized enzyme-responsive and pro-apoptotic peptide-modified vinyl monomers to prepare cytotoxic peptide brush polymers, which disrupted the mitochondrial membrane and triggered the death of cancer cells.<sup>69</sup> Later, copolymerization of these peptide-functionalized monomers with hydrophobic acrylamide monomers, and subsequent PISA resulted in synthesis of peptide brush polymer NPs, proposing their applications for peptide delivery systems.<sup>329</sup> Regardless of the applications, the discovery of high-performing synthetic polymers has been boosted by PET-RAFT polymerization (mostly catalyzed by ZnTPP in DMSO due to its excellent oxygen tolerance), specifically in combination with HTP synthesis (please see Section 4.4.4) and very recently with machine learning approaches and automated polymer chemistry,<sup>266,330–332</sup> which has enabled the facile preparation of a large number of polymers at a time.

#### 4.4. Advanced techniques

**4.4.1. Surface functionalization.** Surface-initiated polymerization from the initiator-functionalized surface allows modulation of physical and chemical properties of material surfaces by the type of monomers and properties of tethered polymers (*e.g.*, composition and molecular weights). Various RDRPs have been employed for surface-initiated polymerization, but were challenged by their oxygen sensitivity.<sup>333</sup> Simple reaction conditions, scalability of the process, and oxygen tolerance are also beneficial for large-scale functionalization of surfaces. In addition, light-driven polymerization affords spatiotemporal control, where the thickness of the polymer film is controlled by irradiation time and patterning of polymer brushes is provided by spatially controlled irradiation using a photomask. Therefore, PET-RAFT polymerization that offers polymerization control over a wide range of monomers under mild and ambient reaction conditions (*i.e.*, in the presence of oxygen) is expected to be a promising method.

Surface-initiated PET-RAFT (SI-PET-RAFT) polymerization was firstly demonstrated by Pester, Boyer and coworkers (Fig. 18a).<sup>334</sup> Given the well-known oxygen tolerance of ZnTPP-catalyzed PET-RAFT polymerization in DMSO, the polymerization from a CTA-functionalized silicon oxide surface was successfully performed without prior deoxygenation. The polymerization mixture deposited on the surface was covered with a glass coverslip and irradiated at 405 or 590 nm ( $1.1 \text{ mW cm}^{-2}$ ). As expected, PET-RAFT polymerization provided polymer brushes with uniform thickness and high end-group fidelity, allowing the synthesis of diblock copolymers by chain extension of the prepared polymer brushes. Fabrication of a patterned surface *via* spatially controlled polymerization using a photomask was also demonstrated.

Since then, ZnTPP in combination with DMSO as a solvent has been widely utilized for oxygen-tolerant SI-PET-RAFT polymerization under violet,<sup>335</sup> green,<sup>336–338</sup> or yellow light



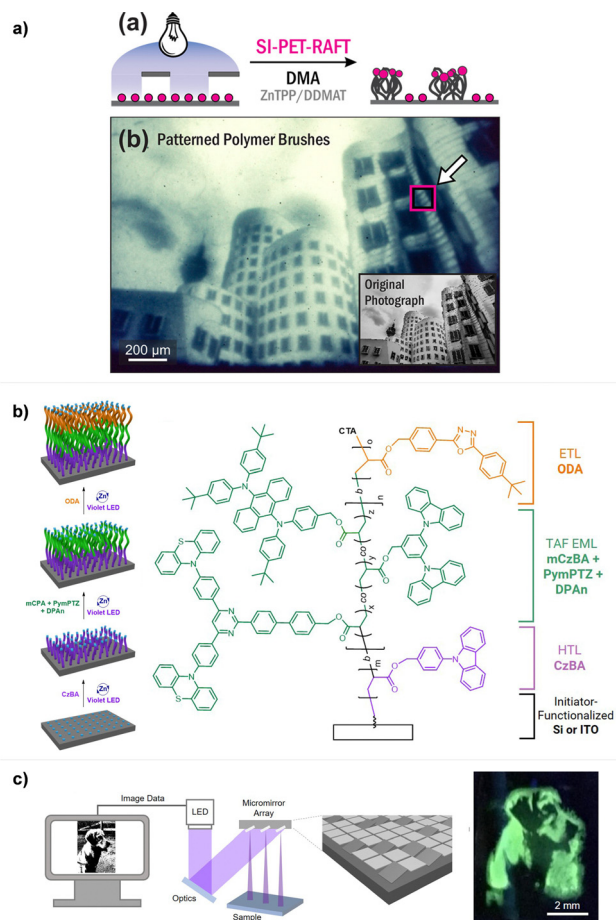


Fig. 18 Schematic representation of (a) spatially controlled SI-PET-RAFT polymerization using a photomask, (b) stepwise polymerization for fabrication of a multilayer architecture, and (c) spatially controlled SI-PET-RAFT polymerization of fluorescent monomers using a digital micromirror device (DMD). Adapted with permission from (a) ref. 334 (Copyright 2019 American Chemical Society), and (b) and (c) ref. 335 (Copyright 2021 John Wiley & Sons, Inc.).

irradiation.<sup>338</sup> A water-soluble  $\text{ZnTPPS}_4^-$  under green light irradiation<sup>339</sup> or EY in the presence of TEOA under blue<sup>140,340</sup> or green light irradiation<sup>138,341</sup> expanded the polymerization media to aqueous systems. The lack of oxygen tolerance in the absence of TEOA required prior degassing<sup>342</sup> or enzymatic degassing strategy using GOx and glucose.<sup>163</sup> Using these various PCs, SI-PET-RAFT polymerization has been employed for fabrication of antifouling surfaces for biomedical and industrial applications,<sup>138,140,336–338,340</sup> polycarbonate surface with tuned hydrophilicity,<sup>339</sup> organic–inorganic hybrid materials,<sup>235,341–344</sup> and functional polymeric materials.<sup>335</sup>

Antifouling surfaces were prepared from hydrophilic, zwitterionic (e.g., carboxybetaine methacrylamide (CBMAM)<sup>140,340</sup>), and low-fouling monomers (e.g., sulfonate<sup>336</sup> or fluorine monomers<sup>337</sup>) to inhibit adsorption of biomolecules such as bacteria, proteins, and cells. Besides its role as a PC, ZnTPP that remained after the polymerization was effective as an antifouling agent through photodynamic inactivation of bacteria owing to its ability to generate singlet oxygen under irradiation.<sup>337</sup> The presence of residual

ZnTPP was ascribed to covalent incorporation of ZnTPP into the polymer chain by radical-mediated polymerization of the reduced porphyrin macrocycle. This photodynamic activity of the residual ZnTPP, on the other hand, likely caused a significant cytotoxicity to mouse macrophage-like (RAW 264.7) cells, implying the need for the use of organic PCs in biomedical applications.<sup>336</sup>

Organic–inorganic hybrid materials were provided *via* grafting-from synthesis of polymers from mesoporous silica NPs,<sup>342</sup> mesoporous silica films,<sup>343</sup> gold-coated silicon wafers,<sup>140</sup> indium tin oxide (ITO)/gold-coated electrodes,<sup>341</sup>  $\text{NaYF}_4\text{:Tm/Yb}$  UCNPs,<sup>344</sup> and CdSe QDs.<sup>235</sup> On the ITO/gold-coated electrode surface, the CTA possessing an electrochemically active carbazole moiety was immobilized by an electrodeposition method.<sup>341</sup>  $\text{NaYF}_4\text{:Tm/Yb}$  UCNPs<sup>344</sup> and CdSe QDs<sup>235</sup> acted as both substrates and PCs for SI-PET-RAFT polymerization, where the synthesized polymers were tethered to the surfaces of nanocomposites *via* ligand exchange between the initial ligands of nanocomposites and TCT groups of the polymers. Encapsulation of gold NPs by the poly(dimethylaminoethyl acrylate) (DMAEA)-tethered surface<sup>341</sup> and subsequent immobilization of antibodies onto the prepared polymer brushes<sup>140</sup> implied that SI-PET-RAFT polymerization would become a promising strategy for the development of organic–inorganic hybrid biosensors.

Very recently, Hudson, Pester, and coworkers employed ZnTPP-catalyzed SI-PET-RAFT polymerization under violet irradiation (405 or 415 nm) for fabrication of multilayer thin films for organic electrodes.<sup>335</sup> Using various acrylic monomers comprised of thermally activated delayed fluorescence (TADF) emitters, stepwise polymerization from CTA-functionalized ITO provided multilayer architectures of hole-transport layer (HTL), emissive layer (EML), and electron-transport layer (ETL), mimicking the structure of multilayer organic light-emitting diodes (OLEDs) (Fig. 18b). Moreover, combined with the recently emerged digital projection lithography technique using arrayed digital micromirror devices (DMDs), a spatial control over complex polymer architectures at high resolution was imparted (Fig. 18c)

A bare surface without prior functionalization with a CTA was also utilized for the preparation of a polyvinyl alcohol (PVA)-based hydrogel. The PVA-based hydrogel was immersed in the reaction mixture of PC (*i.e.*,  $\text{Ru}(\text{bpy})_3\text{Cl}_2$ ,<sup>345,346</sup> fluorescein,<sup>347</sup> EY,<sup>348</sup> and aluminum phthalocyanine chloride<sup>349</sup>), CTA, monomers, and TEA. It was proposed that alkoxyl radicals generated from PVA by a one-electron oxidized PC or by irradiation participated in PET-RAFT polymerization. Zwitterionic monomers such as CBMA were polymerized to provide antifouling properties to PVA-based materials for biomedical applications.<sup>345–349</sup> Thermo-responsive poly(NIPAm) brushes provided surface properties which were adjustable by temperature.<sup>347</sup>

**4.4.2. 3D/4D printing – living additive manufacturing.** 3D printing is an additive manufacturing technology which enables the fabrication of objects with complex structures using a layer-by-layer approach from digitally sliced computer-aided designs. Since the development of the first 3D printing process by Charles Hull in the early 1980s,<sup>350,351</sup> this technique has had scientific, technological, and economic impacts<sup>352,353</sup> by shifting from a

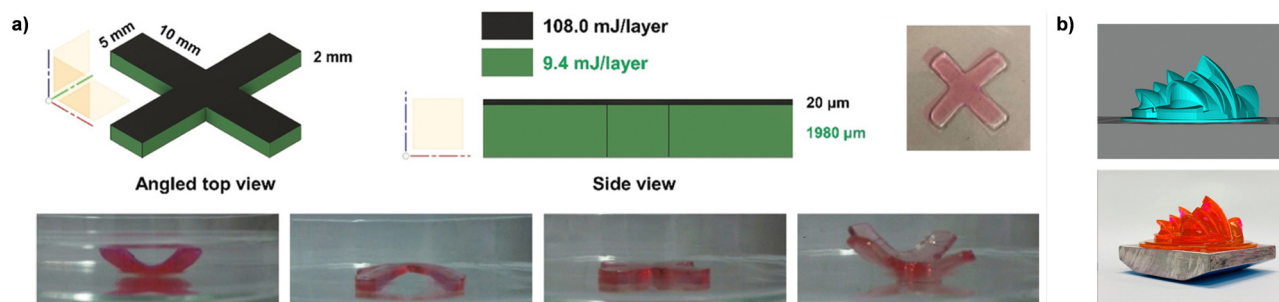


rapid prototyping technology to an advanced material manufacturing platform for diverse applications ranging from biomaterials<sup>354</sup> and soft robotics,<sup>355</sup> to construction.<sup>356</sup> More specifically, vat photopolymerization-based 3D printing techniques, including DLP<sup>357,358</sup> and stereolithography (SLA),<sup>351</sup> where light is used to activate polymerization and cure a liquid resin to form solid materials, have been widely applied.<sup>359</sup> Most of the photopolymerization-based 3D printing techniques employ uncontrolled polymerization methods, *i.e.*, photoinduced conventional free radical or cationic polymerization, to cure the polymers and form the object due to their fast polymerization rates and simplicity.<sup>360</sup> However, the polymers prepared during these photoinduced conventional free radical or cationic polymerizations cannot be reactivated, limiting the opportunity for the functionalization of 3D printed objects. To overcome these limitations, in recent years, PET-RAFT polymerization has been implemented in additive manufacturing to 3D print functional objects.<sup>361</sup> To achieve a reasonable polymerization rate and oxygen tolerance, polymerization *via* RQP was first implemented using xanthene dyes, such as erythrosin and EY, in the presence of a tertiary amine. For example, Boyer and coworkers reported an ultrafast DLP 3D printing system using EB and TEOA as the PC and cocatalyst, respectively, under green light irradiation (525 nm, 0.32 mW cm<sup>-2</sup>).<sup>142</sup> In contrast to conventional free radical polymerization, the network growth was controlled by the RAFT equilibrium, *i.e.*, the degenerative chain transfer between active and dormant chains.<sup>18</sup> Careful optimization of the stoichiometry of reagents in the resin formulation (EB, TEOA, DMAM and PEG diacrylate (PEGDA) ( $M_n = 250$  g mol<sup>-1</sup>)) resulted in a build speed of 1.2 cm h<sup>-1</sup> allowing 3D printing of complex objects. A 4D printed object capable of swelling- and desolvation-induced actuation by differentiation of mechanical properties of two layers based on the control of light dose and curing time was also fabricated (Fig. 19a). The same research group then investigated the effect of various CTAs (TTCs, dithioesters, xanthates, and DTCs) under otherwise identical reaction conditions (Fig. 19b).<sup>362</sup> Interestingly, the structure of the CTA, such as Z and R groups, significantly affected the kinetics of network formation. This result is in alignment with the well-established design rules in conventional RAFT polymerization.<sup>61,363,364</sup> In parallel, Jin, Bagheri, and coworkers in collaboration with the research group of Boyer

utilized EY and TEA under blue (483 nm, 4.16 mW cm<sup>-2</sup>) or green light irradiation (532 nm, 0.48 mW cm<sup>-2</sup>).<sup>134</sup> However, the fastest build speeds were 0.08 and 0.14 cm h<sup>-1</sup> under blue or green light irradiation, respectively, which were lower than that achieved by EB.<sup>142</sup> This was attributed to more favorable photophysical and electrochemical properties of EB over EY.<sup>204,214</sup> The build speed still reached 0.23 cm h<sup>-1</sup> after further optimization of the formulation of resin utilizing EY and TEOA under violet light irradiation (405 nm, 0.10 mW cm<sup>-2</sup>).<sup>139</sup>

ZnTPP then extended the operation wavelength to red (635 nm, 0.5 mW cm<sup>-2</sup>) although 3D printing was performed under a N<sub>2</sub> atmosphere to achieve a reasonable maximum build speed of 0.1 cm h<sup>-1</sup> due to the long inhibition period in the presence of air.<sup>365</sup> Nevertheless, there is still a need to develop new PCs capable of achieving faster polymerization, which would enable 3D printing with a reasonable build speed. To overcome the slow printing speed achieved by PET-RAFT polymerization, Norrish type I photoinitiator diphenyl (2,4,6-trimethylbenzoyl) phosphine oxide (TPO) replaced the PC, which resulted in the fabrication of 3D printing objects at a faster printing rate (up to 9 cm h<sup>-1</sup>).<sup>366</sup> The incorporation of the CTA conferred additional properties to the 3D printed objects, including capability for surface modification<sup>366</sup> and self-healing property.<sup>367</sup> More recently, the incorporation of macro-CTAs in the 3D printing resins enabled the preparation of 3D printed materials containing defined nanostructures *via* polymerization-induced microphase separation.<sup>368–370</sup> This technique would open opportunities for on-demand fabrication of nanostructured polymer materials with tunable mechanical properties and ion conductivity for energy storage applications.<sup>371,372</sup>

**4.4.3. Flow chemistry.** Flow chemistry has improved the practicality and scalability of photomediated synthesis of advanced functional materials including QDs, NPs, and dyes.<sup>373</sup> According to the Beer–Lambert law, it is difficult to perform the light-driven reactions on a large scale because the intensity of light significantly decreases with increasing optical path length. In a continuous flow reactor, the reaction mixtures flow inside a light-permeable tubing which is irradiated.<sup>374</sup> High surface area-to-volume ratio of the tubing ensures effective light penetration and a concomitant increase in the photon flux and reaction



**Fig. 19** (a) Synthesis of a 4D printed object capable of swelling- and desolvation-induced actuation owing to difference in mechanical properties of two layers by the spatially resolved light doses. (b) Original stl file image and 3D printed theater complex. Adapted with permission from (a) ref. 142 (Copyright 2019 John Wiley & Sons, Inc.) and (b) ref. 362 (Copyright 2021 American Chemical Society).





efficiency. Therefore, flow chemistry is expected to expand the versatility of photomediated polymerization.<sup>375–378</sup>

Among visible-light-driven RAFT polymerizations, PET-RAFT polymerization was the first to be performed in a continuous flow reactor, owing to its superior oxygen tolerance.<sup>145</sup> In contrast, there were a few reports employing flow chemistry techniques to (UV light-induced) photoiniferter<sup>379–381</sup> and photomediated cationic RAFT polymerizations, owing to their sensitivity to oxygen.<sup>382</sup> Oxygen tolerance is not a prerequisite for flow chemistry techniques; nevertheless, the high surface-area-to-volume of tubing reactors may facilitate the diffusion of oxygen into the reaction mixtures, causing a negative impact on oxygen-sensitive reactions.<sup>264</sup> In this regard, the more rapid polymerization kinetics of PET-RAFT polymerization compared to other polymerizations is also beneficial for operationally reasonable reaction conditions.<sup>380</sup>

Flow chemistry has been applied to rapid syntheses of homopolymers<sup>209</sup> or multiblock copolymers,<sup>136,204</sup> photo-PISA<sup>135,305</sup> and gram-scale synthesis of discrete pentamers *via* sequential SUMI.<sup>273</sup> Theoretically, the synthesis of polymers within minutes could enable their large-scale production (*e.g.*, multi-gram within a day). In addition to enhanced polymerization kinetics, the molecular weights and monomer compositions can be controlled by simply adjusting the compositions of the reaction mixtures, flow rates (*i.e.*, residence time), and irradiation times. In the case of block copolymer synthesis, different monomers can be sequentially added in order at defined times through separate channels (Fig. 20). Furthermore, in a one-pass reaction system, each batch can be irradiated at a different wavelength and separately turned on and off, such that multiple polymerization reactions are sequentially and selectively activated during the reaction in one pass. This approach was then employed to the synthesis of diverse polymers with complex architectures.<sup>280</sup> At last, dispersity control was achieved *via* temporally regulated initiation and/or adjustment of the reaction parameters (*e.g.*, flow rate and wavelength and intensity of irradiation).<sup>288–290</sup>

Nevertheless, to fully realize the potential of flow chemistry for expanding the current lab-scale polymerization system into the industrial scale, the influences of fluid dynamics and reactor parameters (such as tubing diameter and operation method) on polymerization control must be thoroughly investigated.<sup>204,290</sup> For example, in the synthesis of high-molecular-weight polymers, the polymer properties were inconsistent because the

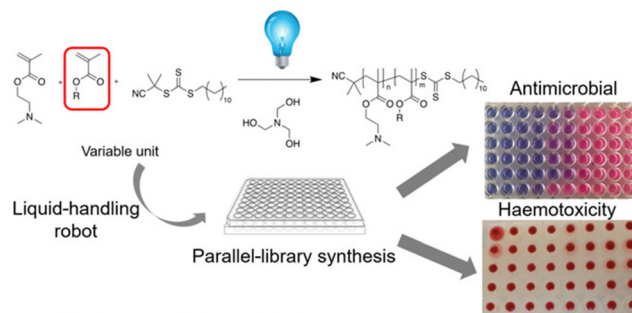


Fig. 21 Combinatorial approach for the discovery of antimicrobial polymers prepared by high-throughput PET-RAFT polymerization. Adapted with permission from ref. 386 (Copyright 2018 John Wiley & Sons, Inc.).

polymers caused reactor fouling and affected the fluidic profiles of the reaction mixture due to low Reynolds number.<sup>204</sup> Homogeneity of the reaction mixture within flow could be improved by applying a plug packed of low-cost and easily accessible silicon oxide beads.<sup>383</sup>

**4.4.4. High-throughput (HTP) synthesis.** HTP synthesis allows facile preparation of a large library of polymers in small volumes, which enables the identification of structure–property relationship. By distributing a stock solution of the reaction mixture into each well, and placing the well plate under a LED, polymerization is performed in each well at the  $\mu\text{L}$  scale (at most 200  $\mu\text{L}$  in the case of a 96-well plate). As deoxygenation is difficult at the  $\mu\text{L}$  scale, PET-RAFT polymerization with intrinsic oxygen tolerance has exclusively been utilized for HTP synthesis,<sup>384</sup> although in some cases, oxygen-tolerant visible-light-driven RAFT polymerization in the absence of a PC was utilized, where  $\text{Zn}_{0.64}\text{Fe}_{2.36}\text{O}_4$ <sup>155</sup> and the tertiary amine,<sup>152,385,386</sup> added instead of the PC, facilitated photomediated deoxygenation and/or photolysis of the excited-state CTA. Polymerization at a low volume scale is also considered to be beneficial for potential bioapplications where it is difficult to prepare reaction substrates (*e.g.*, proteins and DNA) in large quantities.<sup>170</sup> Moreover, new polymers with desired biological activities can be efficiently discovered *via* a combinatorial approach (Fig. 21).<sup>386</sup>

Among PCs, ZnTPP dissolved in DMSO demonstrating extreme oxygen tolerance without additives was extensively employed. ZnTPP-catalyzed HTP polymerization has enabled the simple and efficient construction of a library of polymers without prior deoxygenation.<sup>262–266,276,387–390</sup> *Via* preparation

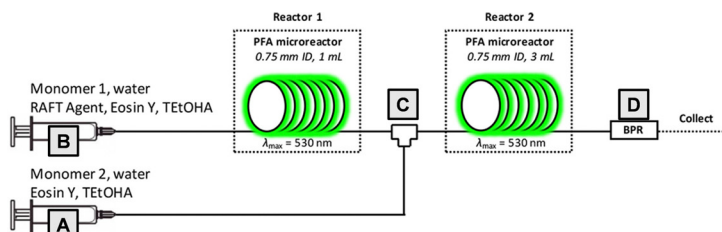


Fig. 20 Schematic representation and photographs of a continuous flow reactor for the block copolymer synthesis. The reactor system is composed of two separated syringe pumps for two tubing reactors, a micromixer tee, and a back-pressure regulator (BPR). Adapted with permission from ref. 136 (Copyright 2019 American Chemical Society).



and investigation of a large combinatorial library of polymers, researchers efficiently optimized polymerization conditions<sup>262,389</sup> and screened structure–activity relationships of polymers synthesized for antimicrobial applications,<sup>155,263,264</sup> polymer–protein binding interactions,<sup>265,266</sup> conjugation of biomolecules,<sup>276</sup> preparation of a glycopolymer library,<sup>390</sup> and design of single-chain polymer NPs.<sup>388</sup> Other than ZnTPP, EY was also employed for photo-PISA in a 96-well plate, but ascorbic acid was necessary to achieve oxygen tolerance.<sup>170</sup>

Apart from its outstanding oxygen tolerance in DMSO, ZnTPP also showed promise in characterization of polymerization at low volumes.<sup>387</sup> Boyer and coworkers noticed that fluorescence emission bands of ZnTPP changed owing to incorporation of ZnTPP into the polymer chain during polymerization. The linear relationship between fluorescence emission and monomer conversion allowed online monitoring of polymerization within a few minutes using plate readers, which was consistent with the results provided by NMR analysis. Herein, polymerization and direct characterization were conducted at below 40  $\mu\text{L}$  scale in a 382-well plate. This ultralow volume is typically difficult to sample for NMR analysis that is carried out to determine monomer conversion in polymerization in batch. Therefore, the merge of HTP synthesis in well-plates and simple online monitoring of polymerization, combined with machine learning approaches and automated polymer chemistry,<sup>266,330,331,391</sup> is expected to accelerate the discovery of novel functional polymers.<sup>392,393</sup>

## 5. Photoiniferter polymerization

In the absence of additives and/or PCs, simplicity and efficiency of the reaction system would be further increased. Moreover, the negative impacts of remaining additives on polymer properties will no longer become a concern. Nevertheless, since the first application of DTCs by Otsu and coworkers,<sup>40</sup> the operating wavelength has been limited to the UV region. Because UV light can lead to undesired decomposition of the CTA and loss of controllability of polymerization, CTAs that can be cleaved by milder visible light have been extensively explored, and the relevant applications have recently emerged. Accordingly, the very recent review article reported by Hartlieb covered the concept, history, and various applications of photoiniferter polymerization irrespective of the irradiation wavelength.<sup>56</sup> In this section, particular emphasis is placed on the examples harnessing visible light rather than UV light.

### 5.1. CTAs for polymerization

Theoretically, visible-light-induced photocleavage of the C–S bond is possible for xanthates or TTCs and DTBs owing to their  $n \rightarrow \pi^*$  electronic transitions. The  $n \rightarrow \pi^*$  electronic transition of TTCs and DTBs occurs under blue and green light irradiation, respectively (Fig. 22).<sup>394</sup> The red-shift effect for DTBs is due to a resonance in the Z group. In contrast, both  $n \rightarrow \pi^*$  and  $\pi \rightarrow \pi^*$  electronic transitions of xanthates<sup>395</sup> and DTCs occur under UV light irradiation because of electron-rich

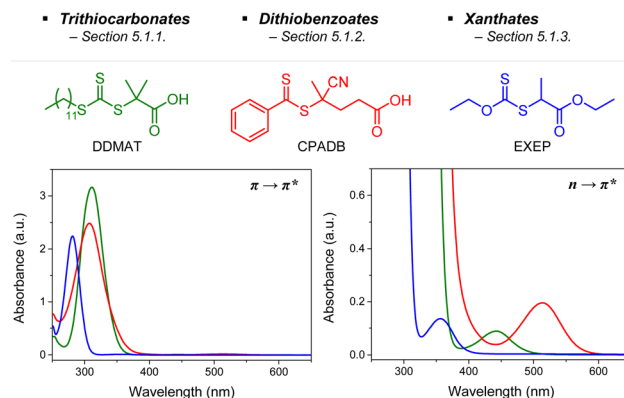
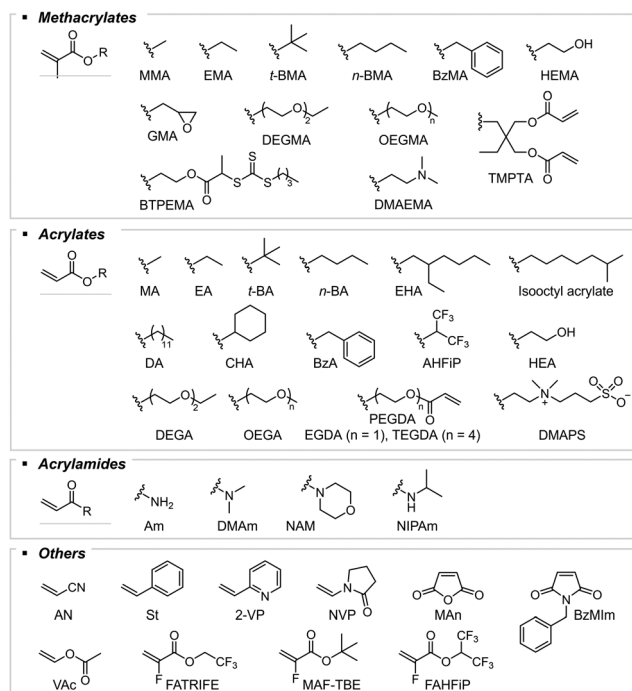


Fig. 22 UV/Vis absorption spectra of DDMAT (green), CPADB (red), and EXEP (blue) in DMSO at 0.2 and 2.0 mM concentration to present  $\pi \rightarrow \pi^*$  and  $n \rightarrow \pi^*$  electronic transitions, respectively.

oxygen and nitrogen in the Z group, respectively. Although  $n \rightarrow \pi^*$  electronic transitions at longer wavelengths are beneficial due to lower energies, their spin-forbidden nature and consequently small molar extinction coefficient make it challenging to achieve visible-light-driven photoiniferter polymerization at a reasonable polymerization rate. Therefore, the recently reported photoiniferter polymerization from TTCs still mostly harnesses UV light to target  $\pi \rightarrow \pi^*$  electronic transition-derived homolysis of the C–S bond regardless of the type of monomers (methacrylates,<sup>396</sup> acrylates,<sup>33,379</sup> acrylamides,<sup>33,58,397</sup> and other monomers<sup>380,397</sup>). The use of a continuous flow reactor and/or high reaction temperature helped to improve the practicality and polymerization kinetics. Johnson and coworkers adapted a flow reactor for UV light irradiation (352 nm)-induced polymerization of acrylates and acrylamides.<sup>379</sup> Junker, Abetz, and coworkers increased the reaction temperature to 120  $^{\circ}\text{C}$  for polymerization of isoprene and styrene in a flow reactor.<sup>380</sup> On the other hand, in this section, we focus on the visible-light-driven photoiniferter polymerization using TTCs, DTBs, xanthates, and others. Scheme 26 depicts the monomers employed thus far.

**5.1.1. Trithiocarbonates.** In 2015, Boyer and coworkers reported the first visible-light-driven photoiniferter polymerization of methacrylates in the presence of a CTA and monomer without the addition of a PC.<sup>32</sup> Among CDTPA, DDMAT, BTPA (TTCs) and CPADB (a DTB), only CDTPA under green light irradiation (530 nm, 5 W) led to controlled polymerization of MMA. The loss of polymerization control under blue light irradiation (461 nm, 5 W) implied that the irradiation wavelength should overlap with the absorption profile of the CTA; however, too high energy would cause partial degradation of the CTA. For other TTCs, the controllability of polymerization was likely affected by the stability of the R group during the fragmentation of the C–S bond. For example, in contrast to CDTPA, BTPA possessing an R group with a secondary carbon led to poorly controlled polymerization of MMA under blue light irradiation because the propagating radical with tertiary carbon was more stable, not favoring the RAFT process. The study of the effect of the R group on blue light (460 nm, 1.5  $\text{mW cm}^{-2}$ )-induced photolysis of the CTA by UV/Vis spectroscopy, by Qiao





**Scheme 26** Chemical structures and abbreviations of monomers employed for visible-light-driven photoiniferter polymerization.

and coworkers, indicated that as the thiol radical generated after photolysis could be irreversibly degraded into carbon disulfide and thiol, polymerization from a CTA with a more stable R group that efficiently generated fragments with extended lifetimes was more prone to lose its living character.<sup>398</sup> The efficient fragmentation, on the other hand, decreased the induction period implying that controlled polymerization of a given monomer with a reasonable induction period would be achieved *via* careful selection of the CTA and light source.

The monomer scope was expanded to methacrylates,<sup>110,157,280,381,399,400</sup> acrylates,<sup>33,88,110,134,157,401–408</sup> acrylamides,<sup>33,110,157,404,407,409</sup> AN,<sup>410</sup> 2-vinylpyridine (2-VP),<sup>411</sup> styrene,<sup>404,406</sup> and fluoro(meth)acrylates<sup>412</sup> (Table 4). Compared to UV light, the use of milder visible light (460 nm, 4.8 W) prohibited the self-initiation of MA although the induction period was increased by four times.<sup>33</sup> The authors ascribed the increase in the induction period to the prolonged time of addition of the first monomer to the CTA. Then, the same authors reported that the induction period was rather related to the R-group stability or inactivation of residual oxygen or trace impurities within the reaction mixture before the polymerization.<sup>398</sup> TTCs with better fragmenting R groups demonstrated significantly reduced induction periods for initiation, whereas during propagation the R-group effect became less important owing to the similar acrylate-inserted R groups of all TTCs. Junker and coworkers also discovered that in the polymerization of MMA under blue light irradiation (450 nm, 14.4 W), the adduct of CTA with one, two, or three MMAs resulted in polymers with lower dispersity.<sup>381</sup> However, to eliminate the need for the preparation of

SUMI adducts, the authors suggested to render the initiation process effective by increasing photon flux in a continuous flow reactor. To achieve fast reaction kinetics, the reaction temperature was also increased to 90 °C, which was sufficiently low not to cause the autoinitiation of MMA or degradation of TTC. As reported by Cameron, Saito, and coworkers, temperature control is particularly important at high irradiation powers.<sup>409</sup> In the aqueous polymerization of acrylamides such as DMAM under irradiation (402 or 451 nm, and 6, 26, 104, or 208 W), high irradiation powers increased not only photon flux and photolysis, but also the reaction temperature, which considerably reduced the polymerization time from 12 hours to 11 minutes, while broadening the dispersity of polymers. Dispersity was narrowed by controlling the temperature to prevent hydrolytic degradation of the CTA and concomitant formation of low molecular weight dead chains.

Very recently, Sumerlin and coworkers reported that irradiation with visible light to target  $n \rightarrow \pi^*$  electronic transitions led to more efficient and well-controlled polymerization than irradiation with UV light to target  $\pi \rightarrow \pi^*$  electronic transitions, if the light intensity was identical ( $0.6 \text{ mW cm}^{-2}$ ).<sup>407</sup> Due to the spin-forbidden nature,  $n \rightarrow \pi^*$  electronic transitions show a much smaller molar extinction coefficient than  $\pi \rightarrow \pi^*$  electronic transitions. Nevertheless, the polymerization results and the radical-trapping experiment using 2,2,6,6-tetramethylpiperidine-1-oxyl (TEMPO) confirmed that  $n \rightarrow \pi^*$  electronic transitions led to the higher quantum yield of photolysis of the C-S bond, higher radical concentration, and more rapid polymerization. This result was consistent with xanthates.

**5.1.2. Dithiobenzoates.** In the first study of visible-light-driven photoiniferter polymerization of MMA and MA by Boyer and coworkers, CPADB was inactive for both monomers under blue light irradiation (461 nm, 5 W) in contrast to CDTPA (a TTC) (Table 5).<sup>32</sup> This was ascribed to the maximum  $n \rightarrow \pi^*$  absorption of CPADB at 513 nm corresponding to green light rather than blue light, although polymerization data under green light irradiation were not shown here. The seminal report demonstrated that green light irradiation (530 nm) was also inefficient for photoiniferter polymerization of MMA in DMSO due to a poor quantum yield of the photochemical relaxation of excited-state CPADB.<sup>398</sup> In DES, on the other hand, MMA was polymerized under green light irradiation (525 nm, 1.2 mW cm<sup>-2</sup>) even in a completely open vial.<sup>158</sup> The effect of DES needs to be investigated.

Meanwhile, Sumerlin and coworkers prepared a UHMW polymer *via* alternative copolymerization of styrene and benzyl maleimide or maleic anhydride under 450 nm irradiation.<sup>413</sup> 2-(dimethylamino)ethyl methacrylate (DMAEMA) also underwent polymerization under irradiation with a household lamp (14 W, 2.4 mW cm<sup>-2</sup>), but here the acceleration effect of the amine incorporated in DMAEMA on the polymerization mechanism needs to be considered. Electron transfer from the amine to excited-state CPADB generated the CPADB anion and facilitated the polymerization as in the case of amine-catalyzed polymerization using TTCs<sup>71,151,152</sup> and DTB.<sup>72</sup> By the addition of TEA, polymerization of MMA from CPDB even under green (520 nm, 5.9 mW cm<sup>-2</sup>) or sunlight irradiation was realized.<sup>72</sup> Recently, Konkolewicz and coworkers reported that an electron-donating substituent at the para position of the benzyl Z group of CPDB

**Table 4** Chemical structures of TTCs employed for visible-light-driven photoiniferter polymerization

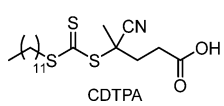
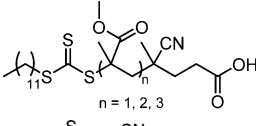
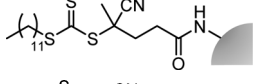
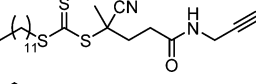
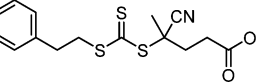
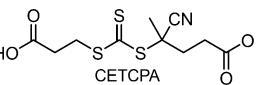
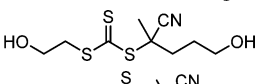
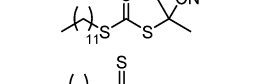
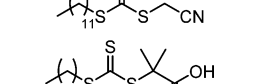
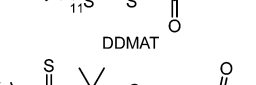
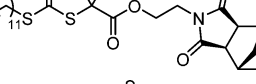
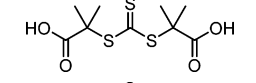
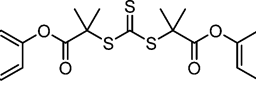
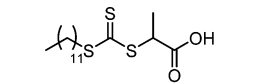
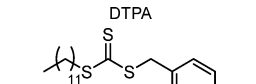
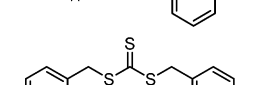

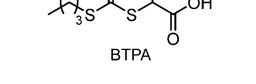
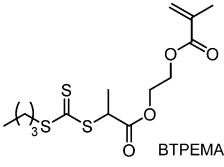
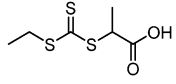
CTA (common name)	Irradiation wavelength	Monomer			
		Methacrylates	Acrylates	Acrylamides	Others
 CDTPA	Violet (405 nm) Blue (455–472 nm)	BzMA	PEGDA <i>n</i> -Bu, <i>t</i> -Bu, BzA, CHA, DA, EA, EHA, HEA, MA, AHFIP		St
 <i>n</i> = 1, 2, 3	Green (520, 530 nm)	<i>n</i> -BMA, BzMA, BTPEMA, DMAEMA, GMA, HEMA, MMA			
	Blue (450 nm) <sup>a</sup>	<i>t</i> -BMA, DEGMA, EMA, HEMA, MMA			
	Blue (460 nm) Green (530 nm)	GMA, HEMA, OEGMA			
	Blue (460 nm)		OEGA		
	White				FATRIFE, FAHFIP, MAF-TBE
 CETCPA	Blue (455 nm)		DMAAPS, HEA, OEGA		
	Blue (455 nm)		<i>n</i> -BA, MA		
	Blue (460, 470 nm)		MA		AN
	Blue (472 nm)		<i>n</i> -BA		
 DDMAT	Violet (420 nm) Blue (450–460 nm)		<i>n</i> -BA, MA	NAM	2-VP St
	Blue (450 nm)		<i>n</i> -BA		
	Violet (402 nm) Blue (450, 451 nm)		MA	Am, DMAm Am	
	Blue (450 nm)	MMA	<i>n</i> -BA, <i>t</i> -BA, DEGA, MA	Am, DMAm, NIPAm	
 DTPA	Blue (460 nm)		MA		
	Blue (460, 480 nm)		MA		
 DBTTC	White Violet (405 nm) Blue (460 nm)		OEGA, TEGDA <i>n</i> -BA, OEGA, TEGDA		FATRIFE
 BTPA	Blue (460 nm)		MA, <i>t</i> -BA, EGDA	NIPAm	

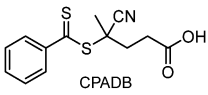
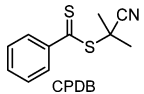
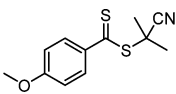


Table 4 (continued)

CTA (common name)	Irradiation wavelength	Monomer			
		Methacrylates	Acrylates	Acrylamides	Others
	Green (520 nm)		MA	DMAm	
	Blue (453 nm)			DMAm	

<sup>a</sup> Performed in a continuous flow reactor, at 90 °C.

Table 5 Chemical structures of DTBs employed for visible-light-driven photoiniferter polymerization

CTA (common name)	Irradiation wavelength	Monomer			
		Methacrylates	Acrylates	Acrylamides	Others
	Blue (440 nm) Green (510 nm) Household lamp	MMA MMA DMAEMA			St and BzMIIm, St and MAn
	Blue (460 nm) <sup>a</sup> Green (520 nm) <sup>a</sup>	MMA			
	Blue (440 nm)	MMA			

<sup>a</sup> Performed in the presence of TEA.

dramatically accelerated the polymerization of MMA under blue light irradiation (440 nm, 11.6 mW cm<sup>-2</sup>) in the absence of an amine additive.<sup>87</sup> The monomer conversion (85%) was comparable to the conversion in polymerization using 1 ppm of Ir(ppy)<sub>3</sub> (*i.e.*, PET-RAFT polymerization). The polymerization rate ( $k_p^{app} = 0.2 \text{ h}^{-1}$ ) was much faster than that using CPDB ( $k_p^{app} = 0.017 \text{ h}^{-1}$ ) despite the slight deviation in molecular weight control ( $\bar{D} = 1.28$ ) and end-group fidelity. The investigation of five CPDB derivatives confirmed the similar molar extinction coefficient at irradiation wavelength, but their Hammett Sigma parameters ( $\sigma_p$ ) and  $E_{red}^0$ s were decreased by the presence of electron-donating substituents. The linear relationship between logarithm of  $k_p^{app}$  and  $\sigma_p$  or  $E_{red}^0$  and  $\sigma_p$  proposed that homolysis of the C–S bond (i) could be enhanced by electronics, (ii) might involve the formation of partial positive charge on the DTB group in the transition state, and thus (iii) the polymerization was accelerated by the electron-donating para methoxy substituent.

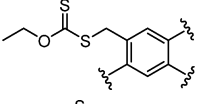
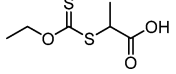
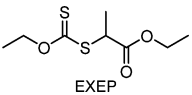
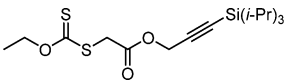
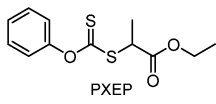
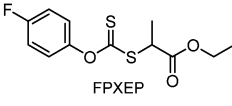
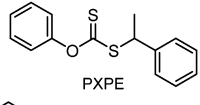
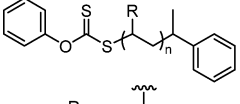
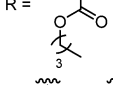
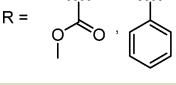
**5.1.3. Xanthates.** Photolysis of EXEP under blue light (460–470 nm) or sunlight irradiation was reported by Zhu, Zhang, and coworkers for the first time (Table 6).<sup>162,394</sup> Introduction of carboxylic acid or triisopropylsilyl-protected alkyne into the R group of EXEP did not interfere in the photoiniferter polymerization of VAc in the bulk. By the way, substitution of the ethyl Z-group of EXEP with a phenyl group (PXEP) led to a

blue-shifted  $n \rightarrow \pi^*$  electronic transition.<sup>159</sup> Under violet light irradiation (390 nm), more-activated monomers such as *n*-butyl and *t*-butyl acrylates (*n*- and *t*-BA) and NIPAm were polymerized in the bulk within an hour, whereas the polymerization of VAc took a far longer time. When fluorine was inserted in the para position of the phenyl Z-group of PXEP (FPXEP), even homopolymerization of VAc and block copolymerization of MA as the first block with VAc as the second block were realized under violet light irradiation (390 nm, 0.72 W).<sup>414</sup> The compatibility of FPXEP with both less- and more-activated monomers was ascribed to the well-balanced addition and fragmentation during the RAFT process, which was induced by the introduction of fluorine. The molecular geometry optimized by DFT implied that fluorine weakened the conjugation between benzene and the C–S double bond and lowered the lowest unoccupied molecular orbital (LUMO) of FPXEP to facilitate the addition of free radicals. PXPE, where the R group of PXEP was further modified to the 1-(phenyl-ethyl) group, was also suitable for more-activated monomers.<sup>415</sup> Similar to FPXEP, only after the polymerization of more-activated monomers (*i.e.*, MA, *n*-BA, or styrene) under blue (465 nm, 1.8 mW cm<sup>-2</sup>) or violet light irradiation (391 nm, 0.6 mW cm<sup>-2</sup>), chain extension with VAc or NVP was possible. Although the wavelength was extended to visible light (blue or violet), still UV light showed the highest





Table 6 Chemical structures of xanthates employed for visible-light-driven photoiniferter polymerization

CTA (common name)	Irradiation wavelengths	Monomer			
		Methacrylates	Acrylates	Acrylamides	Others
	Violet (401 nm)			DMAm	
	Blue (460–470 nm)				VAc
	Blue (460–470 nm)				VAc
	Blue (460–470 nm)				VAc
	Violet (390 nm)		<i>n</i> -BA, <i>t</i> -BA	NIPAm	
	Violet (390 nm)		<i>n</i> -BA, MA	NIPAm	VAc
	Violet (391 nm) Blue (465 nm) Violet (391 nm)		<i>n</i> -BA MA		St
	Violet (391 nm) Blue (465 nm)				VAc NVP
					
	Violet (391 nm)				NVP, VAc

$k_p^{app}$  albeit with higher dispersity due to the generation of dead chains.

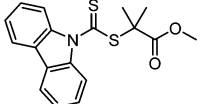
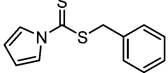
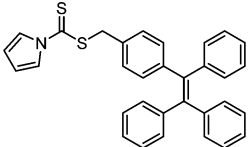
**5.1.4. Others.** In 1982, Otsu and coworkers demonstrated the living polymerization using DTCs as an iniferter under UV light irradiation.<sup>39</sup> In order to extend the absorption of DTCs from UV to longer wavelength, Poly and coworkers conjugated carbazole in the Z group. Therefore, photoiniferter polymerization of *n*-BA was realized even under blue (472 nm, 96 mW cm<sup>-2</sup>) or green (525 nm, 26.5 mW cm<sup>-2</sup>) light irradiation (Table 7).<sup>401</sup> An *N*-heterocyclic DTC-based CTA possessing tetraphenylethylene (TPE) as the R group showed absorption at 400–500 nm.<sup>416</sup> Not only acrylates, MMA, and styrene were polymerized under blue light irradiation (460 nm, 4.8 W), but also the polymerization could be monitored *in situ* by naked eyes *via* aggregation-induced emission of TPE. As the polymerization proceeded, the viscosity of the solution increased, and photoluminescence intensity quantitatively increased to reflect monomer conversion during polymerization. When TPE was physically blended within the reaction mixture, the PL intensity increased in an irregular manner due to the indirect interaction between TPE and the growing polymer network.

## 5.2. Recent developments and applications

Visible-light-driven photoiniferter polymerization has recently been employed in numerous applications; nevertheless, the range of applications is still narrower than those reported for PET-RAFT polymerization owing to the lack of oxygen tolerance of the reaction system and the decreased polymerization rate caused by the absence of a PC. For example, photomediated expansion of the polymer network through incorporation of additional monomers was significantly efficient in the presence of PTH in terms of reaction rate and controllability of polymerization.<sup>208</sup> Moreover, direct photolysis of TTC under visible-light irradiation, which was less efficient than EY/TEA-catalyzed PET-RAFT polymerization, was impractical for 3D printing application where a sufficiently fast photocuring (*i.e.*, a high build speed) is required.<sup>134</sup> In this section, the reported examples of applications that were realized solely by visible-light-driven photoiniferter polymerization are described. The other examples which were aided by PET-RAFT polymerization are mentioned in the relevant subsections throughout Sections 4.3 and 4.4. Herein, the applications driven by UV light are basically excluded, whereas several noteworthy examples which show implications for their expansion to visible-light-driven



Table 7 Chemical structures of other CTAs employed for visible-light-driven photoiniferter polymerization

CTA (common name)	Irradiation wavelengths	Monomer			
		Methacrylates	Acrylates	Acrylamides	Others
	Blue (472 nm) Green (525 nm)		<i>n</i> -BA	DMAm	
	Blue (460 nm)		MA		
	Blue (460 nm)	MMA	<i>n</i> -BA, MA, OEGA, isooctyl acrylate		St

reaction systems are mentioned. For the applications under UV light irradiation, please refer to the review article by Hartlieb.<sup>56</sup>

**5.2.1. Multiblock copolymer synthesis.** Hartlieb and coworkers successfully synthesized an acrylamide-based multiblock copolymer with up to 20 blocks and relatively low dispersity ( $\bar{D} = 1.29$ ) from a xanthate under UV light irradiation (365 nm, 2 W).<sup>417</sup> The high livingness of the polymerization was ascribed to reduction in the feeding rate of monomers. The authors postulated that the slow monomer addition increased the number of reversible deactivations per monomer addition owing to the low chain transfer coefficient of acrylamide monomers for xanthate, and suppressed irreversible termination; however, too slow feeding rate would cause the degradation of the CTA and broad dispersity. Therefore, to prepare polymers with narrow dispersity, a series of chain extensions rather than one polymerization reaction was recommended. Although oxygen had to be removed before each addition of monomers, and molecular weights of the obtained polymers were consistently lower than the theoretical values in every step, this work demonstrated the promise of photoiniferter polymerization for the synthesis of multiblock copolymers.

If different types of monomers have to be involved in each block, the monomer that would become a better leaving group needs to be polymerized first to favor fragmentation and chain extension with the second monomer during addition–fragmentation in the RAFT process. If the order is inverted, the second monomer with a better leaving group, instead of the first block, is likely to favor fragmentation and propagation, and will be homo-polymerized in the presence of an exogenous radical derived from external initiators. As a result, a mixture of homopolymers rather than the desired uniform block copolymers comprising two types of monomers is provided. Sumerlin and coworkers surmised that this restriction regarding the order of blocks in a copolymer would be resolved *via* photoiniferter polymerization.<sup>418</sup> Photoiniferter polymerization that is mediated by (i) direct photolysis of the C–S bond, which does not require an exogenous radical initiator, and (ii) reversible termination rather than degenerative chain transfer is thus expected not to restrict the sequence of blocks in copolymers

based on the difference in leaving group abilities. Initially, DMAm was polymerized as the first block from TTC by conventional RAFT polymerization or from xanthate by photoiniferter polymerization. As expected, subsequent photoiniferter polymerization of poly(DMAm)-xanthate under UV light irradiation (365 nm, 5.0 mW cm<sup>−2</sup>) successfully extended poly(DMAm)-xanthate with MMA, whereas thermally initiated polymerization provided a mixture of homopolymers of DMAm and MMA. Poly(DMAm)-TTC was also extended with MMA under blue light irradiation, but the rate of photolysis was slower. Using xanthate that was efficiently cleaved under UV light irradiation as a CTA, not only DMAm but also MA and *N*-vinylcarbazole were used as the first blocks and were extended by MMA.

Diblock copolymers of poly(acrylamide)s and polyethers were synthesized by combined photoiniferter polymerization under UV light irradiation (365 nm, 3.5 mW cm<sup>−2</sup>) and *t*-Bu-P<sub>2</sub>/triethylborane-catalyzed ROP at room temperature.<sup>122</sup> As TTCs remained intact under the reaction conditions of ROP, either sequentially or simultaneously performed photoiniferter polymerization and ROP from the mono-hydroxyl-functionalized TTC provided the diblock copolymers.  $\alpha,\omega$ -Di-hydroxyl-functionalized TTC provided the  $\alpha,\omega$ -di-hydroxyl-functionalized polyacrylates that could serve as building blocks for polyurethane (PU).<sup>88</sup> After the preparation of poly(*n*-BA) ( $M_{n,GPC} = 3100$  g mol<sup>−1</sup> and  $\bar{D} = 1.03$ ) under blue light irradiation (455 nm, 5 mW cm<sup>−2</sup>), thermoplastic PU elastomer was synthesized from the mixture of 5 mol% poly(*n*-BA) and 95 mol% poly(tetramethylene ether glycol) as a soft segment, isophorone diisocyanate as a hard segment, and ethylene glycol as a chain extender. The prepared elastomer surprisingly overcame the strength–elongation and robustness–self-healing ability trade-off relationships typically observed in elastomers. As various monomers can be incorporated as a part of soft segments to influence phase separation behavior and chain mobility within the polymer network, the development of thermoplastic PU elastomers with unprecedented properties was expected. In addition, *via* copper-catalyzed azide–alkyne reaction, polymers prepared from  $\alpha$ -alkyne-functionalized TTC under blue light irradiation (460 nm, 4 mW cm<sup>−2</sup>) could be linked to bioactive peptides possessing the *N*-terminal azide functionality.<sup>408</sup> Thus, high end-group fidelity



under mild reaction conditions of visible-light-driven photoiniferter polymerization was highlighted.

**5.2.2. Single unit monomer insertion (SUMI).** Photoiniferter polymerization has only been applied in the first step (*i.e.*, the preparation of monoadducts) of sequential SUMI, as discussed in Section 4.3.1.2. For the synthesis of trimers and pentamers, a styrene and indene were inserted into CDTPA *via* direct photolysis under green light irradiation (530 nm,  $0.6 \text{ mW cm}^{-2}$ )<sup>89</sup> and blue light irradiation (460 nm,  $0.8 \text{ mW cm}^{-2}$ ),<sup>269</sup> respectively. Postma, Moad, and coworkers investigated the potential for sequential SUMI by successive photoiniferter polymerizations.<sup>272</sup> Using DMAM as a monomer and CETCPA as a CTA under irradiation with various light sources (402, 451, 512, and 633 nm), red light (633 nm,  $8 \text{ W m}^{-2}$ ) provided the most selective formation of the monoadduct with almost no byproduct formation but at the slowest reaction rate. Nevertheless, red light was not appropriate for the second SUMI owing to significantly less overlap between the emission of the LED and the absorption profile of the resulting monoadduct as the absorption band for the  $n \rightarrow \pi^*$  transition was changed from 442.9 to 427.0 nm. Instead, irradiation at lower wavelengths (402, 451, and 512 nm with 20, 8, and  $14 \text{ W m}^{-2}$ , respectively) with diminished yet sufficient overlap led to the formation of not only the desired diadducts but also byproducts *via* multiple insertions of monomers and photodecomposition of the TTC moiety.

In the absence of a PC, sequence-defined oligomers could be prepared *via* an iterative method rather than sequential SUMI (Fig. 23).<sup>419</sup> Boyer and coworkers in collaboration with Moad and Hawker confirmed the high end-group fidelity of the monoadduct of MA and CDTPA and functionalized the TTC moiety. Aminolysis of TTC into thiol was followed by a thiol-ene reaction with a second monomer containing a hydroxy group (2-hydroxyethyl acrylate (2-HEA)). Thereafter, the hydroxy group underwent esterification with CDTPA to introduce a new

CDTPA for another SUMI using DMAM as a third monomer. Finally, aminolysis, thiol-ene reaction with a fourth monomer (2-hydroxy butyl acrylate), and esterification with CDTPA were repeated to insert BzA as the last monomer to provide a sequence-defined pentamer. Although the monomer scope was expanded to acrylates and acrylamides, pre-functionalization of the carboxylic acid group of the starting CDTPA with a 3-trimethylsilyl protecting group to block its esterification with the lately introduced monomers with hydroxy groups and isolation of each intermediate can be cumbersome in this strategy.

**5.2.3. Ultrahigh-molecular-weight (UHMW) polymer synthesis.** Successful synthesis of UHMW polymers requires fast photolysis of the CTA, high radical concentration, and high  $k_p$  of monomers, while keeping the probability of termination low. Thus, photoiniferter polymerization in the absence of an initiator and initiator-derived radicals is advantageous. Owing to the weaker C-S bond in xanthates compared to that in TTCs and accordingly more efficient generation of initiating radicals through photolysis, xanthates have been extensively employed for synthesis of UHMW polymers.<sup>278,395,420</sup> With regard to the fast polymerization kinetics, acrylamides with high  $k_p$  were selected as monomers. Sumerlin and coworkers synthesized UHMW poly(DMAM)s in water under UV light irradiation.<sup>395</sup> Moreover, a highly viscous reaction mixture prevented termination reactions between propagating radicals. Both xanthate and TTC underwent photolysis, but the reaction time was significantly lowered for xanthate (30 minutes) as compared to TTC (10 hours) because the  $n \rightarrow \pi^*$  transition of xanthate led to more efficient photolytic cleavage compared to the  $\pi \rightarrow \pi^*$  transition of TTC at 365 nm. To facilitate the  $n \rightarrow \pi^*$  transition of TTC, Cameron, Saito, and coworkers used visible light (402 or 451 nm, 6 W), but higher intensity (208 W) was required to achieve a reasonably short reaction time (12 hours *vs.* 11 minutes).<sup>409</sup> However, higher intensity of irradiation also

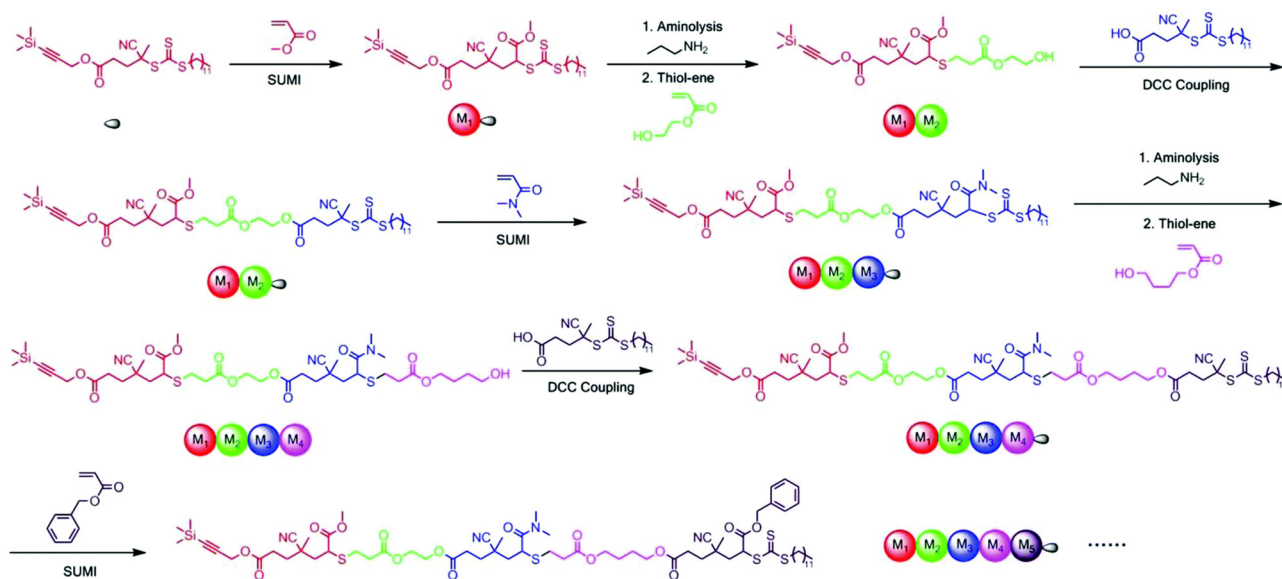


Fig. 23 Schematic representation of the synthesis of a sequence-defined pentamer *via* iterative SUMI, aminolysis, thiol-ene, and esterification reactions. Adapted with permission from ref. 419 (Copyright 2017 The Royal Society of Chemistry).



caused heating of the reaction mixture and subsequent hydrolysis of the CTA resulted in the loss of polymerization control. Qiao and coworkers synthesized UHMW star polymers from 4- and 21-arm xanthates in DMSO.<sup>278</sup> UV light irradiation was more efficient than violet light to reach 96% monomer conversion after 6 and 102 hours, respectively, although UV light could lead to unselective activation of the monomer and loss of polymerization control. UHMW linear and branched block copolymers of acrylic acid and various acrylamides for application as microgel viscosifiers for water-based drilling fluids were synthesized in water under UV light irradiation (350 nm, 7.2 mW cm<sup>-2</sup>).<sup>420</sup>

Sumerlin and coworkers expanded the monomer scope to monomers with relatively low  $k_p$  such as (meth)acrylates and styrene in DMSO.<sup>413</sup> In DMSO, monomer concentrations should be higher than those in water to achieve sufficiently high polymerization kinetics. In particular, synthesis of UHMW poly(MMA) from TTC under UV light irradiation (365 nm, 7.0 mW cm<sup>-2</sup>) required the addition of tertiary amine PMDETA. It was presumed that in the absence of PMDETA, the TTC sulfanyl radical abstracted the hydrogen atom from the propagating methacryloyl chain end, thereby affording a dead chain *via* disproportionation. The lower  $k_p$  of styrene needed to be compensated by alternatively copolymerizing styrene with maleic anhydride or maleimide *via* charge-transfer complex formation. However, because of absorption and background initiation from the charge-transfer complex in the UV region, TTC was replaced with DTB to shift the irradiation wavelength from 365 nm to 450 nm.

**5.2.4. Photo-PISA.** Boyer and coworkers, for the first time, demonstrated the potential of photo-PISA in the absence of a PC to encapsulate hydrophobic drug molecules into polymer micelles.<sup>421</sup> A poly(OEGMA)-based macro-CTA was initially synthesized from CDTPA by thermally initiated RAFT polymerization. Photoiniferter polymerization of BzMAS from the macro-CTA in acetonitrile/ethanol cosolvent under blue (460 nm, 0.7 mW cm<sup>-2</sup>) or green light irradiation (530 nm, 0.7 mW cm<sup>-2</sup>) led to the formation of worm-like micelles. When Nile Red, a model hydrophobic drug, was introduced into the reaction mixture, Nile Red was *in situ* encapsulated in the worm-like micelles, suggesting the potential application of photo-PISA for delivery of hydrophobic drugs. Blue light degraded the end group of CTAs and broadened the dispersity of polymers, but was appropriate for the polymerization in the presence of Nile Red as the polymerization under green light irradiation was significantly inhibited by the absorption of green light by Nile Red. This encapsulation methodology *via* photo-PISA was successfully expanded to another hydrophobic drug doxorubicin using a continuous flow reactor equipped with a 460 nm LED strip.<sup>422</sup> The continuous flow reactor not only enabled the scalable synthesis of polymeric NPs, but also the facile control of NP morphologies by simply adjusting the flow rate and residence time to modulate the length of a solvophobic block. Besides the drug encapsulation, spherical NPs prepared from photo-PISA served as a template to synthesize 3D mesoporous carbon materials.<sup>406</sup>

**5.2.5. Surface functionalization.** Photoiniferter polymerization from CDTPA grafted on UCNPs led to the grafting-from

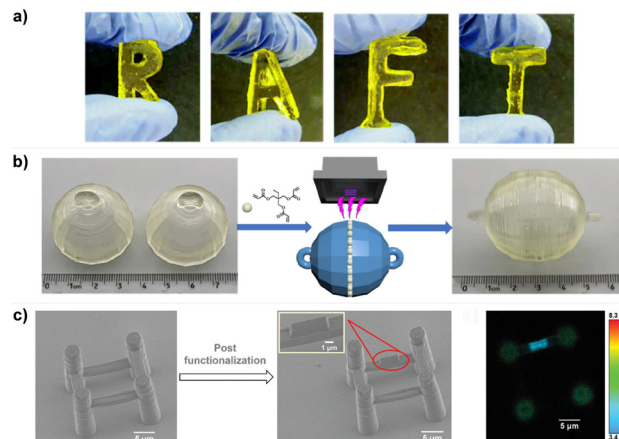


Fig. 24 (a) 3D printed objects. (b) Welding two 3D printed balls by adding fresh TMPTA on the interface and subsequent irradiation. (c) SEM images of the 3D printed bridge before and after post-modification with fluorescein-conjugated TMPTA. The fluorescein-embedded layer was visualized by fluorescence lifetime imaging microscopy (FLIM). Adapted with permission from (a) ref. 403 (Copyright 2020 The Royal Society of Chemistry), (b) ref. 161 (Copyright 2022 American Chemical Society), and (c) ref. 424 (Copyright 2021 John Wiley & Sons, Inc.).

surface functionalization with polymers comprised of glycidyl methacrylate (GMA), OEGMA, and hydroxyethyl methacrylate (HEMA) under blue (460 nm, 0.7 mW cm<sup>-2</sup>) or green light irradiation (530 nm, 0.7 mW cm<sup>-2</sup>).<sup>400</sup> The absence of a PC was advantageous because the remaining PC would interfere with the optical or upconversion properties of the resulting particles.

**5.2.6. 3D printing.** Jin, Bagheri, and coworkers in collaboration with the research group of Boyer applied photoiniferter polymerization of TTCs under violet light irradiation (405 nm, 1.8 mW cm<sup>-2</sup>) to 3D printing (Fig. 24a).<sup>403</sup> The build speed was limited by the slow and inefficient photolysis of TTC. Nevertheless, reactivation of TTC units after 3D printing allowed transformation of the 3D printed object. Soaking the 3D printed object in *n*-BA dissolved in DMSO followed by blue light irradiation (460 nm, 0.7 mW cm<sup>-2</sup>) facilitated insertion of hydrophobic *n*-BA into outer layers of the object and modified surface hydrophilicity. This report was the first to present implementation of photoiniferter polymerization in 3D printing, but 3D printing was performed under a N<sub>2</sub> atmosphere with degassed reaction solutions.

Open-to-air 3D printing by the DLP technique under violet light irradiation (405 nm, 2.0 mW cm<sup>-2</sup>) was performed using EXEP.<sup>161</sup> DFT calculations and ESR spin-trapping experiments confirmed that photolysis of EXEP under irradiation at 325–480 nm was more efficient than that of structurally similar TTC due to the lower bond dissociation energy of EXEP (38.06 kcal mol<sup>-1</sup> vs. 41.5 kcal mol<sup>-1</sup>). Although oxidation-induced loss of end-group fidelity of polymers was previously observed for photoiniferter polymerization using EXEP under blue light irradiation (460–470 nm),<sup>162</sup> the end-group fidelity of polymers within 3D printed objects seemed to be preserved allowing post-functionalization with the freshly added PEGDA and trimethylolpropane triacrylate (TMPTA) or welding,





without an additional introduction of the photoinitiator or PC (Fig. 24b). When this photoiniferter polymerization was combined with cationic RAFT polymerization using diphenyliodonium hexafluorophosphate onium salt, welding of 3D printed objects was realized by either photoiniferter polymerization under violet light irradiation (405 nm, 60 mW cm<sup>-2</sup>) or ZnCl<sub>2</sub>-mediated conventional cationic RAFT polymerization without irradiation.<sup>423</sup> Herein, polymerization (*i.e.*, 3D printing) was initiated by photolysis of two types of CTAs which were expected to orthogonally proceed radical and cationic RAFT polymerization, which would allow tailoring of the mechanical properties of polymeric materials by adjusting the ratio of radically and cationically polymerizable monomers.

DTC bearing conjugated carbazole in the Z group was also applied to prepare 3D microstructures by the direct laser writing technique in the presence of air.<sup>424</sup> Photoiniferter polymerization of *n*-BA under blue light irradiation (480 nm) followed by subsequent photoiniferter polymerization with TMPTA under green light irradiation (532 nm) provided mechanically stable 3D microstructures. Owing to the preserved DTC units, fabrication of multilayered microstructures comprised of multiple polymeric materials *via* repeated polymerization was successfully realized. Post-modification by polymerization with thermoresponsive NIPAm provided the printed object capable of heating-induced shrinkage and cooling-induced swelling, whereas polymerization with fluorescein-conjugated TMPTA allowed the visualization of the modified layer by fluorescence lifetime imaging microscopy (FLIM) (Fig. 24c).

## 6. Photomediated cationic RAFT polymerization

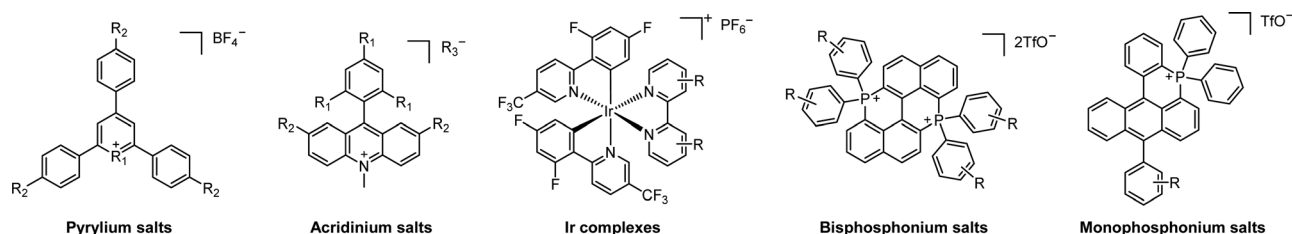
### 6.1. PCs for polymerization

A strongly oxidizing pyrylium salt was first employed for the photomediated cationic RAFT polymerization of vinyl ethers under blue light irradiation (450 nm) (Scheme 27).<sup>43</sup> The excited-state pyrylium salt oxidized the vinyl ether-derived CTA to generate a carbocation intermediate and reversible generation of the carbocations enabled the regulation of cationic RAFT polymerization by light. iBVE and other vinyl ethers (*i.e.*, ethyl, 2-chloroethyl, *n*-propyl, and *n*-butyl-vinyl ethers) were polymerized from DTC and TTC, respectively. In contrast to PET-RAFT polymerization, photomediated cationic RAFT polymerization required CTAs possessing vinyl ether as the R group. However, imperfect temporal control and monomer conversion in the

absence of irradiation were observed in further studies, which was ascribed to the decomposition of the PC. Moreover, the experimental molecular weights of polymers were significantly lower than the theoretical value when the authors targeted to synthesize polymers with molecular weight above 20 kg mol<sup>-1</sup>.

Other oxidizing PCs including the Ru complex and acridinium salt, however, were unsuccessful for the polymerization of iBVE from DTCs.<sup>90</sup> Thereafter, Kamigaito, Ohkubo, and coworkers discovered that acridinium salts at doubled catalyst loadings to that of the previous study<sup>90</sup> could catalyze the polymerization from TTC at -40 °C despite imperfect temporal control,<sup>91</sup> where the polymerization rate was somehow affected by the type of counter-anions of acridinium salts which possessed the same structure and similar redox potentials. Although the polymerization of the chloroethyl vinyl monomer from DTC was uncontrolled because the high  $E_{ox}^*$  (2.06–2.25 V *vs.* SCE) oxidized the chloroethyl substituent of the monomer or the amino substituent of the CTA, acridinium salts extended the polymerization wavelength from blue to white and green.

The imperfect temporal control (*i.e.*, monomer conversion in the dark), observed particularly at high monomer conversion, that was noticed for both pyrylium and acridinium salts was ascribed to low stability of the PC or high  $E_{ox}^*$ . Instead, Ir complexes with enhanced stability demonstrated no monomer conversion in the dark.<sup>425</sup> Moreover, appropriate redox potentials of Ir complexes enabled the synthesis of high-molecular-weight polymers owing to the well-balanced rates of activation and deactivation steps, and the preferential oxidation of the CTA over that of vinyl ether monomers. Owing to more reducing  $E_{red}^0$ , Ir complex in contrast to pyrylium salt efficiently generated the thiolate anion that recaps the propagating cation intermediates and completely prevented the polymerization in the dark.<sup>426</sup> Herein, a thioacetal instead of a dithioester was used as a CTA, but the mechanism was technically identical except that the sulfonium intermediate participated in degenerative chain transfer. The importance of an appropriate redox potential was also verified by Liao and coworkers in the case of bisphosphonium salt ( $E_{ox}^* = 2.01$ – $2.06$  V *vs.* SCE).<sup>427</sup> The bisphosphonium salt allowed the polymerization of a variety of vinyl ethers from TTC with excellent temporal control at low catalyst loadings (in the ppm range) under sunlight irradiation. Similarly, the monophosphonium salt synthesized by the same research group exhibited excellent temporal control.<sup>428</sup> The relationship between the structure of the PC and polymerization activity was explored based on high modularity of the structure of the PC and the concomitantly widened redox window. The controllability of



Scheme 27 Chemical structures of PCs employed for photomediated cationic RAFT polymerization.



polymerization was dependent on the successful oxidation of the CTA by the excited-state PC, which was influenced by the redox potential, lifetime, and  $\Phi_{\text{FL}}$  of the excited-state PC.

On the other hand, cationic RAFT polymerization under NIR light irradiation (788 nm, 14 mW cm<sup>-2</sup>) was induced by Fe<sub>2</sub>(Cp)<sub>2</sub>(CO)<sub>4</sub> in combination with alkyl bromide as an initiating system,<sup>429</sup> where *in situ*-generated FeCp(CO<sub>2</sub>)Br upon irradiation oxidizes a carbon-centered radical to provide an initiating cation *via* a mechanistic process similar to photoinduced radical oxidation/addition/deactivation (PROAD) that was previously reported by Yagci and coworkers.<sup>430</sup> Zhu, Perrier, and coworkers employed Mn(CO)<sub>10</sub>/alkyl bromide<sup>431</sup> or Mn(CO)<sub>5</sub>Br alone under blue light irradiation (440 nm, 10 mW cm<sup>-2</sup>).<sup>432</sup> Mn(CO)<sub>5</sub>Br, a bench-stable PC with reduced sensitivity to oxygen compared to the Mn(CO)<sub>10</sub>/alkyl bromide system, for the first time facilitated the polymerization of iBVE without prior deoxygenation either in a batch or continuous flow reactor.

## 6.2. Applications

Selective activation of Ir(ppy)<sub>3</sub>-catalyzed PET-RAFT and pyrylium salt-catalyzed photomediated cationic RAFT polymerization of MA and iBVE, respectively, by simply changing the irradiation wavelength was applied in one-pot synthesis of a multiblock copolymer (Table 2, entry 1).<sup>124</sup> According to the absorption profile of PCs, absorption of Ir(ppy)<sub>3</sub> and subsequent PET-RAFT polymerization of MA under blue light (450 nm), and absorption of the pyrylium salt and subsequent photomediated cationic RAFT polymerization of iBVE under green light (520 nm) were expected. However, partially overlapping absorption profiles of two PCs also resulted in photomediated cationic RAFT polymerization at 450 nm and the problematic synthesis of tapered block copolymers. Fors and coworkers took advantage of the simultaneous PET-RAFT and photomediated cationic RAFT polymerizations to modulate the mechanical properties of thermoset polymers.<sup>126</sup> Cross-linking of 1,4-butanediol divinyl ethers under green light irradiation (525 nm, 142 mW cm<sup>-2</sup>) generated the polymer network, whereas by switching to blue light (456 nm, 108 mW cm<sup>-2</sup>), butanediol diacrylates were also incorporated into the network and increased the cross-linking density and Young's modulus. Thus, the mechanical properties of the polymer network became easily adjustable by the amount of diacrylates, irradiation time and light intensity, and *via* spatially controlled PET-RAFT polymerization by applying a photomask. Nevertheless, photomediated cationic RAFT polymerization is still at an early stage for numerous applications owing to the narrow scope of monomers, PCs, and solvents and lack of oxygen tolerance in the reaction system. The recent development of PCs<sup>92</sup> or use of continuous flow reactors<sup>382</sup> combined with further studies would expand the utility of the polymerization.

## 7. Summary and outlook

Among photocontrolled RAFT polymerization reactions, visible-light-driven RAFT polymerization which harnesses visible light or even sunlight has drawn attention in various fields including

polymer chemistry, materials science, and bioengineering to name a few. As visible light is an environmentally benign and easily accessible energy source and visible-light photocatalysis provides oxygen tolerance that simplifies the reaction design by eliminating laborious deoxygenation, visible-light-driven RAFT polymerization is expected to be soon utilized at an industrial scale and face the new era in the near future. In particular, PET-RAFT polymerization with highly efficient oxygen tolerance has been successfully adapted for bioapplications, surface functionalization, 3D/4D printing, and HTP synthesis in readily accessible reactor system designs without prior degassing.

In addition, polymers synthesized by RAFT polymerization have recently been subjected to depolymerization, drawing attention to a sustainable future of polymer chemistry. Anastasaki and coworkers reported radical-mediated, catalyst-free, and near-quantitative depolymerization of various methacrylic polymers.<sup>433</sup> Thermally induced homolytic cleavage of the C–S bond at 120 °C generated chain-end radicals and released monomers from the end of the polymer. Depolymerization of the polymer became favored over re-insertion of the released monomers under highly dilute conditions (5 mM relative to the monomer; 200 times lower than that of typical polymerization conditions). Again, *via* visible-light-driven photocatalysis both in the presence<sup>434</sup> and absence of a PC,<sup>435</sup> faster rates and higher conversions of depolymerization were achieved despite the temperature being lowered to 100 °C. The improved reaction efficiencies were attributed to more efficient generation of chain-end radicals *via* the combined thermally and photo-induced homolytic cleavage of the C–S bond. In all cases, high end-group fidelity of polymers provided by RAFT polymerization was essential for efficient depolymerization. These initial demonstrations of depolymerization are expected to be applied for a wider scope of polymers (*i.e.*, prepared from non-methacrylic monomers and various CTAs) under milder reaction conditions. Combined with the synthesis of degradable vinyl polymers *via* copolymerization with macrocyclic allylic sulfones,<sup>100,185</sup> radical-mediated depolymerization would provide further opportunities for polymer chemistry.

However, there is still room for improvement. First, although the interest in comprehensively elucidating mechanistic backgrounds using computational chemistry and kinetic modeling has increased, it is currently limited to only a few types of PCs and/or CTAs. Only when the discrepancy in each combination of PC and/or CTA is considered, a fully optimized reaction system for the intended applications may be designed.<sup>436</sup> Second, compared to PET-RAFT polymerization, the applications of photoiniferter and photomediated cationic RAFT polymerizations are still limited by the lack of oxygen tolerance and a rather narrow range of operational irradiation wavelengths and solvents for the polymerization reactions. Regardless of the polymerization method, a fundamental understanding of the mechanisms of the photomediated process (*e.g.*, the involvement of singlet or triplet excited states, the transfer of electron or energy, and the fate of the reaction intermediates) would improve the reaction system. Third, although the introduction of flow chemistry has enhanced the scalability of visible-light-driven RAFT polymerizations, the design of a reactor that could provide an accurate control over the light



intensity (*i.e.*, photon flux) and reaction temperature is necessary for consistency of polymer properties. This influence of the reactor geometry and volume on PET-RAFT polymerization was also reported for a cylindrical batch system.<sup>437</sup>

In summary, we have provided herein a brief history, progress, and future challenges of photocontrolled RAFT polymerization. Recent studies on degradation and thermally or photo-induced depolymerization of polymers synthesized *via* RAFT polymerization, which potentially provide closed-loop recycling of the polymers synthesized by RAFT polymerization, have also been mentioned. Therefore, photocontrolled RAFT polymerization holds significant promise in polymer chemistry ranging from an environmentally friendly synthesis to a green future of polymers such as commercial vinyl polymers including plastics.<sup>438</sup> We anticipate that this review will provide guidance on how and to what extent the photocontrolled RAFT polymerization could be utilized, and attract researchers from various fields to achieve the full potential of the method, which pose a greater impact on our society in line with the ever-growing need for environmental compatibility.

## Conflicts of interest

There are no conflicts to declare.

## Acknowledgements

This work at SNU was supported by the National Research Foundation of Korea (NRF) funded by the Korean government (MSIT) (2022R1A2C2011627 and 2021R1A5A1030054) and the Challengeable Future Defense Technology Research and Development Program (No. 912909601) of Agency for Defense Development in 2022. Professor Cyrille Boyer (or C.B.) is the recipient of an Australian Research Council Australian Laureate Fellowship (FL220100016) funded by the Australian government.

## References

- 1 L. J. Malone and T. Dolter, *Basic Concepts of Chemistry*, John Wiley & Sons, Inc., 2008.
- 2 G. Ciamician, *Science*, 1912, **36**, 385–394.
- 3 B. König, *Eur. J. Org. Chem.*, 2017, 1979–1981.
- 4 D. A. Nicewicz and D. W. C. MacMillan, *Science*, 2008, **322**, 77–80.
- 5 M. A. Ischay, M. E. Anzovino, J. Du and T. P. Yoon, *J. Am. Chem. Soc.*, 2008, **130**, 12886–12887.
- 6 J. M. R. Narayanam, J. W. Tucker and C. R. J. Stephenson, *J. Am. Chem. Soc.*, 2009, **131**, 8756–8757.
- 7 T. P. Yoon, M. A. Ischay and J. Du, *Nat. Chem.*, 2010, **2**, 527–532.
- 8 J. M. R. Narayanam and C. R. J. Stephenson, *Chem. Soc. Rev.*, 2011, **40**, 102–113.
- 9 C. K. Prier, D. A. Rankic and D. W. C. MacMillan, *Chem. Rev.*, 2013, **113**, 5322–5363.
- 10 L. Marzo, S. K. Pagire, O. Reiser and B. König, *Angew. Chem., Int. Ed.*, 2018, **57**, 10034–10072.
- 11 N. A. Romero and D. A. Nicewicz, *Chem. Rev.*, 2016, **116**, 10075–10166.
- 12 T. Rigotti and J. Alemán, *Chem. Commun.*, 2020, **56**, 11169–11190.
- 13 V. Srivastava, P. K. Singh and P. P. Singh, *J. Photochem. Photobiol., C*, 2022, **50**, 100488.
- 14 J.-F. Lutz, J.-M. Lehn, E. W. Meijer and K. Matyjaszewski, *Nat. Rev. Mater.*, 2016, **1**, 16024.
- 15 W. A. Braunecker and K. Matyjaszewski, *Prog. Polym. Sci.*, 2007, **32**, 93–146.
- 16 K. Matyjaszewski, *Adv. Mater.*, 2018, **30**, 1706441.
- 17 J.-S. Wang and K. Matyjaszewski, *Macromolecules*, 1995, **28**, 7901–7910.
- 18 J. Chiefari, Y. K. (Bill) Chong, F. Ercole, J. Krstina, J. Jeffery, T. P. T. Le, R. T. A. Mayadunne, G. F. Meijs, C. L. Moad, G. Moad, E. Rizzardo and S. H. Thang, *Macromolecules*, 1998, **31**, 5559–5562.
- 19 M. Chen, M. Zhong and J. A. Johnson, *Chem. Rev.*, 2016, **116**, 10167–10211.
- 20 N. Corrigan, S. Shanmugam, J. Xu and C. Boyer, *Chem. Soc. Rev.*, 2016, **45**, 6165–6212.
- 21 S. Dadashi-Silab, M. Atilla Tasdelen and Y. Yagci, *J. Polym. Sci., Part A: Polym. Chem.*, 2014, **52**, 2878–2888.
- 22 Y. Yagci, S. Jockusch and N. J. Turro, *Macromolecules*, 2010, **43**, 6245–6260.
- 23 M. A. Tasdelen, M. Uygun and Y. Yagci, *Macromol. Rapid Commun.*, 2011, **32**, 58–62.
- 24 A. Anastasaki, V. Nikolaou, Q. Zhang, J. Burns, S. R. Samanta, C. Waldron, A. J. Haddleton, R. McHale, D. Fox, V. Percec, P. Wilson and D. M. Haddleton, *J. Am. Chem. Soc.*, 2014, **136**, 1141–1149.
- 25 R. Ran, Y. Yu and T. Wan, *J. Appl. Polym. Sci.*, 2007, **105**, 398–404.
- 26 H. Wang, Q. Li, J. Dai, F. Du, H. Zheng and R. Bai, *Macromolecules*, 2013, **46**, 2576–2582.
- 27 Y. Kwak and K. Matyjaszewski, *Macromolecules*, 2010, **43**, 5180–5183.
- 28 B. P. Fors and C. J. Hawker, *Angew. Chem., Int. Ed.*, 2012, **51**, 8850–8853.
- 29 D. Konkolewicz, K. Schröder, J. Buback, S. Bernhard and K. Matyjaszewski, *ACS Macro Lett.*, 2012, **1**, 1219–1223.
- 30 M. A. Tasdelen, M. Ciftci and Y. Yagci, *Macromol. Chem. Phys.*, 2012, **213**, 1391–1396.
- 31 J. Xu, K. Jung, A. Atme, S. Shanmugam and C. Boyer, *J. Am. Chem. Soc.*, 2014, **136**, 5508–5519.
- 32 J. Xu, S. Shanmugam, N. A. Corrigan and C. Boyer, *Controlled Radical Polymerization: Mechanisms*, American Chemical Society, Washington, DC, 2015, vol. 1187, pp. 247–267.
- 33 T. G. McKenzie, Q. Fu, E. H. H. Wong, D. E. Dunstan and G. G. Qiao, *Macromolecules*, 2015, **48**, 3864–3872.
- 34 N. Corrigan, K. Jung, G. Moad, C. J. Hawker, K. Matyjaszewski and C. Boyer, *Prog. Polym. Sci.*, 2020, **111**, 101311.
- 35 C. Aydogan, G. Yilmaz, A. Shegiwal, D. M. Haddleton and Y. Yagci, *Angew. Chem., Int. Ed.*, 2022, **61**, e202117377.



- 36 D. A. Corbin and G. M. Miyake, *Chem. Rev.*, 2022, **122**, 1830–1874.
- 37 S. Perrier, *Macromolecules*, 2017, **50**, 7433–7447.
- 38 J. F. Quinn, L. Barner, C. Barner-Kowollik, E. Rizzardo and T. P. Davis, *Macromolecules*, 2002, **35**, 7620–7627.
- 39 T. Otsu and M. Yoshida, *Macromol. Rapid Commun.*, 1982, **3**, 127–132.
- 40 T. Otsu, M. Yoshida and T. Tazaki, *Macromol. Rapid Commun.*, 1982, **3**, 133–140.
- 41 M. Uchiyama, K. Satoh and M. Kamigaito, *Angew. Chem., Int. Ed.*, 2015, **54**, 1924–1928.
- 42 S. Sugihara, N. Konegawa and Y. Maeda, *Macromolecules*, 2015, **48**, 5120–5131.
- 43 V. Kottisch, Q. Michaudel and B. P. Fors, *J. Am. Chem. Soc.*, 2016, **138**, 15535–15538.
- 44 J. Phommalsack-Lovan, Y. Chu, C. Boyer and J. Xu, *Chem. Commun.*, 2018, **54**, 6591–6606.
- 45 S. Dadashi-Silab, S. Doran and Y. Yagci, *Chem. Rev.*, 2016, **116**, 10212–10275.
- 46 S. Shanmugam, J. Xu and C. Boyer, *Macromol. Rapid Commun.*, 2017, **38**, 1700143.
- 47 X. Pan, M. A. Tasdelen, J. Laun, T. Junkers, Y. Yagci and K. Matyjaszewski, *Prog. Polym. Sci.*, 2016, **62**, 73–125.
- 48 M. L. Allegranza and D. Konkolewicz, *ACS Macro Lett.*, 2021, **10**, 433–446.
- 49 J. Yeow, R. Chapman, A. J. Gormley and C. Boyer, *Chem. Soc. Rev.*, 2018, **47**, 4357–4387.
- 50 N. Corrigan, J. Yeow, P. Judzewitsch, J. Xu and C. Boyer, *Angew. Chem., Int. Ed.*, 2019, **58**, 5170–5189.
- 51 S. Li, G. Han and W. Zhang, *Polym. Chem.*, 2020, **11**, 1830–1844.
- 52 V. Bellotti and R. Simonutti, *Polymers*, 2021, **13**, 1119.
- 53 K. Parkatzidis, H. S. Wang, N. P. Truong and A. Anastasaki, *Chem*, 2020, **6**, 1575–1588.
- 54 T. G. McKenzie, Q. Fu, M. Uchiyama, K. Satoh, J. Xu, C. Boyer, M. Kamigaito and G. G. Qiao, *Adv. Sci.*, 2016, **3**, 1500394.
- 55 M. D. Nothling, Q. Fu, A. Reyhani, S. Allison-Logan, K. Jung, J. Zhu, M. Kamigaito, C. Boyer and G. G. Qiao, *Adv. Sci.*, 2020, **7**, 2001656.
- 56 M. Hartlieb, *Macromol. Rapid Commun.*, 2022, **43**, 2100514.
- 57 C. A. Figg, J. D. Hickman, G. M. Scheutz, S. Shanmugam, R. N. Carmean, B. S. Tucker, C. Boyer and B. S. Sumerlin, *Macromolecules*, 2018, **51**, 1370–1376.
- 58 H. Zhou and J. A. Johnson, *Angew. Chem., Int. Ed.*, 2013, **52**, 2235–2238.
- 59 Q. Wang, F.-Y. Bai, Y. Wang, F. Niu, Y. Zhang, Q. Mi, K. Hu and X. Pan, *J. Am. Chem. Soc.*, 2022, **144**, 19942–19952.
- 60 E. E. Stache, V. Kottisch and B. P. Fors, *J. Am. Chem. Soc.*, 2020, **142**, 4581–4585.
- 61 G. Moad, E. Rizzardo and S. H. Thang, *Aust. J. Chem.*, 2012, **65**, 985–1076.
- 62 L. T. Strover, A. Cantalice, J. Y. L. Lam, A. Postma, O. E. Hutt, M. D. Horne and G. Moad, *ACS Macro Lett.*, 2019, **8**, 1316–1322.
- 63 F. Izadi, E. Arthur-Baidoo, L. T. Strover, L.-J. Yu, M. L. Coote, G. Moad and S. Denifl, *Angew. Chem., Int. Ed.*, 2021, **60**, 19128–19132.
- 64 Z. Wu, K. Jung, C. Wu, G. Ng, L. Wang, J. Liu and C. Boyer, *J. Am. Chem. Soc.*, 2022, **144**, 995–1005.
- 65 C. Yu, J. Song, T. I. Kim, Y. Lee, Y. Kwon, J. Kim, J. Park, J. Choi, J. Doh, S. K. Min, S. Cho and M. S. Kwon, *ACS Catal.*, 2023, **13**, 665–680.
- 66 J. Xu, S. Shanmugam, H. T. Duong and C. Boyer, *Polym. Chem.*, 2015, **6**, 5615–5624.
- 67 J. Niu, D. J. Lunn, A. Pusuluri, J. I. Yoo, M. A. O'Malley, S. Mitragotri, H. T. Soh and C. J. Hawker, *Nat. Chem.*, 2017, **9**, 537–545.
- 68 B. S. Tucker, M. L. Coughlin, C. A. Figg and B. S. Sumerlin, *ACS Macro Lett.*, 2017, **6**, 452–457.
- 69 H. Sun, W. Choi, N. Zang, C. Battistella, M. P. Thompson, W. Cao, X. Zhou, C. Forman and N. C. Gianneschi, *Angew. Chem., Int. Ed.*, 2019, **58**, 17359–17364.
- 70 C. Fu, B. Demir, S. Alcantara, V. Kumar, F. Han, H. G. Kelly, X. Tan, Y. Yu, W. Xu, J. Zhao, C. Zhang, H. Peng, C. Boyer, T. M. Woodruff, S. J. Kent, D. J. Searles and A. K. Whittaker, *Angew. Chem., Int. Ed.*, 2020, **59**, 4729–4735.
- 71 Q. Fu, T. G. McKenzie, S. Tan, E. Nam and G. G. Qiao, *Polym. Chem.*, 2015, **6**, 5362–5368.
- 72 M. L. Allegranza, Z. M. DeMartini, A. J. Kloster, Z. A. Digby and D. Konkolewicz, *Polym. Chem.*, 2016, **7**, 6626–6636.
- 73 B. Nomeir, O. Fabre and K. Ferji, *Macromolecules*, 2019, **52**, 6898–6903.
- 74 J. W. Beatty and C. R. J. Stephenson, *Acc. Chem. Res.*, 2015, **48**, 1474–1484.
- 75 J.-H. Back, Y. Kwon, H. Cho, H. Lee, D. Ahn, H.-J. Kim, Y. Yu, Y. Kim, W. Lee and M. S. Kwon, *Adv. Mater.*, 2022, 2204776.
- 76 F. Strieth-Kalthoff, M. J. James, M. Teders, L. Pitzer and F. Glorius, *Chem. Soc. Rev.*, 2018, **47**, 7190–7202.
- 77 F. Strieth-Kalthoff and F. Glorius, *Chem*, 2020, **6**, 1888–1903.
- 78 D. L. Dexter, *J. Chem. Phys.*, 1953, **21**, 836–850.
- 79 S. S. Skourtis, C. Liu, P. Antoniou, A. M. Virshup and D. N. Beratan, *Proc. Natl. Acad. Sci. U. S. A.*, 2016, **113**, 8115–8120.
- 80 R. A. Marcus, *Rev. Mod. Phys.*, 1993, **65**, 599–610.
- 81 P. Seal, J. Xu, S. Luca, C. Boyer, S. C. Smith, S. De Luca, C. Boyer and S. C. Smith, *Adv. Theory Simulations*, 2019, **2**, 1900038.
- 82 M. D. Thum, S. Wolf and D. E. Falvey, *J. Phys. Chem. A*, 2020, **124**, 4211–4222.
- 83 J. Christmann, A. Ibrahim, V. Charlot, C. Croutxé-Barghorn, C. Ley and X. Allonas, *ChemPhysChem.*, 2016, **17**, 2309–2314.
- 84 N. Corrigan, J. Xu, C. Boyer and X. Allonas, *ChemPhotoChem*, 2019, **3**, 1193–1199.
- 85 L. R. Kuhn, M. L. Allegranza, N. J. Dougher and D. Konkolewicz, *J. Polym. Sci.*, 2020, **58**, 139–144.
- 86 T. Otsu, *J. Polym. Sci., Part A: Polym. Chem.*, 2000, **38**, 2121–2136.
- 87 M. L. Allegranza, N. De Alwis Watuthanthrige, Y. Wang, G. A. Garcia, H. Ren and D. Konkolewicz, *Polym. Chem.*, 2020, **11**, 6129–6133.
- 88 C. Yu, J.-K. Ha, J. Ahn, J. Lee, J. Choi, T. Chang, S. K. Min and M. S. Kwon, *Chemrxiv*, 2023, DOI: [10.26434/chemrxiv-2023-dl842](https://doi.org/10.26434/chemrxiv-2023-dl842).





- 89 J. Xu, C. Fu, S. Shanmugam, C. J. Hawker, G. Moad and C. Boyer, *Angew. Chem., Int. Ed.*, 2017, **56**, 8376–8383.
- 90 Q. Michaudel, T. Chauviré, V. Kottisch, M. J. Supej, K. J. Stawiasz, L. Shen, W. R. Zipfel, H. D. Abruña, J. H. Freed and B. P. Fors, *J. Am. Chem. Soc.*, 2017, **139**, 15530–15538.
- 91 M. Matsuda, M. Uchiyama, Y. Itabashi, K. Ohkubo and M. Kamigaito, *Polym. Chem.*, 2022, **13**, 1031–1039.
- 92 R. J. Sifri, Y. Ma and B. P. Fors, *Acc. Chem. Res.*, 2022, **55**, 1960–1971.
- 93 S. Shanmugam, J. Xu and C. Boyer, *Macromolecules*, 2017, **50**, 1832–1846.
- 94 M. Chen, S. Deng, Y. Gu, J. Lin, M. J. MacLeod and J. A. Johnson, *J. Am. Chem. Soc.*, 2017, **139**, 2257–2266.
- 95 Y. Huang, X. R. Zhang, S. Ye, J. Le Li, X. Li and T. Cai, *Nanoscale*, 2019, **11**, 13502–13510.
- 96 C. Wu, H. Chen, N. Corrigan, K. Jung, X. Kan, Z. Li, W. Liu, J. Xu and C. Boyer, *J. Am. Chem. Soc.*, 2019, **141**, 8207–8220.
- 97 X. Li, Y. C. Zhang, Y. Zhao, H. P. Zhao, B. Zhang and T. Cai, *Macromolecules*, 2020, **53**, 1550–1556.
- 98 S. Shanmugam, J. Xu and C. Boyer, *Polym. Chem.*, 2016, **7**, 6437–6449.
- 99 L. Zhang, C. Wu, K. Jung, Y. H. Ng and C. Boyer, *Angew. Chem., Int. Ed.*, 2019, **58**, 16811–16814.
- 100 W. Wang, Z. Zhou, D. Sathe, X. Tang, S. Moran, J. Jin, F. Haeffner, J. Wang and J. Niu, *Angew. Chem., Int. Ed.*, 2022, **61**, e202113302.
- 101 X. Li, S. Ye, Y. C. Zhang, H. P. Zhao, Y. Huang, B. Zhang and T. Cai, *Nanoscale*, 2020, **12**, 7595–7603.
- 102 X. Li, J. Le Li, W. G. Huang, X.-Z. Zhang, B. Zhang and T. Cai, *Nanoscale*, 2018, **10**, 19254–19261.
- 103 L. Hu, Q. Wang, X. Zhang, H. Zhao, Z. Cui, P. Fu, M. Liu, N. Liu, S. He, X. Pang and X. Qiao, *RSC Adv.*, 2020, **10**, 6850–6857.
- 104 C. A. Cox, A. N. Ogorek, J. P. Habumugisha and J. D. Martell, *J. Am. Chem. Soc.*, 2023, **145**, 1818–1825.
- 105 S. Shanmugam, J. Xu and C. Boyer, *J. Am. Chem. Soc.*, 2015, **137**, 9174–9185.
- 106 J. Xu, S. Shanmugam, C. Fu, K. F. Aguey-Zinsou and C. Boyer, *J. Am. Chem. Soc.*, 2016, **138**, 3094–3106.
- 107 S. Houshyar, D. J. Keddie, G. Moad, R. J. Mulder, S. Saubern and J. Tsanaksidis, *Polym. Chem.*, 2012, **3**, 1879–1889.
- 108 J. Vandenbergh, G. Reekmans, P. Adriaenssens and T. Junkers, *Chem. Commun.*, 2013, **49**, 10358–10360.
- 109 J. Xu, *Macromolecules*, 2019, **52**, 9068–9093.
- 110 S. Shanmugam, J. Cuthbert, T. Kowalewski, C. Boyer and K. Matyjaszewski, *Macromolecules*, 2018, **51**, 7776–7784.
- 111 C. Wu, K. Jung, Y. Ma, W. Liu and C. Boyer, *Nat. Commun.*, 2021, **12**, 478.
- 112 N. Corrigan, M. Ciftci, K. Jung and C. Boyer, *Angew. Chem., Int. Ed.*, 2021, **60**, 1748–1781.
- 113 P. Lu, D. Ahn, R. Yunis, L. Delafresnaye, N. Corrigan, C. Boyer, C. Barner-Kowollik and Z. A. Page, *Matter*, 2021, **4**, 2172–2229.
- 114 N. Corrigan and C. Boyer, *ACS Macro Lett.*, 2019, **8**, 812–818.
- 115 Z. Zhang, T.-Y. Zeng, L. Xia, C.-Y. Hong, D.-C. Wu and Y.-Z. You, *Nat. Commun.*, 2018, **9**, 2577.
- 116 M. J. Supej, B. M. Peterson and B. P. Fors, *Chem*, 2020, **6**, 1794–1803.
- 117 A. Nikolaev, Z. Lu, A. Chakraborty, L. Sepunaru and J. Read de Alaniz, *J. Am. Chem. Soc.*, 2021, **143**, 12278–12285.
- 118 C. Fu, J. Xu and C. Boyer, *Chem. Commun.*, 2016, **52**, 7126–7129.
- 119 B. M. Peterson, V. Kottisch, M. J. Supej and B. P. Fors, *ACS Cent. Sci.*, 2018, **4**, 1228–1234.
- 120 L. Xia, Z. Zhang and Y.-Z. You, *Polym. J.*, 2020, **52**, 1323–1331.
- 121 K. Satoh, Z. Sun, M. Uchiyama, M. Kamigaito, J. Xu and C. Boyer, *Polym. J.*, 2020, **52**, 65–73.
- 122 Y. Xia, G. M. Scheutz, C. P. Easterling, J. Zhao and B. S. Sumerlin, *Angew. Chem., Int. Ed.*, 2021, **60**, 18537–18541.
- 123 C. Fu, J. Xu, M. Kokotovic and C. Boyer, *ACS Macro Lett.*, 2016, **5**, 444–449.
- 124 V. Kottisch, Q. Michaudel and B. P. Fors, *J. Am. Chem. Soc.*, 2017, **139**, 10665–10668.
- 125 J. C. Theriot, G. M. Miyake and C. A. Boyer, *ACS Macro Lett.*, 2018, **7**, 662–666.
- 126 Y. Ma, V. Kottisch, E. A. McLoughlin, Z. W. Rouse, M. J. Supej, S. P. Baker and B. P. Fors, *J. Am. Chem. Soc.*, 2021, **143**, 21200–21205.
- 127 M. Fromel, E. M. Benetti and C. W. Pester, *ACS Macro Lett.*, 2022, 415–421.
- 128 P. Xiao, J. Zhang, F. Dumur, M. A. Tehfe, F. Morlet-Savary, B. Graff, D. Gigmes, J. P. Fouassier and J. Lalevée, *Prog. Polym. Sci.*, 2015, **41**, 32–66.
- 129 J. Xu, K. Jung and C. Boyer, *Macromolecules*, 2014, **47**, 4217–4229.
- 130 I.-H. Lee, E. H. Discekici, A. Anastasaki, J. R. de Alaniz and C. J. Hawker, *Polym. Chem.*, 2017, **8**, 3351–3356.
- 131 S. Shanmugam, J. Xu and C. Boyer, *Macromolecules*, 2016, **49**, 9345–9357.
- 132 H. Lu, Y. Huang, E. Zhang, Y. Liu, F. Lv, L. Liu, Y. Ma and S. Wang, *ACS Macro Lett.*, 2021, **10**, 996–1001.
- 133 M. Fromel, D. M. Sweeder, S. Jang, T. A. Williams, S. H. Kim and C. W. Pester, *ACS Appl. Polym. Mater.*, 2021, **3**, 5291–5301.
- 134 A. Bagheri, C. W. A. Bainbridge, K. E. Engel, G. G. Qiao, J. Xu, C. Boyer and J. Jin, *ACS Appl. Polym. Mater.*, 2020, **2**, 782–790.
- 135 N. Zaquen, W. A. A. W. Azizi, J. Yeow, R. P. Kuchel, T. Junkers, P. B. Zetterlund and C. Boyer, *Polym. Chem.*, 2019, **10**, 2406–2414.
- 136 N. Zaquen, A. M. N. B. P. H. A. Kadir, A. Iasa, N. Corrigan, T. Junkers, P. B. Zetterlund and C. Boyer, *Macromolecules*, 2019, **52**, 1609–1619.
- 137 E. Roeven, A. R. Kuzmyn, L. Scheres, J. Baggerman, M. M. J. Smulders and H. Zuilhof, *Langmuir*, 2020, **36**, 10187–10199.
- 138 A. R. Kuzmyn, A. T. Nguyen, L. W. Teunissen, H. Zuilhof and J. Baggerman, *Langmuir*, 2020, **36**, 4439–4446.
- 139 C. W. A. Bainbridge, K. E. Engel and J. Jin, *Polym. Chem.*, 2020, **11**, 4084–4093.
- 140 A. R. Kuzmyn, L. W. Teunissen, P. Fritz, B. van Lagen, M. M. J. Smulders and H. Zuilhof, *Adv. Mater. Interfaces*, 2022, **9**, 2101784.



- 141 M. Kovaliov, M. L. Allegranza, B. Richter, D. Konkolewicz and S. Averick, *Polymer*, 2018, **137**, 338–345.
- 142 Z. Zhang, N. Corrigan, A. Bagheri, J. Jin and C. Boyer, *Angew. Chem., Int. Ed.*, 2019, **58**, 17954–17963.
- 143 Q. Fu, Q. Ruan, T. G. McKenzie, A. Reyhani, J. Tang and G. G. Qiao, *Macromolecules*, 2017, **50**, 7509–7516.
- 144 E. Paola Fonseca Parra, B. Chouchene, J.-L. Six, R. Schneider and K. Ferji, *ACS Appl. Polym. Mater.*, 2021, **3**, 3649–3658.
- 145 N. Corrigan, D. Rosli, J. W. J. Jones, J. Xu and C. Boyer, *Macromolecules*, 2016, **49**, 6779–6789.
- 146 G. Ng, J. Yeow, J. Xu and C. Boyer, *Polym. Chem.*, 2017, **8**, 2841–2851.
- 147 S. Xu, J. Yeow and C. Boyer, *ACS Macro Lett.*, 2018, **7**, 1376–1382.
- 148 S. Xu, G. Ng, J. Xu, R. P. Kuchel, J. Yeow and C. Boyer, *ACS Macro Lett.*, 2017, **6**, 1237–1244.
- 149 Y. Huang, W. L. Guo, J. C. He, X. Li and T. Cai, *Macromol. Rapid Commun.*, 2022, **43**, 2200020.
- 150 J. Niu, Z. A. Page, N. D. Dolinski, A. Anastasaki, A. T. Hsueh, H. T. Soh and C. J. Hawker, *ACS Macro Lett.*, 2017, **6**, 1109–1113.
- 151 Q. Fu, K. Xie, T. G. McKenzie and G. G. Qiao, *Polym. Chem.*, 2017, **8**, 1519–1526.
- 152 C. Stubbs, T. Congdon, J. Davis, D. Lester, S.-J. Richards and M. I. Gibson, *Macromolecules*, 2019, **52**, 7603–7612.
- 153 Y. Huang, Y. Sun, Y. Weng and W. Zhang, *ChemistrySelect*, 2022, **7**, e202201583.
- 154 J. Wang, M. Rivero, A. Muñoz Bonilla, J. Sanchez-Marcos, W. Xue, G. Chen, W. Zhang and X. Zhu, *ACS Macro Lett.*, 2016, **5**, 1278–1282.
- 155 Y. Zheng, Y. Luo, K. Feng, W. Zhang and G. Chen, *ACS Macro Lett.*, 2019, **8**, 326–330.
- 156 Y. Zhou, C. Gu, L. Zheng, F. Shan and G. Chen, *Polym. Chem.*, 2022, **13**, 989–996.
- 157 J. R. Lamb, K. P. Qin and J. A. Johnson, *Polym. Chem.*, 2019, **10**, 1585–1590.
- 158 C.-Y. Li and S.-S. Yu, *Macromolecules*, 2021, **54**, 9825–9836.
- 159 J. Li, C. Ding, Z. Zhang, X. Pan, N. Li, J. Zhu and X. Zhu, *Macromol. Rapid Commun.*, 2017, **38**, 1600482.
- 160 K. M. Burridge, N. De Alwis Watuthanthrige, C. Payne, R. C. Page and D. Konkolewicz, *J. Polym. Sci.*, 2021, **59**, 2530–2536.
- 161 B. Zhao, J. Li, Y. Xiu, X. Pan, Z. Zhang and J. Zhu, *Macromolecules*, 2022, **55**, 1620–1628.
- 162 C. Ding, C. Fan, G. Jiang, X. Pan, Z. Zhang, J. Zhu and X. Zhu, *Macromol. Rapid Commun.*, 2015, **36**, 2181–2185.
- 163 S. E. Seo, E. H. Discekici, Y. Zhang, C. M. Bates and C. J. Hawker, *J. Polym. Sci.*, 2020, **58**, 70–76.
- 164 R. Li and Z. An, *Angew. Chem., Int. Ed.*, 2020, **59**, 22258–22264.
- 165 F. Zhou, R. Li, X. Wang, S. Du and Z. An, *Angew. Chem., Int. Ed.*, 2019, **58**, 9479–9484.
- 166 J. Lalevée, A. Dirani, M. El-Roz, X. Allonas and J. P. Fouassier, *Macromolecules*, 2008, **41**, 2003–2010.
- 167 S. C. Ligon, B. Husár, H. Wutz, R. Holman and R. Liska, *Chem. Rev.*, 2014, **114**, 557–589.
- 168 D. Ahn, L. M. Stevens, K. Zhou and Z. A. Page, *ACS Cent. Sci.*, 2020, **6**, 1555–1563.
- 169 D. Ahn, L. M. Stevens, K. Zhou and Z. A. Page, *Adv. Mater.*, 2021, **33**, 2104906.
- 170 J. Yeow, R. Chapman, J. Xu and C. Boyer, *Polym. Chem.*, 2017, **8**, 5012–5022.
- 171 L. Yu, Y. Wei, Y. Tu, S. Lin, Z. Huang, J. Hu, Y. Chen, H. Qiao and W. Zou, *J. Polym. Sci., Part A: Polym. Chem.*, 2018, **56**, 2437–2444.
- 172 H. Yang, Z. Lu, X. Fu, Q. Li, Y. Zhao, L. Xiao and L. Hou, *Polym. Chem.*, 2022, **13**, 4776–4781.
- 173 Z. Wu, W. Fang, C. Wu, N. Corrigan, T. Zhang, S. Xu and C. Boyer, *Chem. Sci.*, 2022, **13**, 11519–11532.
- 174 J. Sun, S. Ren, H. Zhao, S. Zhang, X. Xu, L. Zhang and Z. Cheng, *ACS Macro Lett.*, 2023, **12**, 165–171.
- 175 H. Yang, Z. Lu, X. Fu, Q. Li, L. Xiao, R. Zhao, Y. Zhao and L. Hou, *Polym. Chem.*, 2021, **12**, 6998–7004.
- 176 Y. Lee, Y. Kwon, Y. Kim, C. Yu, S. Feng, J. Park, J. Doh, R. Wannemacher, B. Koo, J. Gierschner and M. S. Kwon, *Adv. Mater.*, 2022, **34**, 2108446.
- 177 C. Lv, C. He and X. Pan, *Angew. Chem., Int. Ed.*, 2018, **57**, 9430–9433.
- 178 O. R. Wilson and A. J. D. Magenau, *ACS Macro Lett.*, 2018, **7**, 370–375.
- 179 Y. Peng, S. Liu, L. Wang, Y. Xu, Z. Wu and H. Chen, *Macromol. Rapid Commun.*, 2022, **43**, 2100920.
- 180 S. Shanmugam and C. Boyer, *Science*, 2016, **352**, 1053–1054.
- 181 J. T. Trotta and B. P. Fors, *Synlett*, 2016, 702–713.
- 182 V. K. Singh, C. Yu, S. Badgular, Y. Kim, Y. Kwon, D. Kim, J. Lee, T. Akhter, G. Thangavel, L. S. Park, J. Lee, P. C. Nandajan, R. Wannemacher, B. Milián-Medina, L. Lüer, K. S. Kim, J. Gierschner and M. S. Kwon, *Nat. Catal.*, 2018, **1**, 794–804.
- 183 C. Wu, N. Corrigan, C.-H. Lim, W. Liu, G. Miyake and C. Boyer, *Chem. Rev.*, 2022, **122**, 5476–5518.
- 184 Y. Lee and M. S. Kwon, *Eur. J. Org. Chem.*, 2020, 6028–6043.
- 185 W. Wang, B. Rondon, Z. Wang, J. Wang and J. Niu, *Macromolecules*, 2023, **56**, 2052–2061.
- 186 S. Shanmugam, J. Xu and C. Boyer, *Macromolecules*, 2014, **47**, 4930–4942.
- 187 J. A. Reeves, N. De Alwis Watuthanthrige, C. Boyer and D. Konkolewicz, *ChemPhotoChem*, 2019, **3**, 1171–1179.
- 188 P. Yang, P. Pageni, M. P. Kabir, T. Zhu and C. Tang, *ACS Macro Lett.*, 2016, **5**, 1293–1300.
- 189 G. Li, W. Feng, N. Corrigan, C. Boyer, X. Wang and J. Xu, *Polym. Chem.*, 2018, **9**, 2733–2745.
- 190 H. Gong, Y. Gu, Y. Zhao, Q. Quan, S. Han and M. Chen, *Angew. Chem., Int. Ed.*, 2020, **59**, 919–927.
- 191 Q. Yang, V. Ladmiral and B. Améduri, *ChemPhotoChem*, 2019, **3**, 1095–1099.
- 192 J. Yeow, J. Xu and C. Boyer, *ACS Macro Lett.*, 2015, **4**, 984–990.
- 193 J. Xu, K. Jung, N. A. Corrigan and C. Boyer, *Chem. Sci.*, 2014, **5**, 3568–3575.



- 194 S. Shanmugam, J. Xu and C. Boyer, *Chem. Sci.*, 2015, **6**, 1341–1349.
- 195 C. Wu, S. Shanmugam, J. Xu, J. Zhu and C. Boyer, *Chem. Commun.*, 2017, **53**, 12560–12563.
- 196 S. Shanmugam, J. Xu and C. Boyer, *Angew. Chem., Int. Ed.*, 2016, **55**, 1036–1040.
- 197 Z. Yajun, Z. Shuaishuai, L. Xiaojing, Z. Xiaoyu, X. Jing, X. Bijin, W. Yong, Z. Xingping and X. Xiaolin, *CCS Chem.*, 2021, **4**, 122–131.
- 198 J. Xu, S. Shanmugam and C. Boyer, *ACS Macro Lett.*, 2015, **4**, 926–932.
- 199 Y. Zhou, Z. Zhang, C. M. Reese, D. L. Patton, J. Xu, C. Boyer, A. Postma and G. Moad, *Macromol. Rapid Commun.*, 2020, **41**, 1900478.
- 200 S. Xu, N. Corrigan and C. Boyer, *Polym. Chem.*, 2021, **12**, 57–68.
- 201 S. Xu, T. Zhang, R. P. Kuchel, J. Yeow and C. Boyer, *Macromol. Rapid Commun.*, 2020, **41**, 1900493.
- 202 L. Shen, Q. Lu, A. Zhu, X. Lv and Z. An, *ACS Macro Lett.*, 2017, **6**, 625–631.
- 203 W. Wang, S. Zhong, G. Wang, H. Cao, Y. Gao and W. Zhang, *Polym. Chem.*, 2020, **11**, 3188–3194.
- 204 N. Corrigan, L. Zhernakov, M. H. Hashim, J. Xu and C. Boyer, *React. Chem. Eng.*, 2019, **4**, 1216–1228.
- 205 D. P. Hari and B. König, *Chem. Commun.*, 2014, **50**, 6688–6699.
- 206 N. J. Treat, H. Sprafke, J. W. Kramer, P. G. Clark, B. E. Barton, J. Read De Alaniz, B. P. Fors and C. J. Hawker, *J. Am. Chem. Soc.*, 2014, **136**, 16096–16101.
- 207 M. Chen, M. J. MacLeod and J. A. Johnson, *ACS Macro Lett.*, 2015, **4**, 566–569.
- 208 M. W. Lampley and E. Harth, *ACS Macro Lett.*, 2018, **7**, 745–750.
- 209 H. Gong, Y. Zhao, X. Shen, J. Lin and M. Chen, *Angew. Chem., Int. Ed.*, 2018, **57**, 333–337.
- 210 Q. Quan, H. Wen, S. Han, Z. Wang, Z. Shao and M. Chen, *ACS Appl. Mater. Interfaces*, 2020, **12**, 24319–24327.
- 211 Y. Zhao, M. Ma, X. Lin and M. Chen, *Angew. Chem., Int. Ed.*, 2020, **59**, 21470–21474.
- 212 K. Jiang, S. Han, M. Ma, L. Zhang, Y. Zhao and M. Chen, *J. Am. Chem. Soc.*, 2020, **142**, 7108–7115.
- 213 Q. Quan, Y. Zhao, K. Chen, H. Zhou, C. Zhou and M. Chen, *ACS Catal.*, 2022, **12**, 7269–7277.
- 214 C. Wu, N. Corrigan, C.-H. Lim, K. Jung, J. Zhu, G. Miyake, J. Xu and C. Boyer, *Macromolecules*, 2019, **52**, 236–248.
- 215 Y. Song, Y. Kim, Y. Noh, V. K. Singh, S. K. Behera, A. Abudulimu, K. Chung, R. Wannemacher, J. Gierschner, L. Lüer and M. S. Kwon, *Macromolecules*, 2019, **52**, 5538–5545.
- 216 B.-H. He, M. Lu, C.-X. Yang, Y. Liu, E. Liang and G.-X. Wang, *J. Macromol. Sci., Part A: Pure Appl. Chem.*, 2018, **55**, 583–587.
- 217 W. Zhang, X. Zhang, Y. Ma, D. Chen and W. Yang, *Macromol. Chem. Phys.*, 2019, **220**, 1900022.
- 218 Q. Yang, X. Zhang, Y. Ma, D. Chen and W. Yang, *J. Polym. Sci., Part A: Polym. Chem.*, 2018, **56**, 2072–2079.
- 219 Q. Yang, X. Zhang, W. Ma, Y. Ma, D. Chen, L. Wang, C. Zhao and W. Yang, *J. Polym. Sci., Part A: Polym. Chem.*, 2018, **56**, 229–236.
- 220 H. Tao, L. Xia, G. Chen, T. Zeng, X. Nie, Z. Zhang and Y. You, *Polymers*, 2019, **11**, 892.
- 221 H. Cao, G. Wang, Y. Xue, G. Yang, J. Tian, F. Liu and W. Zhang, *ACS Macro Lett.*, 2019, **8**, 616–622.
- 222 Q. Ma, W. Wang, L. Zhang and H. Cao, *Macromol. Rapid Commun.*, 2022, **43**, 2200122.
- 223 S. Allison-Logan, Q. Fu, Y. Sun, M. Liu, J. Xie, J. Tang and G. G. Qiao, *Angew. Chem., Int. Ed.*, 2020, **59**, 21392–21396.
- 224 L. Zhang, G. Ye, X. Huo, S. Xu, J. Chen and K. Matyjaszewski, *ACS Omega*, 2019, **4**, 16247–16255.
- 225 S. Han, T. Qiu, C. Xiong, X. Li and L. Guo, *Macromolecules*, 2022, **55**, 5314–5325.
- 226 L. Xia, B.-F. Cheng, T.-Y. Zeng, X. Nie, G. Chen, Z. Zhang, W.-J. Zhang, C.-Y. Hong and Y.-Z. You, *Adv. Sci.*, 2020, **7**, 1902451.
- 227 Z. Lu, H. Yang, X. Fu, Y. Zhao, L. Xiao, Z. Zhang and L. Hou, *Macromol. Rapid Commun.*, 2021, **42**, 2100384.
- 228 J. Jiang, G. Ye, Z. Wang, Y. Lu, J. Chen and K. Matyjaszewski, *Angew. Chem., Int. Ed.*, 2018, **57**, 12037–12042.
- 229 T. Zhang, J. Yeow and C. Boyer, *Polym. Chem.*, 2019, **10**, 4643–4654.
- 230 J. Jiang, G. Ye, F. Lorandi, Z. Liu, Y. Liu, T. Hu, J. Chen, Y. Lu and K. Matyjaszewski, *Angew. Chem., Int. Ed.*, 2019, **58**, 12096–12101.
- 231 E. Liang, M. Liu, B. He and G.-X. Wang, *Adv. Polym. Technol.*, 2018, **37**, 2879–2884.
- 232 K. Hakobyan, T. Gegenhuber, C. S. P. McErlean and M. Müllner, *Angew. Chem., Int. Ed.*, 2019, **58**, 1828–1832.
- 233 K. P. McClelland, T. D. Clemons, S. I. Stupp and E. A. Weiss, *ACS Macro Lett.*, 2020, **9**, 7–13.
- 234 Y. Liang, H. Ma, W. Zhang, Z. Cui, P. Fu, M. Liu, X. Qiao and X. Pang, *Polym. Chem.*, 2020, **11**, 4961–4967.
- 235 Y. Zhu and E. Egap, *Polym. Chem.*, 2020, **11**, 1018–1024.
- 236 Q. Wang, L. Hu, Z. Cui, P. Fu, M. Liu, X. Qiao and X. Pang, *ACS Appl. Mater. Interfaces*, 2020, **12**, 42161–42168.
- 237 Y. Zhu, Y. Liu, K. A. Miller, H. Zhu and E. Egap, *ACS Macro Lett.*, 2020, **9**, 725–730.
- 238 C. Ding, J. Wang, W. Zhang, X. Pan, Z. Zhang, W. Zhang, J. Zhu and X. Zhu, *Polym. Chem.*, 2016, **7**, 7370–7374.
- 239 Y. Zhu and E. Egap, *ACS Polym. Au*, 2021, **1**, 76–99.
- 240 Y. Chu, N. Corrigan, C. Wu, C. Boyer and J. Xu, *ACS Sustainable Chem. Eng.*, 2018, **6**, 15245–15253.
- 241 Y. Chu, Z. Huang, K. Liang, J. Guo, C. Boyer and J. Xu, *Polym. Chem.*, 2018, **9**, 1666–1673.
- 242 Y. Huang, X. Li, J. Le Li, B. Zhang and T. Cai, *Macromolecules*, 2018, **51**, 7974–7982.
- 243 Y. Chu, Z. Huang, R. Liu, C. Boyer and J. Xu, *ChemPhotoChem*, 2020, **4**, 5201–5208.
- 244 S. Shanmugam, S. Xu, N. N. M. Adnan and C. Boyer, *Macromolecules*, 2018, **51**, 779–790.
- 245 K. Bell, S. Freeburne, A. Wolford and C. W. Pester, *Polym. Chem.*, 2022, **13**, 6120–6126.
- 246 K. Bell, S. Freeburne, M. Fromel, H. J. Oh and C. W. Pester, *J. Polym. Sci.*, 2021, **59**, 2844–2853.
- 247 R. A. Olson, J. S. Levi, G. M. Scheutz, J. J. Lessard, C. A. Figg, M. N. Kamat, K. B. Basso and B. S. Sumerlin, *Macromolecules*, 2021, **54**, 4880–4888.



- 248 J. J. Lessard, G. M. Scheutz, A. B. Korpusik, R. A. Olson, C. A. Figg and B. S. Sumerlin, *Polym. Chem.*, 2021, **12**, 2205–2209.
- 249 X. Li, Y. C. Zhang, S. Ye, X. R. Zhang and T. Cai, *J. Mater. Chem. A*, 2020, **8**, 25363–25370.
- 250 Y. Zhao, S. Shao, J. Xia, Y. Huang, Y. C. Zhang, X. Li and T. Cai, *J. Mater. Chem. A*, 2020, **8**, 9825–9831.
- 251 C. Chen, G. A. Zhou, H. R. Zhang, X. Tang, J. N. Cheng, Y. H. Zhao, X. Li and T. Cai, *Chem. Eng. J.*, 2021, **424**, 130395.
- 252 M. Zhao, S. Zhu, X. Yang, Y. Wang, X. Zhou and X. Xie, *Macromol. Rapid Commun.*, 2022, **43**, 2200173.
- 253 F. Li, Y. Yu, H. Lv, G. Cai and Y. Zhang, *Polym. Chem.*, 2021, **12**, 2258–2270.
- 254 F. Li, Y. Yu, H. Lv, Y. Wan, X. Gao, Y. Li and Y. Zhang, *Eur. Polym. J.*, 2022, **178**, 111519.
- 255 Y. Zhu, D. Zhu, Y. Chen, Q. Yan, C.-Y. Liu, K. Ling, Y. Liu, D. Lee, X. Wu, T. P. Senftle and R. Verduzco, *Chem. Sci.*, 2021, **12**, 16092–16099.
- 256 H. Yang, Z. Lu, X. Fu, Q. Li, L. Xiao, Y. Zhao and L. Hou, *Eur. Polym. J.*, 2022, **173**, 111306.
- 257 L. Zhang, X. Shi, Z. Zhang, R. P. Kuchel, R. Namivandi-Zangeneh, N. Corrigan, K. Jung, K. Liang and C. Boyer, *Angew. Chem., Int. Ed.*, 2021, **60**, 5489–5496.
- 258 L. Zhang, G. Ng, N. Kapoor-Kaushik, X. Shi, N. Corrigan, R. Webster, K. Jung and C. Boyer, *Angew. Chem., Int. Ed.*, 2021, **60**, 22664–22671.
- 259 X. Li, Y. Huang, W. F. Wei, W. L. Guo, Z. Luo, J. Xu and T. Cai, *Chem. Eng. J.*, 2022, **434**, 134692.
- 260 V. P. Beyer, J. Kim and C. R. Becer, *Polym. Chem.*, 2020, **11**, 1271–1291.
- 261 C. Fu, J. Xu, L. Tao and C. Boyer, *ACS Macro Lett.*, 2014, **3**, 633–638.
- 262 G. Ng, J. Yeow, R. Chapman, N. Isahak, E. Wolvetang, J. J. Cooper-White and C. Boyer, *Macromolecules*, 2018, **51**, 7600–7607.
- 263 P. R. Judzewitsch, L. Zhao, E. H. H. Wong and C. Boyer, *Macromolecules*, 2019, **52**, 3975–3986.
- 264 P. R. Judzewitsch, N. Corrigan, F. Trujillo, J. Xu, G. Moad, C. J. Hawker, E. H. H. Wong and C. Boyer, *Macromolecules*, 2020, **53**, 631–639.
- 265 A. J. Gormley, J. Yeow, G. Ng, Ó. Conway, C. Boyer and R. Chapman, *Angew. Chem., Int. Ed.*, 2018, **57**, 1557–1562.
- 266 M. J. Tamasi, R. A. Patel, C. H. Borca, S. Kosuri, H. Mugnier, R. Upadhy, N. S. Murthy, M. A. Webb and A. J. Gormley, *Adv. Mater.*, 2022, **34**, 2201809.
- 267 Q. Ma, X. Zhang, Y. Jiang, J. Lin, B. Graff, S. Hu, J. Lalevée and S. Liao, *Polym. Chem.*, 2022, **13**, 209–219.
- 268 C. Boyer, M. Kamigaito, K. Satoh and G. Moad, *Prog. Polym. Sci.*, 2023, **138**, 101648.
- 269 Z. Huang, B. B. Noble, N. Corrigan, Y. Chu, K. Satoh, D. S. Thomas, C. J. Hawker, G. Moad, M. Kamigaito, M. L. Coote, C. Boyer and J. Xu, *J. Am. Chem. Soc.*, 2018, **140**, 13392–13406.
- 270 S. Lin, L. Zhang, Z. Huang, P. V. Kumar and J. Xu, *Macromolecules*, 2019, **52**, 7157–7166.
- 271 L. Zhang, S. Lin and J. Xu, *Macromolecules*, 2022, **55**, 2463–2474.
- 272 A. Aerts, R. W. Lewis, Y. Zhou, N. Malic, G. Moad and A. Postma, *Macromol. Rapid Commun.*, 2018, **39**, 1800240.
- 273 Z. Huang, N. Corrigan, S. Lin, C. Boyer and J. Xu, *J. Polym. Sci., Part A: Polym. Chem.*, 2019, **57**, 1947–1955.
- 274 Y. Yang, K. Yu, S. Liu, J. Yan, H. Lai, F. Xing and P. Xiao, *Macromolecules*, 2021, **54**, 10923–10930.
- 275 L. Zhang, R. Liu, S. Lin and J. Xu, *Chem. Commun.*, 2021, **57**, 10759–10762.
- 276 Z. Li, S. Kosuri, H. Foster, J. Cohen, C. Jumeaux, M. M. Stevens, R. Chapman and A. J. Gormley, *J. Am. Chem. Soc.*, 2019, **141**, 19823–19830.
- 277 H. Foster, M. H. Stenzel and R. Chapman, *Macromolecules*, 2022, **55**, 5938–5945.
- 278 S. Allison-logan, F. Karimi, Y. Sun, T. G. McKenzie, M. D. Nothling, G. Bryant and G. G. Qiao, *ACS Macro Lett.*, 2019, **8**, 1291–1295.
- 279 X. Shi, J. Zhang, N. Corrigan and C. Boyer, *Mater. Chem. Front.*, 2021, **5**, 2271–2282.
- 280 N. Corrigan, F. J. Trujillo, J. Xu, G. Moad, C. J. Hawker and C. Boyer, *Macromolecules*, 2021, **54**, 3430–3446.
- 281 A. J. Teator, T. P. Varner, P. C. Knutson, C. C. Sorensen and F. A. Leibfarth, *ACS Macro Lett.*, 2020, **9**, 1638–1654.
- 282 S. Shanmugam and C. Boyer, *J. Am. Chem. Soc.*, 2015, **137**, 9988–9999.
- 283 N. Li, D. Ding, X. Pan, Z. Zhang, J. Zhu, C. Boyer and X. Zhu, *Polym. Chem.*, 2017, **8**, 6024–6027.
- 284 S.-H. Shim, M. Ham, J. Huh, Y.-K. Kwon and Y.-J. Kwark, *Polym. Chem.*, 2013, **4**, 5449–5455.
- 285 D. T. Gentekos, R. J. Sifri and B. P. Fors, *Nat. Rev. Mater.*, 2019, **4**, 761–774.
- 286 S. Xu, F. J. Trujillo, J. Xu, C. Boyer and N. Corrigan, *Macromol. Rapid Commun.*, 2021, **42**, 2100212.
- 287 R. Whitfield, N. P. Truong, D. Messmer, K. Parkatzidis, M. Rolland and A. Anastasaki, *Chem. Sci.*, 2019, **10**, 8724–8734.
- 288 N. Corrigan, A. Almasri, W. Taillades, J. Xu and C. Boyer, *Macromolecules*, 2017, **50**, 8438–8448.
- 289 N. Corrigan, R. Manahan, Z. T. Lew, J. Yeow, J. Xu and C. Boyer, *Macromolecules*, 2018, **51**, 4553–4563.
- 290 K. Liu, N. Corrigan, A. Postma, G. Moad and C. Boyer, *Macromolecules*, 2020, **53**, 8867–8882.
- 291 K. Parkatzidis, N. P. Truong, M. N. Antonopoulou, R. Whitfield, D. Konkolewicz and A. Anastasaki, *Polym. Chem.*, 2020, **11**, 4968–4972.
- 292 R. Whitfield, K. Parkatzidis, N. P. Truong, T. Junkers and A. Anastasaki, *Chem*, 2020, **6**, 1340–1352.
- 293 T. Nwoko, N. De Alwis Watuthanthrige, B. Parnitzke, K. Yehl and D. Konkolewicz, *Polym. Chem.*, 2021, **12**, 6761–6770.
- 294 R. Whitfield, N. P. Truong and A. Anastasaki, *Angew. Chem., Int. Ed.*, 2021, **60**, 19383–19388.
- 295 M.-N. Antonopoulou, R. Whitfield, N. P. Truong, D. Wyers, S. Harrison, T. Junkers and A. Anastasaki, *Nat. Chem.*, 2022, **14**, 304–312.





- 296 Z. An, *ACS Macro Lett.*, 2020, **9**, 350–357.
- 297 Y. Yang and Z. An, *Polym. Chem.*, 2019, **10**, 2801–2811.
- 298 B. Ameduri, *Chem. – Eur. J.*, 2018, **24**, 18830–18841.
- 299 L. D. Blackman, K. E. B. Doncom, M. I. Gibson and R. K. O'Reilly, *Polym. Chem.*, 2017, **8**, 2860–2871.
- 300 J. Wan, B. Fan and S. H. Thang, *Chem. Sci.*, 2022, **13**, 4192–4224.
- 301 J. Yeow, S. Shanmugam, N. Corrigan, R. P. Kuchel, J. Xu and C. Boyer, *Macromolecules*, 2016, **49**, 7277–7285.
- 302 L. Zhang, L. Xie, S. Xu, R. P. Kuchel, Y. Dai, K. Jung and C. Boyer, *Biomacromolecules*, 2020, **21**, 3887–3897.
- 303 S. Han, Y. Gu, M. Ma and M. Chen, *Chem. Sci.*, 2020, **11**, 10431–10436.
- 304 J. Zhou, C. Hong and C. Pan, *Mater. Chem. Front.*, 2017, **1**, 1200–1206.
- 305 N. Zaquen, H. Zu, A. M. N. B. P. H. A. Kadir, T. Junkers, P. B. Zetterlund and C. Boyer, *ACS Appl. Polym. Mater.*, 2019, **1**, 1251–1256.
- 306 A. B. Korpusik, Y. Tan, J. B. Garrison, W. Tan and B. S. Sumerlin, *Macromolecules*, 2021, **54**, 7354–7363.
- 307 C. Lin, S. K. Katla and J. Perez-Mercader, *J. Photochem. Photobiol., A*, 2021, **406**, 112992.
- 308 J. Wang, X. Hu, N. Zhu and K. Guo, *Chem. Eng. J.*, 2021, **420**, 127663.
- 309 R. A. Olson, A. B. Korpusik and B. S. Sumerlin, *Chem. Sci.*, 2020, **11**, 5142–5156.
- 310 M. S. Messina, K. M. M. Messina, A. Bhattacharya, H. R. Montgomery and H. D. Maynard, *Prog. Polym. Sci.*, 2020, **100**, 101186.
- 311 T. Lueckerath, T. Strauch, K. Koynov, C. Barner-Kowollik, D. Y. W. Ng and T. Weil, *Biomacromolecules*, 2019, **20**, 212–221.
- 312 A. Watanabe, J. Niu, D. J. Lunn, J. Lawrence, A. S. Knight, M. Zhang and C. J. Hawker, *J. Polym. Sci., Part A: Polym. Chem.*, 2018, **56**, 1259–1268.
- 313 J. M. Harris and R. B. Chess, *Nat. Rev. Drug Discovery*, 2003, **2**, 214–221.
- 314 E. M. Pelegri-O'Day, E.-W. Lin and H. D. Maynard, *J. Am. Chem. Soc.*, 2014, **136**, 14323–14332.
- 315 A. Abuchowski, T. van Es, N. C. Palczuk and F. F. Davis, *J. Biol. Chem.*, 1977, **252**, 3578–3581.
- 316 C. DelRe, Y. Jiang, P. Kang, J. Kwon, A. Hall, I. Jayapurna, Z. Ruan, L. Ma, K. Zolkin, T. Li, C. D. Scown, R. O. Ritchie, T. P. Russell and T. Xu, *Nature*, 2021, **592**, 558–563.
- 317 W.-H. Leung, P.-K. So, W.-T. Wong, W.-H. Lo and P.-H. Chan, *RSC Adv.*, 2016, **6**, 106837–106846.
- 318 M. Liu, L. Jia, Z. Zhao, Y. Han, Y. Li, Q. Peng and Q. Zhang, *Chem. Eng. J.*, 2020, **390**, 124667.
- 319 A. J. Russell, S. L. Baker, C. M. Colina, C. A. Figg, J. L. Kaar, K. Matyjaszewski, A. Simakova and B. S. Sumerlin, *AIChE J.*, 2018, **64**, 3230–3245.
- 320 Y. Yu, W. Xu, X. Huang, X. Xu, R. Qiao, Y. Li, F. Han, H. Peng, T. P. Davis, C. Fu and A. K. Whittaker, *ACS Macro Lett.*, 2020, **9**, 799–805.
- 321 W. L. Guo, Y. Zhou, B. Duan, W. F. Wei, C. Chen, X. Li and T. Cai, *Chem. Eng. J.*, 2022, **429**, 132120.
- 322 Y. Huang, X. Li, Y. C. Zhang, Z. Shi, L. Zeng, J. Xie, Y. Du, D. Lu, Z. Hu, T. Cai and Z. Luo, *ACS Appl. Mater. Interfaces*, 2021, **13**, 44488–44496.
- 323 C. Ma, X. Liu, G. Wu, P. Zhou, Y. Zhou, L. Wang and X. Huang, *ACS Macro Lett.*, 2017, **6**, 689–694.
- 324 G. Szczepaniak, J. Jeong, K. Kapil, S. Dadashi-Silab, S. S. Yerneni, P. Ratajczyk, S. Lathwal, D. J. Schild, S. R. Das and K. Matyjaszewski, *Chem. Sci.*, 2022, **13**, 11540–11550.
- 325 B. Panganiban, B. Qiao, T. Jiang, C. DelRe, M. M. Obadia, T. D. Nguyen, A. A. Smith, A. Hall, I. Sit, M. G. Crosby and P. B. Dennis, *Science*, 2018, **359**, 1239–1243.
- 326 C. DelRe, B. Chang, I. Jayapurna, A. Hall, A. Wang, K. Zolkin and T. Xu, *Adv. Mater.*, 2021, **33**, 2105707.
- 327 P. R. Judzewitsch, T.-K. Nguyen, S. Shanmugam, E. H. H. Wong and C. Boyer, *Angew. Chem., Int. Ed.*, 2018, **57**, 4559–4564.
- 328 P. R. Judzewitsch, N. Corrigan, E. H. H. Wong and C. Boyer, *Angew. Chem., Int. Ed.*, 2021, **60**, 24248–24256.
- 329 H. Sun, W. Cao, N. Zang, T. D. Clemons, G. M. Scheutz, Z. Hu, M. P. Thompson, Y. Liang, M. Vratsanos, X. Zhou, W. Choi, B. S. Sumerlin, S. I. Stupp and N. C. Gianneschi, *Angew. Chem., Int. Ed.*, 2020, **59**, 19136–19142.
- 330 A. J. Gormley and M. A. Webb, *Nat. Rev. Mater.*, 2021, **6**, 642–644.
- 331 M. Tamasi, S. Kosuri, J. DiStefano, R. Chapman and A. J. Gormley, *Adv. Intell. Syst.*, 2020, **2**, 1900126.
- 332 R. Upadhyaya, A. Punia, M. J. Kanagala, L. Liu, M. Lamm, T. A. Rhodes and A. J. Gormley, *ACS Appl. Polym. Mater.*, 2021, **3**, 1525–1536.
- 333 J. O. Zoppe, N. C. Ataman, P. Mocny, J. Wang, J. Moraes and H.-A. Klok, *Chem. Rev.*, 2017, **117**, 1105–1318.
- 334 M. Li, M. Fromel, D. Ranaweera, S. Rocha, C. Boyer and C. W. Pester, *ACS Macro Lett.*, 2019, **8**, 374–380.
- 335 J. Poisson, A. M. Polgar, M. Fromel, C. W. Pester and Z. M. Hudson, *Angew. Chem., Int. Ed.*, 2021, **60**, 19988–19996.
- 336 X. Xu, X. Huang, Y. Chang, Y. Yu, J. Zhao, N. Isahak, J. Teng, R. Qiao, H. Peng, C.-X. Zhao, T. P. Davis, C. Fu and A. K. Whittaker, *Biomacromolecules*, 2021, **22**, 330–339.
- 337 G. Ng, P. Judzewitsch, M. Li, C. W. Pester, K. Jung and C. Boyer, *Macromol. Rapid Commun.*, 2021, **42**, 2100106.
- 338 G. Ng, M. Li, J. Yeow, K. Jung, C. W. Pester and C. Boyer, *ACS Appl. Mater. Interfaces*, 2020, **12**, 55243–55254.
- 339 M. Fromel and C. W. Pester, *Macromolecules*, 2022, **55**, 4907–4915.
- 340 A. R. Kuzmyn, L. W. Teunissen, M. V. Kroese, J. Kant, S. Venema and H. Zuilhof, *ACS Omega*, 2022, **7**, 38371–38379.
- 341 L.-H. Rong, X. Cheng, J. Ge, O. K. Krebs, J. R. Capadona, E. B. Caldona and R. C. Advincula, *ACS Appl. Polym. Mater.*, 2022, **4**, 6449–6457.
- 342 T. Joshi and L. Nebhani, *Surf. Interfaces*, 2022, **29**, 101764.
- 343 C. Förster, L. Veith and A. Andrieu-Brunsen, *RSC Adv.*, 2022, **12**, 27109–27113.
- 344 L. Hu, Q. Hao, L. Wang, Z. Cui, P. Fu, M. Liu, X. Qiao and X. Pang, *Polym. Chem.*, 2021, **12**, 545–553.



- 345 J. Zhou, L. Ye, Y. Lin, L. Wang, L. Zhou, H. Hu, Q. Zhang, H. Yang and Z. Luo, *J. Appl. Polym. Sci.*, 2019, **136**, 47653.
- 346 J. Zhou, Y. Lin, L. Ye, L. Wang, L. Zhou, H. Hu, Q. Zhang, H. Yang and Z. Luo, *Macromol. Res.*, 2019, **27**, 1144–1154.
- 347 J. Zhou, Y. Sun, Z. Huang, Z. Luo and H. Hu, *J. Appl. Polym. Sci.*, 2021, **138**, 51395.
- 348 Y. Lin, L. Wang, J. Zhou, L. Ye, H. Hu, Z. Luo and L. Zhou, *Polymer*, 2019, **162**, 80–90.
- 349 J. Zhou, Y. Lin, L. Wang, L. Zhou, B. Yu, X. Zou, Z. Luo and H. Hu, *Colloids Surf., A*, 2021, **617**, 126369.
- 350 H. Kodama, *Rev. Sci. Instrum.*, 1981, **52**, 1770–1773.
- 351 C. W. Hull, *US Pat.*, **4575330**, 1986.
- 352 S. C. Ligon, R. Liska, J. Stampfl, M. Gurr and R. Mülhaupt, *Chem. Rev.*, 2017, **117**, 10212–10290.
- 353 T. T. Wohlers, W. A. (Firm), R. I. Campbell, O. Diegel, J. Kowen, R. Huff, N. Mostow, I. Fidan, D. L. Bourell, J. Van Rensburg and others, *Wohlers Report 2022: 3D Printing and Additive Manufacturing Global State of the Industry*, Wohlers Associates, 2022.
- 354 H. N. Chia and B. M. Wu, *J. Biol. Eng.*, 2015, **9**, 4.
- 355 T. J. Wallin, J. Pikul and R. F. Shepherd, *Nat. Rev. Mater.*, 2018, **3**, 84–100.
- 356 A. Paolini, S. Kollmannsberger and E. Rank, *Addit. Manuf.*, 2019, **30**, 100894.
- 357 C. Sun, N. Fang, D. M. Wu and X. Zhang, *Sens. Actuators, A*, 2005, **121**, 113–120.
- 358 X. Zheng, J. Deotte, M. P. Alonso, G. R. Farquar, T. H. Weisgraber, S. Gemberling, H. Lee, N. Fang and C. M. Spadaccini, *Rev. Sci. Instrum.*, 2012, **83**, 125001.
- 359 K. Jung, N. Corrigan, M. Ciftci, J. Xu, S. E. Seo, C. J. Hawker and C. Boyer, *Adv. Mater.*, 2020, **32**, 1903850.
- 360 A. Bagheri and J. Jin, *ACS Appl. Polym. Mater.*, 2019, **1**, 593–611.
- 361 V. A. Bobrin, J. Zhang, N. Corrigan and C. Boyer, *Adv. Mater. Technol.*, 2022, 2201054.
- 362 Z. Zhang, N. Corrigan and C. Boyer, *Macromolecules*, 2021, **54**, 1170–1182.
- 363 G. Moad, E. Rizzardo and S. H. Thang, *Polymer*, 2008, **49**, 1079–1131.
- 364 G. Moad, E. Rizzardo and S. H. Thang, *Acc. Chem. Res.*, 2008, **41**, 1133–1142.
- 365 A. Bagheri, H. Ling, C. William Anderson Bainbridge and J. Jin, *ACS Appl. Polym. Mater.*, 2021, **3**, 2921–2930.
- 366 K. Lee, N. Corrigan and C. Boyer, *Angew. Chem., Int. Ed.*, 2021, **60**, 8839–8850.
- 367 Z. Zhang, N. Corrigan and C. Boyer, *Angew. Chem., Int. Ed.*, 2022, **61**, e202114111.
- 368 V. A. Bobrin, K. Lee, J. Zhang, N. Corrigan and C. Boyer, *Adv. Mater.*, 2022, **34**, 2107643.
- 369 X. Shi, V. A. Bobrin, Y. Yao, J. Zhang, N. Corrigan and C. Boyer, *Angew. Chem., Int. Ed.*, 2022, **61**, e202206272.
- 370 V. A. Bobrin, Y. Yao, X. Shi, Y. Xiu, J. Zhang, N. Corrigan and C. Boyer, *Nat. Commun.*, 2022, **13**, 3577.
- 371 D. Melodia, A. Bhadra, K. Lee, R. Kuchel, D. Kundu, N. Corrigan and C. Boyer, *Small*, 2023, 2206639.
- 372 K. Lee, Y. Shang, V. A. Bobrin, R. Kuchel, D. Kundu, N. Corrigan and C. Boyer, *Adv. Mater.*, 2022, **34**, 2204816.
- 373 R. M. Myers, D. E. Fitzpatrick, R. M. Turner and S. V. Ley, *Chem. – A Eur. J.*, 2014, **20**, 12348–12366.
- 374 M. B. Plutschack, B. Pieber, K. Gilmore and P. H. Seeberger, *Chem. Rev.*, 2017, **117**, 11796–11893.
- 375 T. Junkers and B. Wenn, *React. Chem. Eng.*, 2016, **1**, 60–64.
- 376 N. Zhu, X. Hu, Z. Fang and K. Guo, *ChemPhotoChem*, 2018, **2**, 831–838.
- 377 B. L. Buss and G. M. Miyake, *Chem. Mater.*, 2018, **30**, 3931–3942.
- 378 M. H. Reis, F. A. Leibfarth and L. M. Pitet, *ACS Macro Lett.*, 2020, **9**, 123–133.
- 379 M. Chen and J. A. Johnson, *Chem. Commun.*, 2015, **51**, 6742–6745.
- 380 F. Lauterbach, M. Rubens, V. Abetz and T. Junkers, *Angew. Chem., Int. Ed.*, 2018, **57**, 14260–14264.
- 381 M. Rubens, P. Latsrisaeng and T. Junkers, *Polym. Chem.*, 2017, **8**, 6496–6505.
- 382 C. Sambiagio, M. Ferrari, K. van Beurden, N. della Ca', J. Van Schijndel and T. Noël, *Org. Lett.*, 2021, **23**, 2042–2047.
- 383 F. Zhong, Y. Zhou and M. Chen, *Polym. Chem.*, 2019, **10**, 4879–4886.
- 384 S. Oliver, L. Zhao, A. J. Gormley, R. Chapman and C. Boyer, *Macromolecules*, 2019, **52**, 3–23.
- 385 C. Stubbs, K. A. Murray, T. Ishibe, R. T. Mathers and M. I. Gibson, *ACS Macro Lett.*, 2020, **9**, 290–294.
- 386 S.-J. Richards, A. Jones, R. M. F. Tomás and M. I. Gibson, *Chem. – A Eur. J.*, 2018, **24**, 13758–13761.
- 387 J. Yeow, S. Joshi, R. Chapman and C. Boyer, *Angew. Chem., Int. Ed.*, 2018, **57**, 10102–10106.
- 388 R. Upadhyaya, N. S. Murthy, C. L. Hoop, S. Kosuri, V. Nanda, J. Kohn, J. Baum and A. J. Gormley, *Macromolecules*, 2019, **52**, 8295–8304.
- 389 G. Ng, K. Jung, J. Li, C. Wu, L. Zhang and C. Boyer, *Polym. Chem.*, 2021, **12**, 6548–6560.
- 390 M. Nagao, Y. Kimoto, Y. Hoshino and Y. Miura, *ACS Omega*, 2022, **7**, 13254–13259.
- 391 S. Kosuri, C. H. Borca, H. Mugnier, M. Tamasi, R. A. Patel, I. Perez, S. Kumar, Z. Finkel, R. Schloss, L. Cai, M. L. Yarmush, M. A. Webb and A. J. Gormley, *Adv. Healthcare Mater.*, 2022, **11**, 2102101.
- 392 R. Upadhyaya, S. Kosuri, M. Tamasi, T. A. Meyer, S. Atta, M. A. Webb and A. J. Gormley, *Adv. Drug Delivery Rev.*, 2021, **171**, 1–28.
- 393 F. Soheilmooghaddam, M. Rumble and J. Cooper-White, *Chem. Rev.*, 2021, **121**, 10792–10864.
- 394 J. Li, M. Zhang, J. Zhu and X. Zhu, *Polymers*, 2019, **11**, 1722.
- 395 R. N. Carmean, T. E. Becker, M. B. Sims and B. S. Sumerlin, *Chem*, 2017, **2**, 93–101.
- 396 K. Ferji, P. Venturini, F. Cleymand, C. Chassenieux and J.-L. Six, *Polym. Chem.*, 2018, **9**, 2868–2872.
- 397 P. Lertturonchai, M. I. A. Ibrahim, A. Durand, P. Sunintaboon and K. Ferji, *Macromol. Rapid Commun.*, 2020, **41**, 2000058.
- 398 T. G. McKenzie, L. P. da, M. Costa, Q. Fu, D. E. Dunstan and G. G. Qiao, *Polym. Chem.*, 2016, **7**, 4246–4253.



- 399 K. Jung, C. Boyer and P. B. Zetterlund, *Polym. Chem.*, 2017, **8**, 3965–3970.
- 400 A. Bagheri, Z. Sadrearhami, N. N. M. Adnan, C. Boyer and M. Lim, *Polymer*, 2018, **151**, 6–14.
- 401 B. Cabannes-Boué, Q. Yang, J. Lalevée, F. Morlet-Savary and J. Poly, *Polym. Chem.*, 2017, **8**, 1760–1770.
- 402 A. Bagheri, C. Bainbridge and J. Jin, *ACS Appl. Polym. Mater.*, 2019, **1**, 1896–1904.
- 403 A. Bagheri, K. E. Engel, C. W. A. Bainbridge, J. Xu, C. Boyer and J. Jin, *Polym. Chem.*, 2020, **11**, 641–647.
- 404 K. J. Arrington and J. B. Matson, *Polym. Chem.*, 2017, **8**, 7452–7456.
- 405 T. G. McKenzie, E. H. H. Wong, Q. Fu, A. Sulistio, D. E. Dunstan and G. G. Qiao, *ACS Macro Lett.*, 2015, **4**, 1012–1016.
- 406 V. Tkachenko, C. Matei Ghimbeu, C. Vaulot, L. Vidal, J. Poly and A. Chemtob, *Polym. Chem.*, 2019, **10**, 2316–2326.
- 407 R. W. Hughes, M. E. Lott, J. I. Bowman and B. S. Sumerlin, *ACS Macro Lett.*, 2023, **12**, 14–19.
- 408 A. Rasines Mazo, T. N. Tran, W. Zhang, Y. Meng, A. Reyhani, S. Pascual, L. Fontaine, G. G. Qiao and S. Piogé, *Polym. Chem.*, 2020, **11**, 5238–5248.
- 409 R. W. Lewis, R. A. Evans, N. Malic, K. Saito and N. R. Cameron, *Polym. Chem.*, 2018, **9**, 60–68.
- 410 J. Li, C. Ding, Z. Zhang, J. Zhu and X. Zhu, *React. Funct. Polym.*, 2017, **113**, 1–5.
- 411 J. Luo, M. Li, M. Xin, W. Sun and W. Xiao, *Macromol. Chem. Phys.*, 2016, **217**, 1777–1784.
- 412 Q. Yang, M. Guerre, V. Ladmiral and B. Ameduri, *Polym. Chem.*, 2018, **9**, 3388–3397.
- 413 R. N. Carmean, M. B. Sims, C. A. Figg, P. J. Hurst, J. P. Patterson and B. S. Sumerlin, *ACS Macro Lett.*, 2020, **9**, 613–618.
- 414 J. Li, X. Pan, N. Li, J. Zhu and X. Zhu, *Polym. Chem.*, 2018, **9**, 2897–2904.
- 415 Y. Wang, M. Wang, L. Bai, L. Zhang, Z. Cheng and X. Zhu, *Polym. Chem.*, 2020, **11**, 2080–2088.
- 416 S. Liu, Y. Cheng, H. Zhang, Z. Qiu, R. T. K. Kwok, J. W. Y. Lam and B. Z. Tang, *Angew. Chem., Int. Ed.*, 2018, **57**, 6274–6278.
- 417 A.-C. Lehen, J. A. M. Kurki and M. Hartlieb, *Polym. Chem.*, 2022, **13**, 1537–1546.
- 418 C. P. Easterling, Y. Xia, J. Zhao, G. E. Fanucci and B. S. Sumerlin, *ACS Macro Lett.*, 2019, **8**, 1461–1466.
- 419 C. Fu, Z. Huang, C. J. Hawker, G. Moad, J. Xu and C. Boyer, *Polym. Chem.*, 2017, **8**, 4637–4643.
- 420 S. Shanmugam, G. Ross, C. Y. Mbuncha and A. Santra, *Polym. Chem.*, 2021, **12**, 6705–6713.
- 421 J. Yeow, O. R. Sugita and C. Boyer, *ACS Macro Lett.*, 2016, **5**, 558–564.
- 422 N. Zaquen, J. Yeow, T. Junkers, C. Boyer and P. B. Zetterlund, *Macromolecules*, 2018, **51**, 5165–5172.
- 423 B. Zhao, J. Li, Z. Li, X. Lin, X. Pan, Z. Zhang and J. Zhu, *Macromolecules*, 2022, **55**, 7181–7192.
- 424 X. Wu, B. Gross, B. Leuschel, K. Mougin, S. Dominici, S. Gree, M. Belqat, V. Tkachenko, B. Cabannes-Boué, A. Chemtob, J. Poly and A. Spangenberg, *Adv. Funct. Mater.*, 2022, **32**, 2109446.
- 425 V. Kottisch, M. J. Supej and B. P. Fors, *Angew. Chem., Int. Ed.*, 2018, **57**, 8260–8264.
- 426 R. J. Sifri, A. J. Kennedy and B. P. Fors, *Polym. Chem.*, 2020, **11**, 6499–6504.
- 427 X. Zhang, Y. Jiang, Q. Ma, S. Hu and S. Liao, *J. Am. Chem. Soc.*, 2021, **143**, 6357–6362.
- 428 Z. Yang, J. Chen and S. Liao, *ACS Macro Lett.*, 2022, **11**, 1073–1078.
- 429 J. Li, M. Chen, X. Lin, Q. Li, W. Zhang, G. Jin, X. Pan, J. Zhu and X. Zhu, *ACS Macro Lett.*, 2020, **9**, 1799–1805.
- 430 M. Ciftci, Y. Yoshikawa and Y. Yagci, *Angew. Chem., Int. Ed.*, 2017, **56**, 519–523.
- 431 J. Li, A. Kerr, S. Häkkinen, T. Floyd, M. Zhang, X. Pan, X. Zhu, S. Perrier and J. Zhu, *Polym. Chem.*, 2020, **11**, 2724–2731.
- 432 J. Li, A. Kerr, Q. Song, J. Yang, S. Häkkinen, X. Pan, Z. Zhang, J. Zhu and S. Perrier, *ACS Macro Lett.*, 2021, **10**, 570–575.
- 433 H. Suk Wang, N. P. Truong, Z. Pei, M. L. Coote, A. Anastasaki, H. S. Wang, N. P. Truong, Z. Pei, M. L. Coote and A. Anastasaki, *J. Am. Chem. Soc.*, 2022, **144**, 4678–4684.
- 434 V. Bellotti, K. Parkatzidis, H. S. Wang, N. De Alwis Watuthanthrige, M. Orfano, A. Monguzzi, N. P. Truong, R. Simonutti and A. Anastasaki, *Polym. Chem.*, 2023, **14**, 253–258.
- 435 J. B. Young, J. I. Bowman, C. B. Eades, A. J. Wong and B. S. Sumerlin, *ACS Macro Lett.*, 2022, **11**, 1390–1395.
- 436 S. V. Wanasinghe, M. Sun, K. Yehl, J. Cuthbert, K. Matyjaszewski and D. Konkolewicz, *ACS Macro Lett.*, 2022, **11**, 1156–1161.
- 437 P. N. Kurek, A. J. Kloster, K. A. Weaver, R. Manahan, M. L. Allegranza, N. De Alwis Watuthanthrige, C. Boyer, J. A. Reeves and D. Konkolewicz, *Ind. Eng. Chem. Res.*, 2018, **57**, 4203–4213.
- 438 Y. Lee, C. Boyer and M. S. Kwon, *Nat. Rev. Mater.*, 2022, **7**, 74–75.

